AD NUMBER

AD481174

NEW LIMITATION CHANGE

TO

Approved for public release, distribution unlimited

FROM

Distribution authorized to U.S. Gov't. agencies and their contractors; Critical Technology; Mar 1966. Other requests shall be referred to Air Force Weapons Lab., Attn: WLRE, Kirtland AFB, NM 87117.

AUTHORITY

Air Force Weapons Lab ltr dtd 30 Nov 1971

AFWL-TR
65-188

ULTRASONIC WAVE VELOCITY-TEMPERATURE STUDIES IN SEVERAL PLASTICS, PLASTIC FOAMS AND NOSE-CONE MATERIALS

James R. Asay
Lt USAF

Anton J. Dorr
Lt USAF

Ned D. Arnold
Capt USAF

Dr. Arthur H. Guenther

TECHNICAL REPORT NO. AFWL-TR-65-188

March 1966

AIR FORCE WEAPONS LABORATORY
Research and Technology Division
Air Force Systems Command
Kirtland Air Force Base
New Mexico

AFWL-TR-65-188

Research and Technology Division
AIR FORCE WEAPONS LABORATORY
Air Force Systems Command
Kirtland Air Force Base
New Mexico

AFWL-TR-65-188

ULTRASONIC WAVE VELOCITY - TEMPERATURE STUDIES IN SEVERAL PLASTICS, PLASTIC FOAMS AND NOSE-CONE MATERIALS

James R. Asay
Lt USAF

Anton J. Dorr
Lt USAF

Ned D. Arnold
Capt USAF

Dr. Arthur H. Guenther

TECHNICAL REPORT NO. AFWL-TR-65-188

FOREWORD

This research concerning the ultrasonic investigations of nose-cone materials extended from April 1964 to June 1965. This document is intended for technical personnel who are familiar with acoustic properties of solids. The research was performed under Program Element 7.60.06.01.D, Project 5710, Subtask 15.018 and was funded by the Defense Atomic Support Agency.

The research was the result of the continuing efforts of four investigators. Dr. Arthur H. Guenther conceived the original requirements and instigated the program. Capt Ned D. Arnold was responsible for setting up the original apparatus, perfecting techniques, and performing many of the early measurements. The authors wish to express gratitude to the following: A1C Richard P. Copeland and A2C Robert D. Goligowski for performing many of the measurements and for calibrating and refining the equipment, and to SSgt Jerry Teal for valuable assistance in machining several components of the apparatus and for preparing the samples. This report was submitted by the Air Force Weapons Laboratory Project Officer, 2Lt James R. Asay (WLRE), 23 February 1966.

This technical report has been reviewed and is approved.

James R. Asay

JAMES R. ASAY
2Lt, USAF
Project Officer

Edgar M. Munyon

EDGAR M. MUNYON
Colonel, USAF
Chief, Effects Branch

William H. Stephens

WILLIAM H. STEPHENS
Colonel, USAF
Chief, Research Division

ABSTRACT

An experimental study with two specific aims was conducted at the Air Force Weapons Laboratory: (1) to show the relationship between temperature and velocity of longitudinal ultrasonic waves through several plastics and nose-cone materials and (2) to establish a convenient apparatus for the determination of elastic properties of materials. The velocity-temperature data were needed for use in another research project where certain inputs were necessary to more completely describe materials under shock-loaded conditions. The experimental procedure was based on measuring the transit times required for ultrasonic waves in the low-megacycle range to pass through samples of different thicknesses. The resulting accuracy for most of the measurements is within about 1 to 2 percent. The temperature range of the measurements extended between room temperature and about 125°C, with a few measurements to 250°C. Velocity-temperature curves were determined for nylon, low- and high-density polyethylene, plexiglass (polymethylmethacrylate), Delrin Acetal, and teflon. Curves were also drawn for several re-entry vehicle nose-cone materials, including chopped nylon phenolic, Castable 124, Avcoat I and 19, pyrolytic graphite, General Electric Phenolic Fibre Glass, Phenolic Carbon, Tape Wound Nylon Phenolic, Rad 58B, Rad 60, and some solid epoxy foams. Less complete data were obtained for Avco phenolic fiber glass and Obiique Tape Wound Refrasil. The angular dependence of velocity was measured for several layered materials, and it was found that the velocity was very dependent on the direction of propagation. For most of the materials studied the velocity was found to decrease more or less linearly with increasing temperature and normally was about 9 - 20 percent lower than at room temperature.

CONTENTS

ILLUSTRATIONS

ILLUSTRATIONS (cont'd)

TABLES

ABBREVIATIONS AND SYMBOLS

E Young's modulus, ratio of applied stress to fractional extension.

G Shear modulus, ratio of shearing stress to shear strain.

L Attenuation of a wave in decibels $L = (20 \log e)\alpha$.

B_s Bulk modulus, ratio of applied pressure to fractional change in volume for uniform hydrostatic compression, $-V\left(\frac{\partial P}{\partial V}\right)$ at constant entropy, s.

c_{ij} Elastic stiffness constants which are the coefficients of the strains in the generalized form of Hooke's law. In matrix form $\sigma_{ij} = \left(c_{ij}\right)\varepsilon_{ij}$.

ε_{ij} Components of strain.

σ_{ij} Components of stress.

μ Lamé constant for isotropic materials. Identical with the shear modulus G.

λ Lamé constant appearing in the stress-strain matrix for isotropic materials.

c_ℓ Longitudinal velocity, defined in isotropic media as $c_\ell = \sqrt{\frac{\lambda + 2\mu}{\rho}}$

c_t Shear velocity, defined in isotropic media as $c_t = \sqrt{\frac{\mu}{\rho}}$.

c_o Hydrodynamic sound velocity, defined as $c_o^2 = \left(\frac{\partial P_o}{\partial \rho}\right)_s$, where s is entropy and P_o is the pressure at normal conditions.

U_S Shock velocity defined as $U_S^2 = \left(\frac{\partial P}{\partial \rho}\right)$, along the actual path in the pressure-density plane.

Z Acoustic impedance, defined as product of velocity (longitudinal or shear) and initial sample density ρ.

u_p Particle velocity.

σ Poisson's ratio, ratio of lateral contraction to longitudinal extension of a specimen.

C_P Specific heat at constant pressure.

α Attenuation of an acoustic wave in nepers.

β Volume coefficient of thermal expansion $\beta = \frac{1}{V}\left(\frac{\partial V}{\partial T}\right)_P$.

γ Grueneisen ratio, defined as $\gamma = V\left(\frac{\partial P}{\partial E}\right)_V$ where P is the pressure, E the internal energy, and V is specific volume.

μ' Compression defined as $\mu' = \frac{\rho - \rho_o}{\rho_o}$, where ρ_o is the initial sample density and ρ is the density behind the pressure wave.

SECTION I

INTRODUCTION

The first fact which becomes apparent to a researcher desiring information on the velocity of ultrasound penetrating through a particular material is that there is a shortage of published specific parametric data on the phenomenon. Such parameters as the frequency of the acoustic waves used and the temperature at which measurements were made are noticeably lacking. For plastics and related materials, in particular, there is a scarcity of information indicating the relationship between velocities and temperatures.

For this reason an investigation was conducted at the Air Force Weapons Laboratory to determine as functions of temperature, the velocities of longitudinal ultrasonic waves through several plastic materials, including some of the nonmetallic materials used in the nose cones of ballistic reentry vehicles. This information was needed as input data in other research programs which were concerned with the dynamic response of materials to shock loading. Without published data showing the effect of temperature upon velocity one might assume the velocity to be constant over fairly large temperature ranges. This is indeed a very broad assumption which the results of this study have shown to be invalid.

In view of the accuracy of other input data and the reproducibility and inhomogeneity of sample material it was determined that a precision of ~5% in velocity values was needed. Considering this and the availability of equipment it was decided to use a simple and straightforward direct timing method in which transit times through samples of different thicknesses are measured.

Before proceeding further, a word on definitions is in order. The term "ultrasonic" is now commonly used to describe vibrational waves with frequencies higher than those normally audible to the ear, i.e., any acoustic wave of a frequency higher than approximately 20 kc is said to be ultrasonic. In some older works the word "supersonic" was used to mean the same thing, but such usage is no longer sanctioned by convention. Similarly, "ultrasonics" is defined as the technology of sound at frequencies above the audio range, and "supersonics" is now defined to be the general subject covering phenomena associated with speed higher than the speed of sound (as in the case of aircraft, projectiles, etc). This study is concerned only with "ultrasonics."

SECTION II

EXPERIMENTAL METHOD

The technique of determing velocity by measuring the time required for pulses to traverse samples of different thicknesses was chosen, whenever possible, to eliminate complicating considerations such as transducer and circuitry delay times, and interfacial effects.

The resulting sample arrangement is best explained by referring to figure 1. If the transit time form A to B through the thick sample is t_1, and the transit time through the thin sample is t_2, the velocity of the pulse through the sample material can be calculated as,

$$c_\ell = \frac{\Delta X}{\Delta t} = \frac{X_1 - X_2}{t_1 - t_2} \qquad (1)$$

where c_ℓ is the longitudinal bulk velocity. If the same aluminum block* and the same transducers are used while making the measurements of t_1 and t_2, it is not necessary to determine the transducer delay times or the transit time through the aluminum buffers, since these constant delays disappear on computing the difference in times, $t_1 - t_2$. This method, of course, assumes that the acoustic units can be reproducibly assembled and that the difference in transit times is due only to the difference in sample thicknesses.

Figure 2 shows an improved bonding clamp based on Sullivan's design (Ref. 1) which was devised to achieve this reproducibility. It was found that with this technique the deviation in time due to assembly was generally within $\pm$ 0.01μ - sec. The transmission blocks were cut from 2 inch diameter bar stock of 2024 aluminum alloy. The ends of the rods were machined and polished so as to be flat, parallel, and smooth, thereby reducing diffraction and edge effects. The length of the rods used in this work were varied to suit the individual experiment and were normally on the order of 3/4 to 2 inches long.

---

*The function of the aluminum block is to make the overall transit time greater than the duration of the ultrasonic pulse so that electrical noise generated by the transmitted pulse does not interfere with the received pulse.

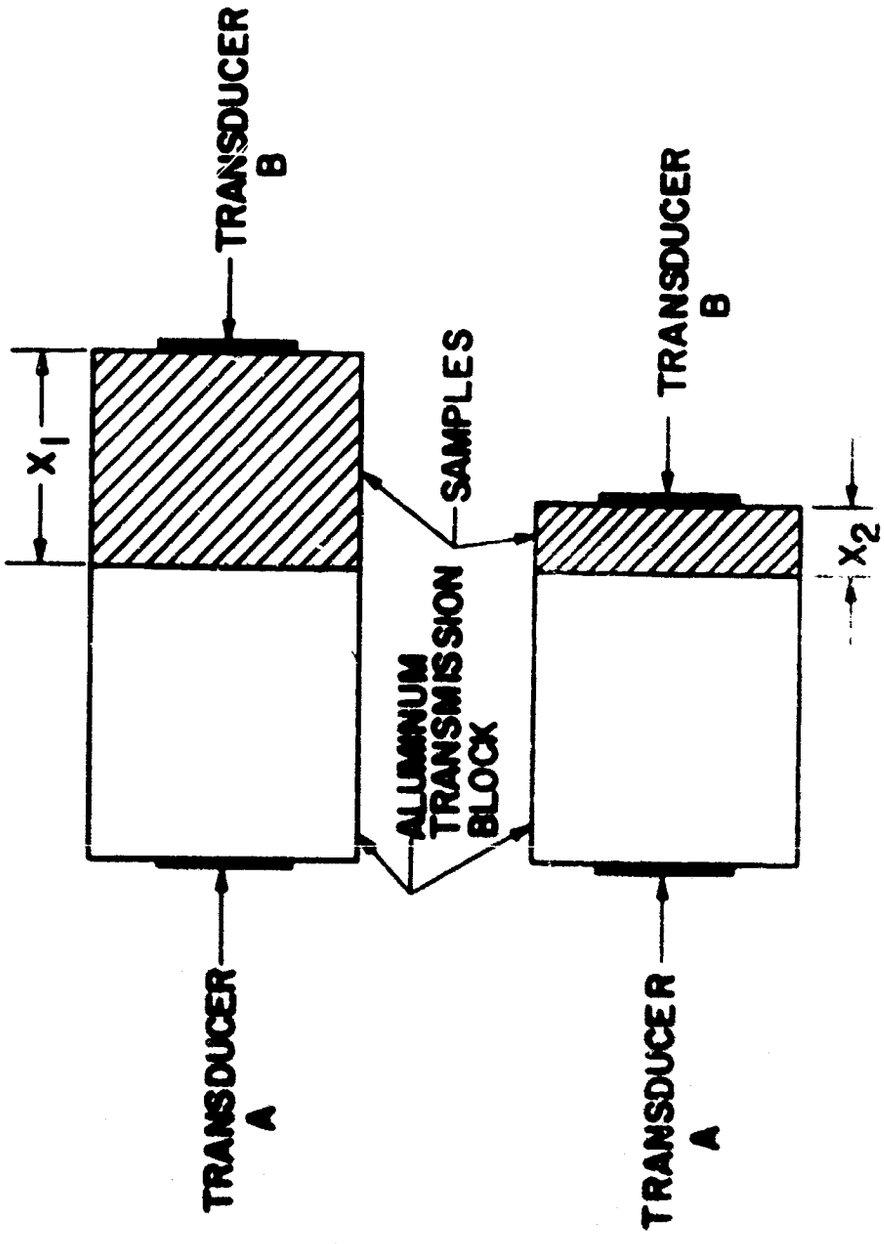

Figure 1. Diagrams of Typical Acoustic Assembly

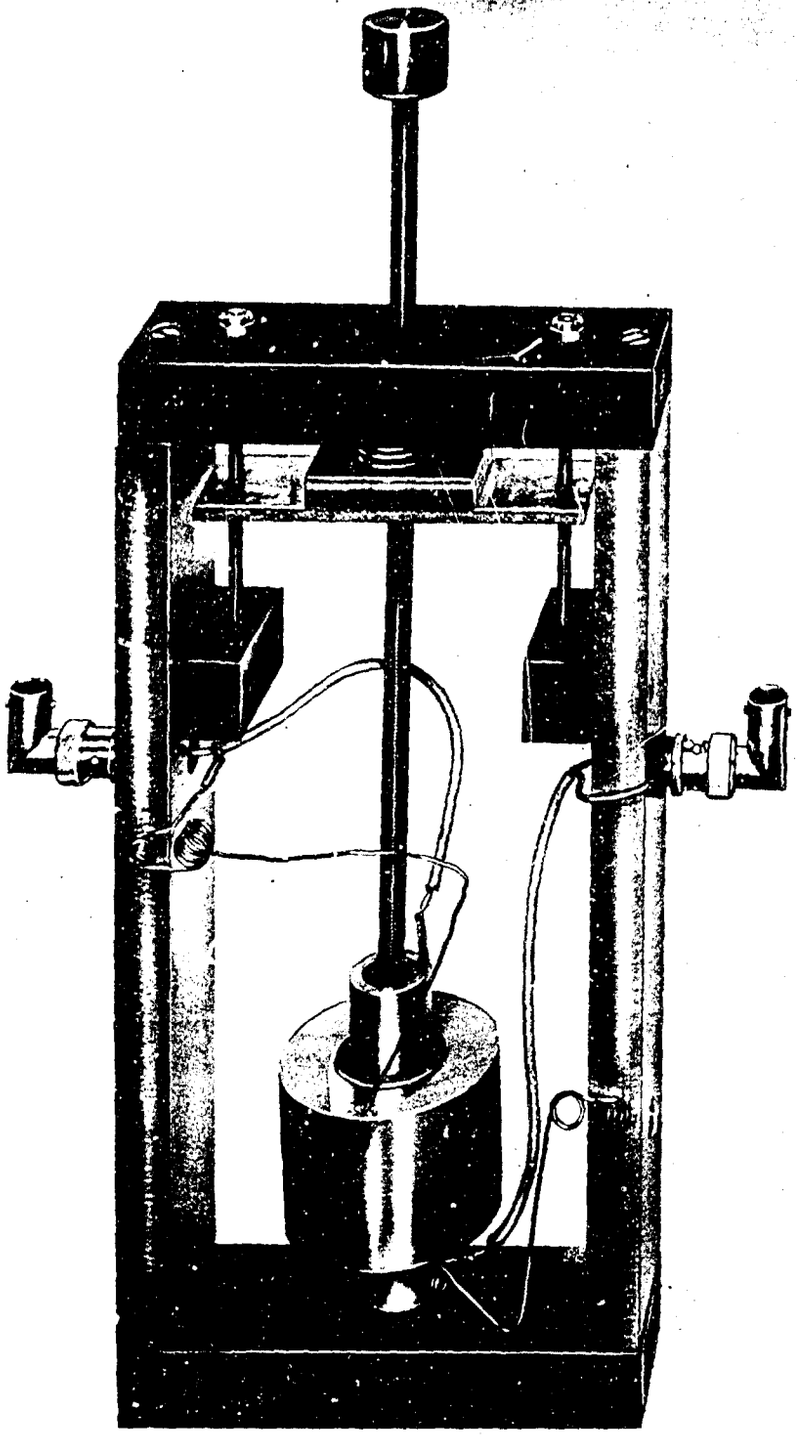

Figure 2. Bonding Clamp with Acoustic Unit in Place

The samples were also cut as right circular cylinders of approximately 2-inch diameter. The exact shape of the sample is immaterial, provided that the lateral and longitudinal dimensions are large enough that the assumption of an infinite medium is valid. Tu, Brennan, and Sauer (Ref. 2) have found ultrasonic velocities to be independent of sample size provided the radius of the sample is at least 2.5 times as great as the wavelength of the stress disturbance. The samples and transmission blocks used in the present study have radii that are generally six or more times greater than the wavelengths used. This ensures the one dimensionality of the hydrodynamic wave so that the longitudinal bulk velocity is essentially the quantity measured.

For the required accuracy it was imperative that the two end faces of the sample be flat and parallel to reduce diffraction and dispersion effects. This was achieved with varying degrees of success depending on the particular sample material and the technique used in preparing it. Normally, however, it was found that the variation of sample thickness was so small that the contribution of the resulting error to the overall error could be neglected. This source of error, which contributed at most a deviation of 0.5 percent, will be treated in more detail in a later section.

The transducers used to produce the acoustic vibrations are composed of lead zirconate/titanate mixtures formed in the shape of circular disks and designed to operate in the thickness mode. Their thicknesses varied depending upon the desired resonant frequency, e.g., the thickness corresponding to a resonant frequency of 3.0 megacycles per second is 0.026 inches. In most cases, the transducers were operated at the fundamental frequencies of 1.5, 3.0, 5.0 and 10.0 megacycles per second, or the respective harmonics.

For most of the measurements a light transformer oil* was used as the coupling agent between the various components of the acoustic units. For temperature measurements (to temperatures of about 125°C) the same oil was used as the liquid in a thermostatically controlled bath used to control sample temperatures. For temperatures higher than this and for samples which were oil absorbant, a thermostatically controlled oven was used for the temperature measurements.

---

*"Special Marcol 42-46", produced by Humble Oil and Refining Company.

The acoustic unit shown in figure 2 is composed of two ceramic transducers (only the upper one is visible), a sample, and an aluminum transmission block. The cylindrical aluminum electrodes of the clamp are mounted on ball joints which ensures that the components of the acoustic unit are held together, accurately aligned, and under constant spring pressure.

For many of the experiments only one buffer rod was used in calculating velocities. A grounding electrode was therefore provided for the side of the transducer next to the sample, since the plastic samples are nonconducting. This was a thin (0.0017 inch thick) piece of aluminum foil which can be seen in figure 2 between the sample and the upper transducer. The wire contact was pressed firmly against the foil with spring pressure to maintain an adequate ground lead. For samples which were highly attenuating or for which it was not possible to obtain a sufficiently thick sample, the foil was eliminated and two aluminum buffer rods were used instead of one. This modification required the transit time measurement of only one sample, and the velocity was computed as in equation (1) with X_2 equal to zero, t_1, the transit time with the sample inserted, and t_2, the transit time through the assembly without the sample. Comparison between the two methods was good, providing proper precaution was taken in assembling the various acoustic units.

The main difference in velocity measurements which could result from the use of these two different methods is that occurring because of the difference in the number of sample-buffer interfaces with and without the sample inserted for the latter method. However, this effect appeared to be insignificant in comparison to the inherent limitations of the technique, and cross checks between the two methods on identical samples agreed regularly to withing 1%. To distinguish between the various methods referred to in the text, the technique of using different samples to calculate the velocity will be referred to as the "comparison method", and that of using only one sample with the corresponding system delay times will be referred to as the "single sample technique".

Since the major objective of the experiment was to determine the longitudinal velocity as a function of temperature, it was necessary to know the heating rate of the samples. This was a very important consideration, since in order to measure the true velocity-temperature dependence it was necessary that all temperature gradients vanished along the path of the acoustic beam. With this in mind, a study of the temperature-time dependence of the samples

was conducted to determine the time required to reach temperature equilibrium in the sample. The detailed results are presented in Appendix I, but a few words about the temperature measurements will be given here.

Sample temperatures were determined by reading the bath or oven temperatures to the nearest degree by means of a mercury thermometer or chromel-alumel thermocouple, respectively. The agreement between the two methods of temperature measurement was found to be within 1°C for the reported temperature range. The results of the work shown in Appendix I indicated that approximately one hour was necessary before the sample reached thermal equilibrium. The thinner samples were allowed somewhat less time for the temperature to stabilize, but in no case was less than one half hour allotted for temperature stabilization. With these precautions taken, it is estimated that the temperature of the sample was uniform to within 1°C and to within 1°C of the desired environment.

The ultrasonic pulse generating equipment is an Arenberg* pulsed oscillator which generates pulses a few microseconds long with a carrier frequency in the low megacycle range. The attenuators indicated in figure 3 are also made by Arenberg and are designed to give from 1 to 122 db of attenuation in 1 db increments. Their main use is to prevent overloading of the oscilloscope for constant input signals and to allow relative attenuation measurements to be made. The time-mark generator** produces 1 microsecond markers and is calibrated to provide an error of less than one part per million. The oscilloscope used for all measurements is a well-adjusted dual beam oscilloscope with two type CA dual trace plug-in units.# The Arenberg pulse oscillator was rated for an output of 600 volts, peak-to-peak, so that most measurements were possible without the use of additional amplifiers. When additional amplification was necessary, the amplifier was inserted on the receiving branch between the attenuator and the receiving transducer.

In many of the pulse methods of measuring ultrasonic velocities which have been reported in the literature, the received pulses are rectified and the pulse

---

*Arenberg Ultrasonic Laboratory, Model PG-650C, Boston, Massachusetts.

**Hickok Model 1817.

#Tektronic Type 555.

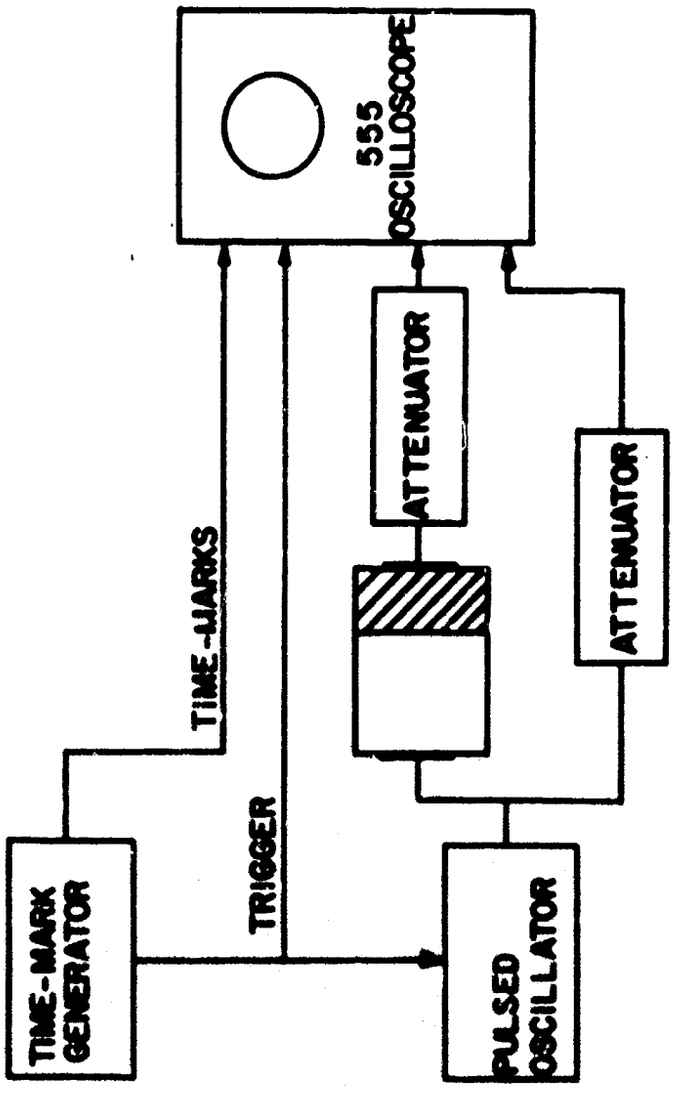

Figure 3. Block Diagram of Measuring Circuit

envelope observed. Eros and Reitz (Ref. 3) have described a single-transducer method based on the observation of the unrectified pulses. This was the practice used in the present work. In making velocity determinations by such a timing method it is necessary to have, on both the transmitted and received pulses, reference points between which the elapsed time can be measured. Therefore, the unrectified pulses were observed in their entirety on the oscilloscope, so that the time could be measured from one particular oscillation of the transmitted pulse to the corresponding oscillation of the received pulse. During the course of this investigation, several different time-measuring techniques were used, and a method was developed which gave the best reproducibility and reliability and for which most of the data are reported.

In the resulting technique, ultrasonic pulses approximately 3 μ sec in duration with a carrier frequency in the low megacycle range were used to measure velocities. The received and transmitted signals were delayed on the oscilloscope by a calibrated delay sweep potentiometer in order to identify two corresponding peaks near the middle of the respective pulses as references. The transit time was then determined by counting and extrapolating the number of time marks between the two reference peaks. Figure 4 illustrates the method.

The illustration shows three hypothetical oscilloscope traces with a fixed time relationship to each other. They represent, from top to bottom, the transmitted pulse, the received pulse, and a series of 1 μ sec time marks. The desired time interval, t, is that between the 4th positive peaks of the transmitted and received pulses. This time is obtained by taking readings of the potentiometer corresponding to the six events marked p_1 through p_6 and calculating the elapsed time by assuming that the oscilloscope delay circuit is sufficiently linear over any 1 μ sec interval to permit linear interpolation. With this time measuring technique, successive measurements, using the same acoustic unit, regularly agreed to within $\pm$ 0.004 μ sec, and most measurements agreed even closer. Most of the velocities reported here were determined by this technique.

In certain cases the thicker samples of some of the materials studied caused either high attenuation or excessive distortion of the acoustic waves. When this condition was encountered, the velocity measurement method employed by Nolle and Sieck (Ref. 4), or the single sample method described earlier was used to make velocity determinations using only one thin sample of the material. In the echo method of Nolle, a sample was placed between two transmission blocks

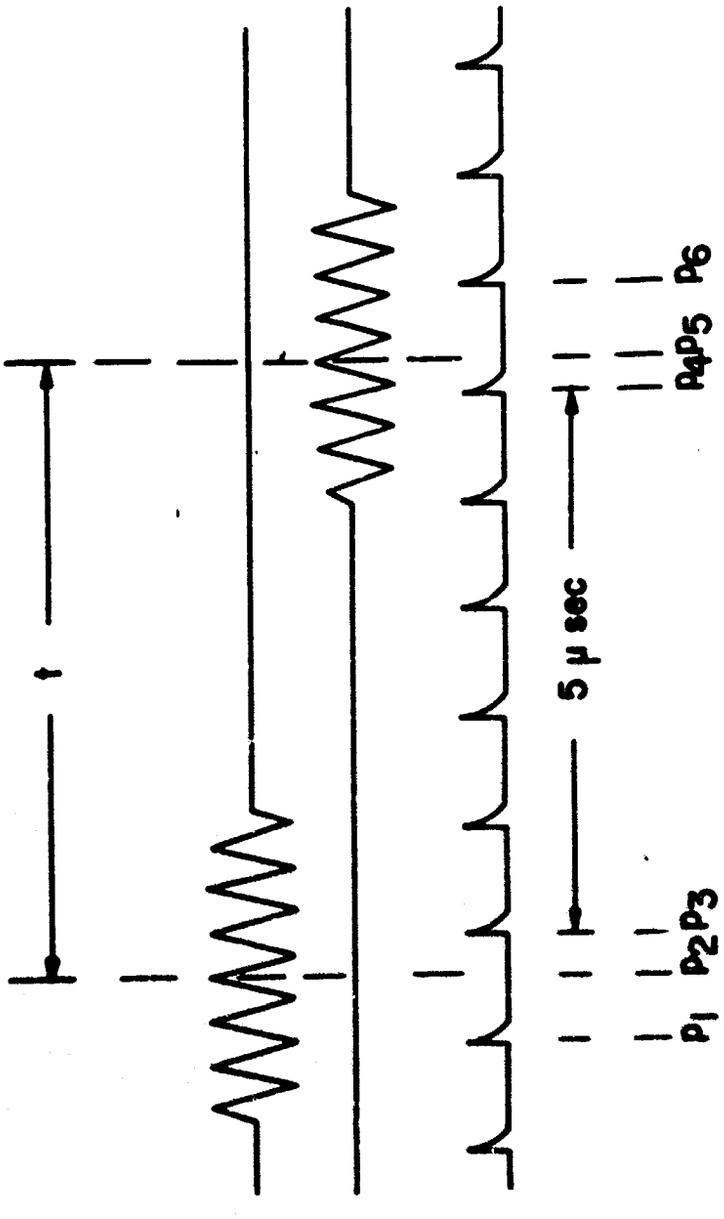

Figure 4. Schematic Representation Illustrating an Interpolation Time-Measuring Technique

with a transducer at each end of the assembly, and the transit time for a pulse to pass from end to end of the assembly was measured. Then the time required for an echo to return from the sample interface to the sending transducer was measured for each of the blocks by transmitting from each of the transducers in turn. The average of the block transmission times was then subtracted from the end-to-end transit time to obtain the transit time through the sample. This method was infrequently used and the results obtained by it were used only for comparison purposes.

SECTION III

EXPERIMENTAL RESULTS

1. Longitudinal Velocity in Common Plastics

The first common plastic studied over a range of temperatures was a nylon.* Temperatures ranged from a low of 25°C to a high of 114°C and the resultant velocity values are shown in figure 5. The frequency used for most of the measurements was 3.0 Mc, although velocity checks at frequencies of 1.5, 4.33 and 10.0 Mc agreed within experimental variation with the values at 3.0 Mc, thus indicating that the material is not dispersive in this frequency range.

Another nylon (Delrin Acetal) was also analyzed as a function of temperature, and the results are plotted in figure 6. The density for this material was 1.43 g/cc, and no apparent dependence with frequency was observed for the longitudinal velocity. In anticipation of velocity-density measurements reported in a later section, it is of interest to point out the differences in velocity for the two nylon materials. The higher density sample exhibits a lower value of longitudinal velocity at room temperature than the lower density material. For materials which are identical in composition and vary only in density characteristics, the effect is generally the opposite, which is shown by the following two materials and by the results to be presented later.

Two different density polyethylene samples were analyzed and the results are shown in figures 7 and 8. It is noted that the velocity at room temperature for the 0.964 g/cc (Fig. 8) sample is greater than that for the 0.916 g/cc sample, agreeing with measurements obtained in velocity-density studies of polyethylene (Ref. 5). The temperature range used here was necessarily limited to about 70°C to avoid melting or distorting the samples.

The longitudinal wave velocity in Plexiglas (polymethylmethacrylate, density 1.19 g/cc) is plotted in figure 9. As indicated in the previous graphs, similar velocities are obtained at various frequencies studied so that, again, dispersion is not evident, within the experimental errors present.

The last common plastic investigated was Teflon (density 2.19 g/cc). For this material the temperature range was extended to below room temperature in

---

*Poly-Penco Nylon (density 1.15 g/cc)

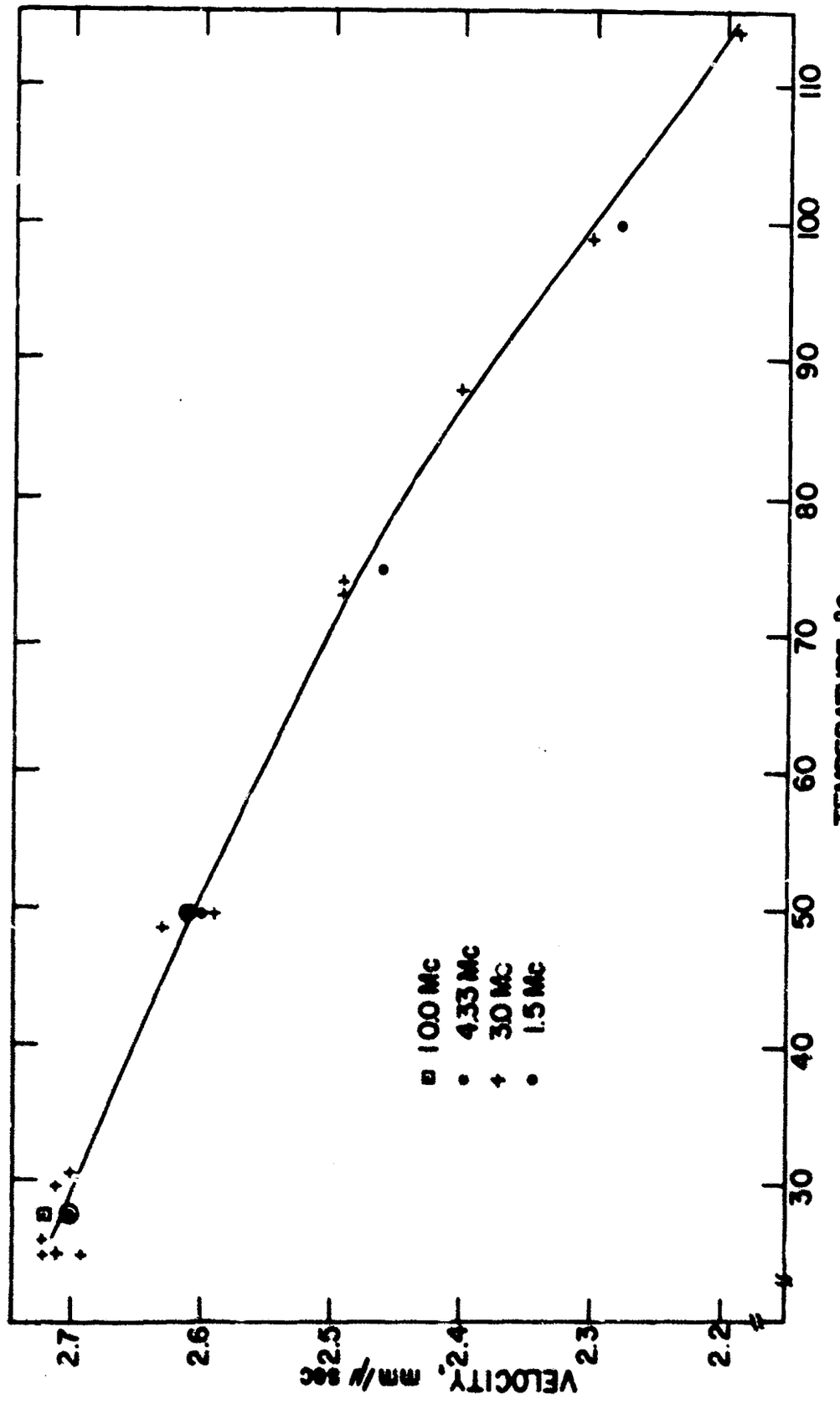

Figure 5. Longitudinal Wave Velocity vs Temperature in Poly Penco Nylon (density 1.15 g/cc)

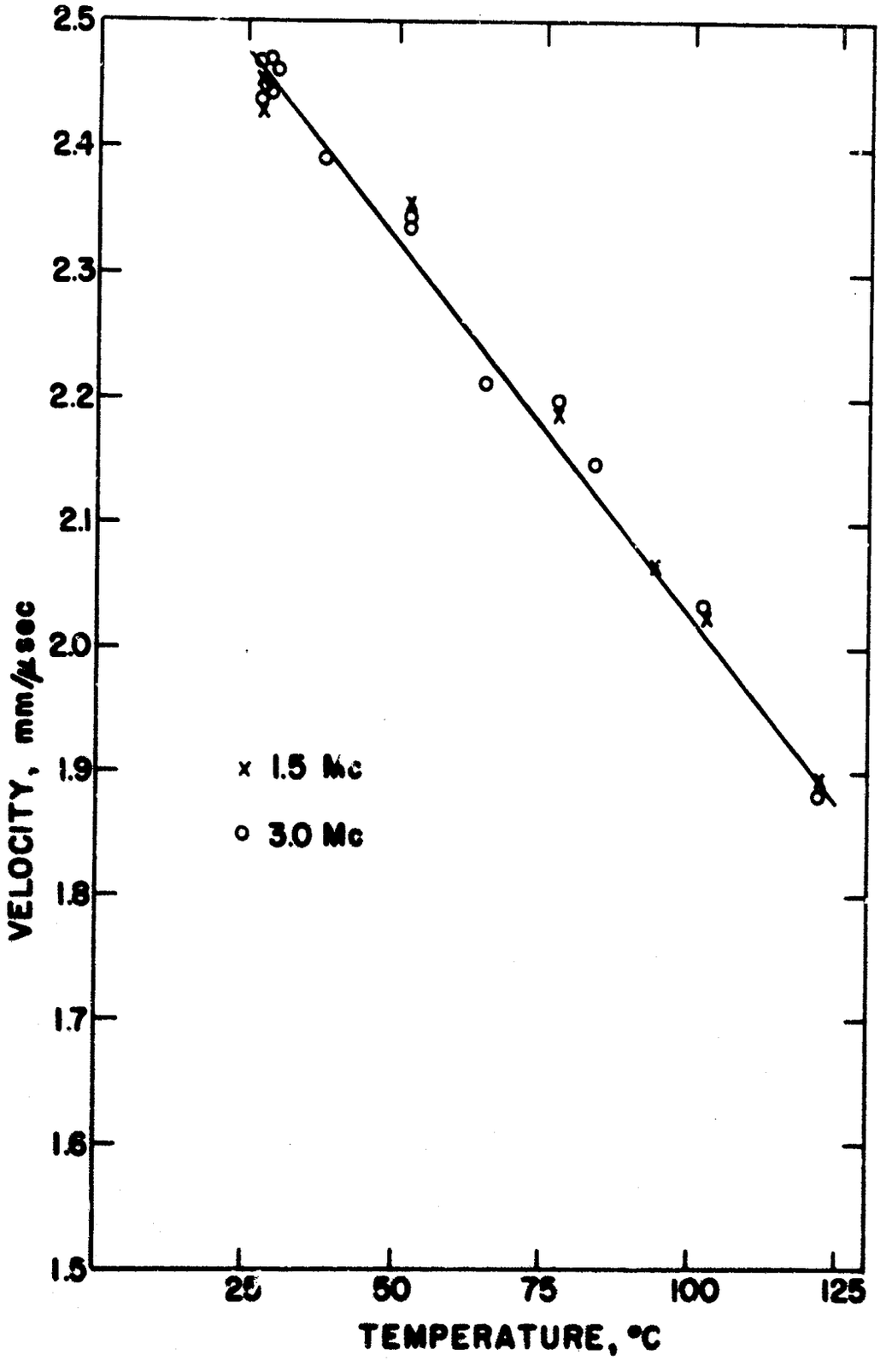

Figure 6. Longitudinal Wave Velocity vs Temperature in Delrin Acetal Nylon (density 1.43 g/cc)

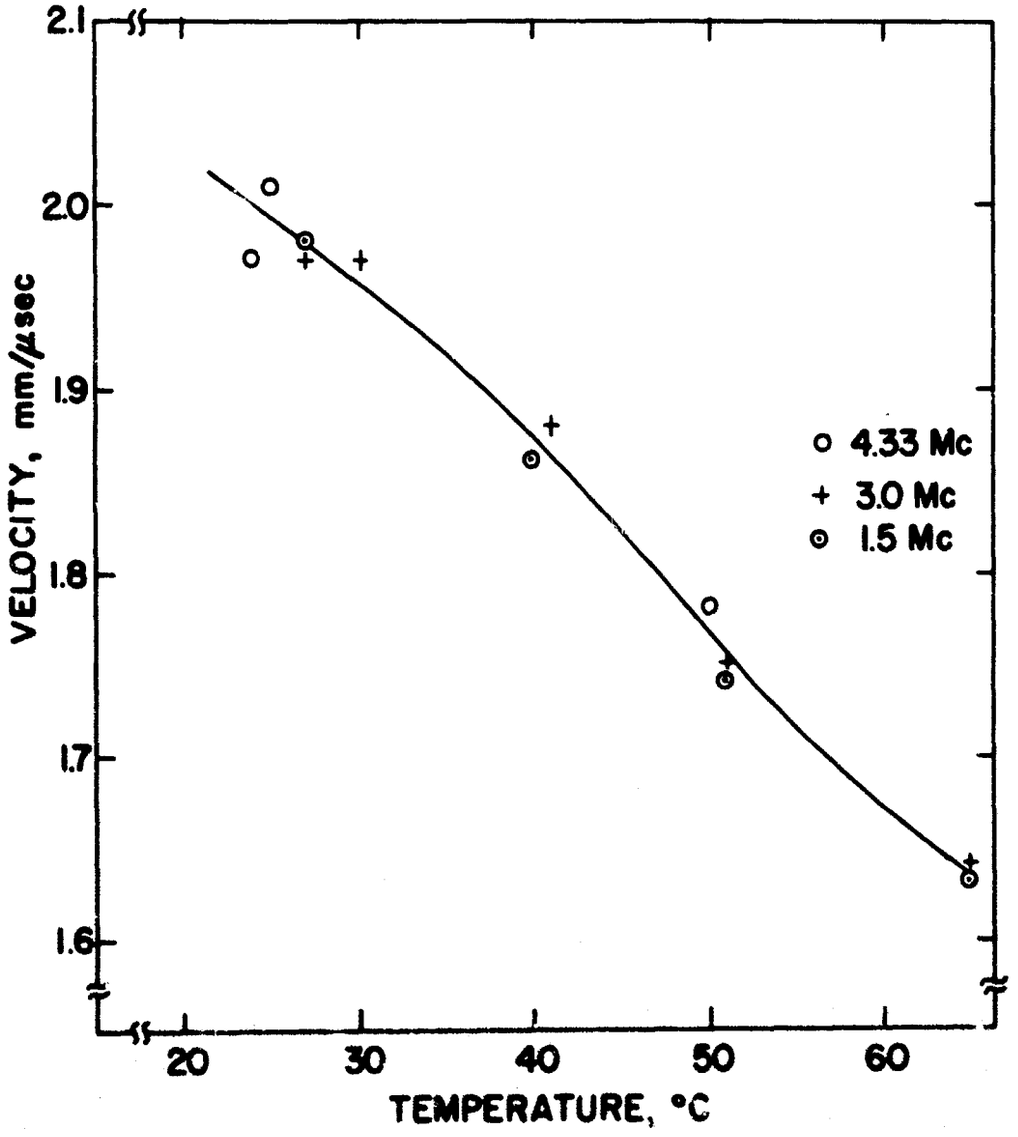

Figure 7. Longitudinal Wave Velocity vs Temperature in Low Density Polyethylene (density 0.916 g/cc)

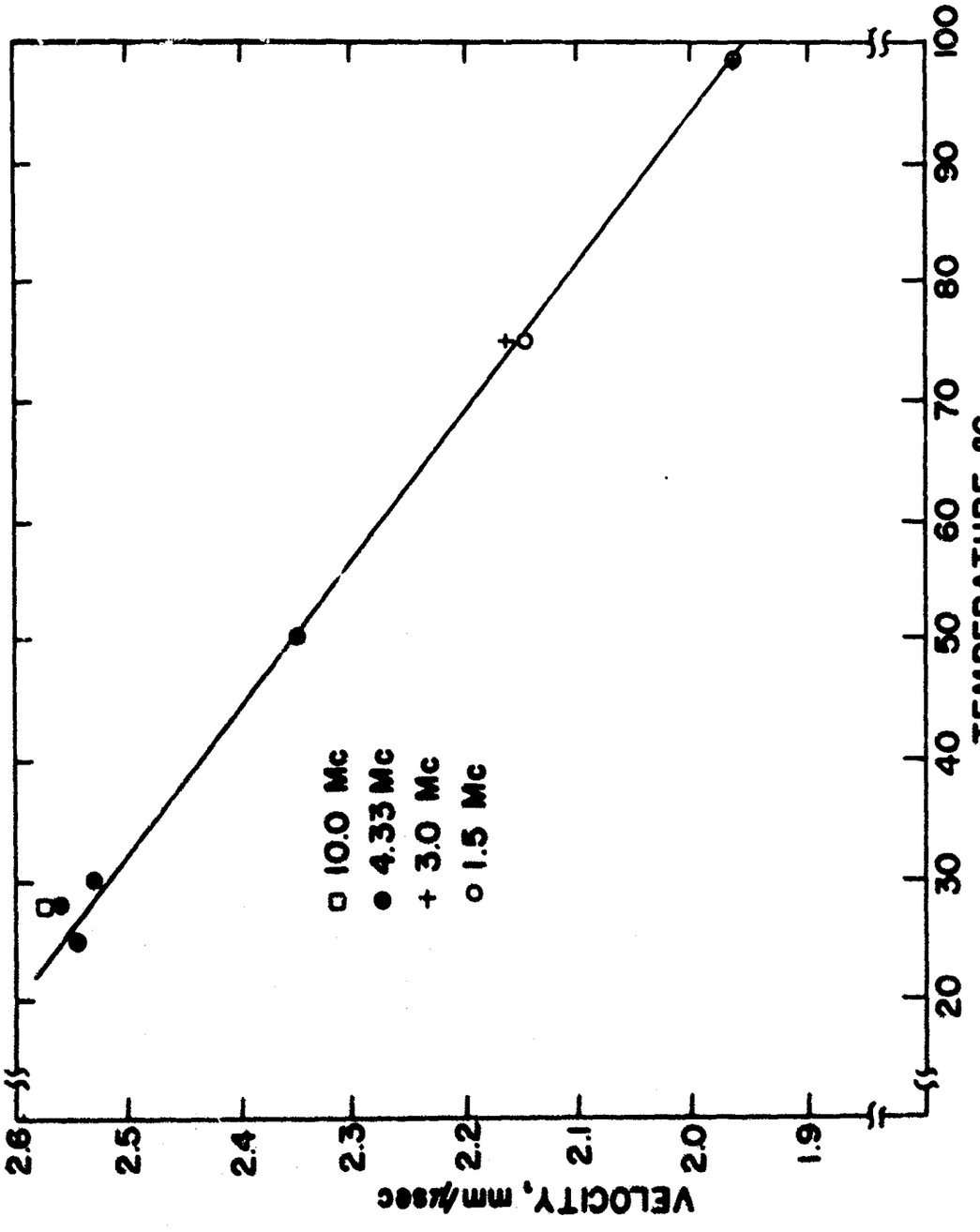

Figure 8. Longitudinal Wave Velocity vs Temperature in High Density Polyethylene (density 0.964 g/cc)

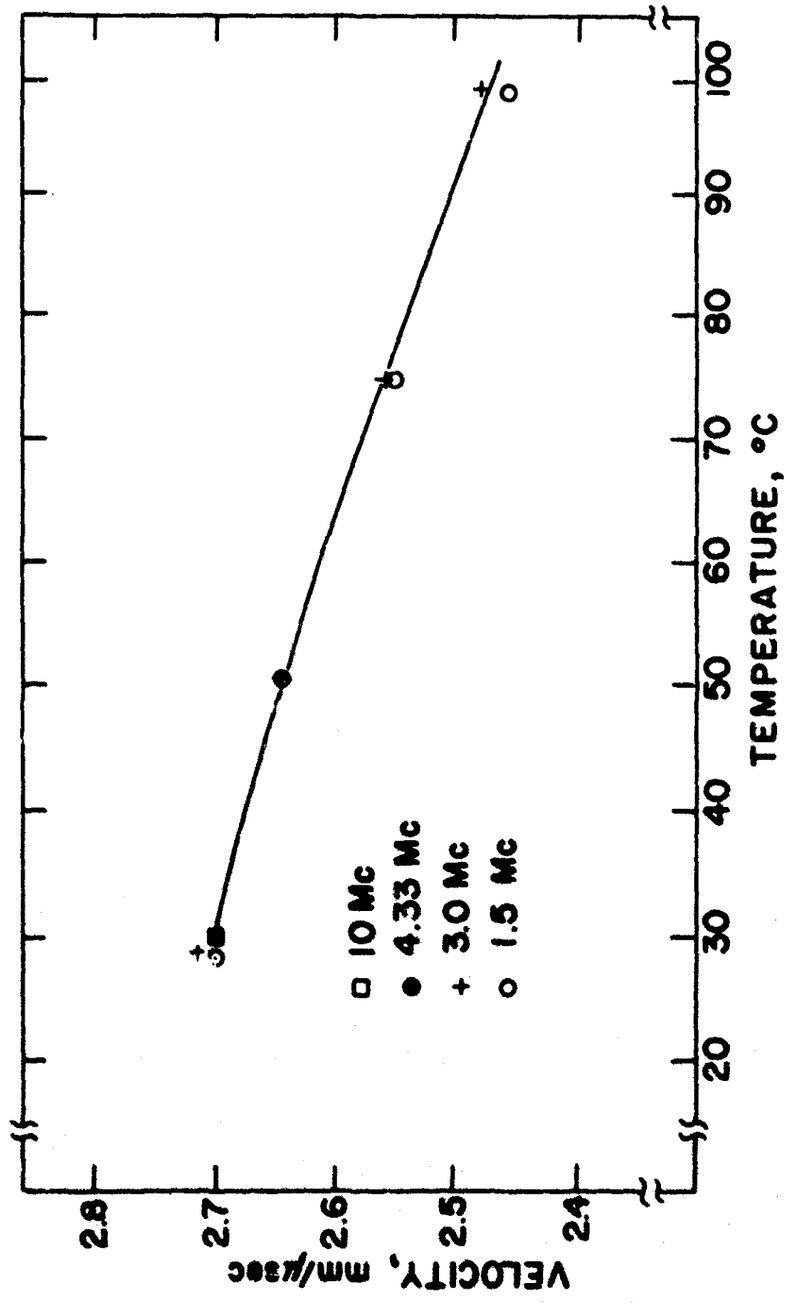

Figure 9. Longitudinal Wave Velocity vs Temperature in Plexiglass (polymethylmethacrylate, density 1.19 g/cc)

order to obtain a more accurate picture of the shape of the velocity curve in the range between 20 and 30°C. As can be seen in figure 10, there is a fairly sharp inflection in the velocity curve in this region. It is noted that Teflon exhibits a well known second order transition in the molecular structure at a temperature of 20°C (Ref. 6), so that it is to be expected that a change in the mechanical properties (and consequently the velocity) would be observed as the temperature is varied over the transition region. The velocities measured in Teflon appear to be somewhat more frequency sensitive than for the previously listed materials. However, the difference is not sufficient to justify separate plots, and all measurements for the three frequencies used are plotted on the same graph.

Table I summarizes the longitudinal velocities at room temperature for the various plastics discussed in this section.

Table I

LONGITUDINAL VELOCITY IN COMMON PLASTICS AT 25°C

Material	Density g/cc	Frequency range Mc	Velocity mm/μsec
Poly-Penco nylon	1.15	1.5-10.0	2.72
Delrin Acetal nylon	1.43	1.5-3.0	2.48
Polyethylene			
low density	0.916	1.5-4.33	1.99
high density	0.964	1.5-10.0	2.55
Plexiglass	1.19	1.5-10.0	2.73
Teflon	2.19	1.5-4.33	1.40

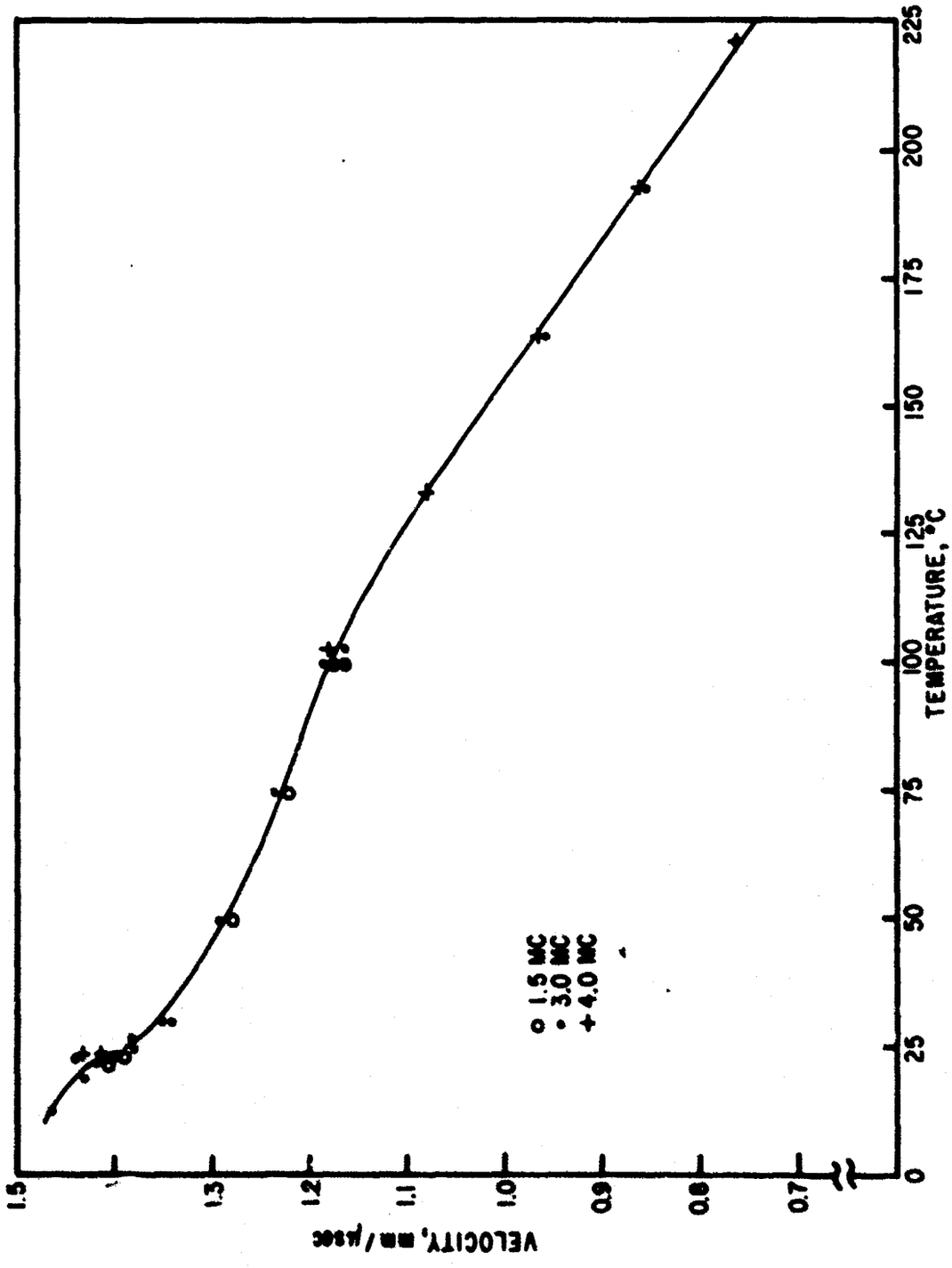

Figure 10. Longitudinal Wave Velocity vs Temperature in Teflon (density 2.19 g/cc)

2. Longitudinal Velocity in Composite Nose-Cone Materials

Another group of materials studied consists of typical nose-cone materials which are generally either composites or laminates. In some of these reentry vehicle materials, the measurement of ultrasonic velocities is very difficult due to excessive attenuation and distortion of the signal and the results obtained should be viewed with caution as far as absolute velocity values are concerned. In the graphs that follow, most of the data are fairly complete and self-consistent, but the cases where the results are suspect will be pointed out. These situations usually result from the fact that in many of the composite materials sampling errors arise because of significant material inhomogeneities and nonuniformities. In some of the layered materials it is often difficult to assign a particular direction to the lamination layers, or to reproduce a particular orientation, so that sampling errors again become important.

The material represented in figure 11 is Castable 124 (C 124), a light-yellow, clear material with a density of 1.23 g/cc. As can be seen, the data are insensitive to the different frequencies utilized and are fairly consistent so that appreciable dispersion is not present in this material for the frequency range of 1.5 - 3.0 Mc. The velocity curve for this material was not corrected for thermal expansion because of the difficulty in obtaining reliable expansion data. When exposed to temperatures higher than $\sim$ 75°C, the specimen showed significant dimensional instabilities when remeasured at room temperature. These dimensional changes, which were as high as 3 percent for exposure to 225°C, more than offset any error resulting from not applying a thermal expansion correction.

The next two graphs show the velocities measured in two similar materials, Avcoat I (yellow, density 1.10 g/cc) and Avcoat 19 (green, density 1.07 g/cc). Attenuation in these samples increased greatly at elevated temperatures so that measurements could be made only by using thinner samples and/or lower frequencies. The velocity curve in Avcoat 19 (Fig. 12) was checked by three different techniques. Measurements were first made at room temperature by measuring transit times through two different thicknesses of material (comparison method), but the method did not work well at higher temperatures because of excessive attenuation through the thicker (19 mm) sample. Therefore, the echo technique described in Section II was used by placing the thinner sample (3.5 mm) between two different aluminum transmission blocks. This method gave good agreement

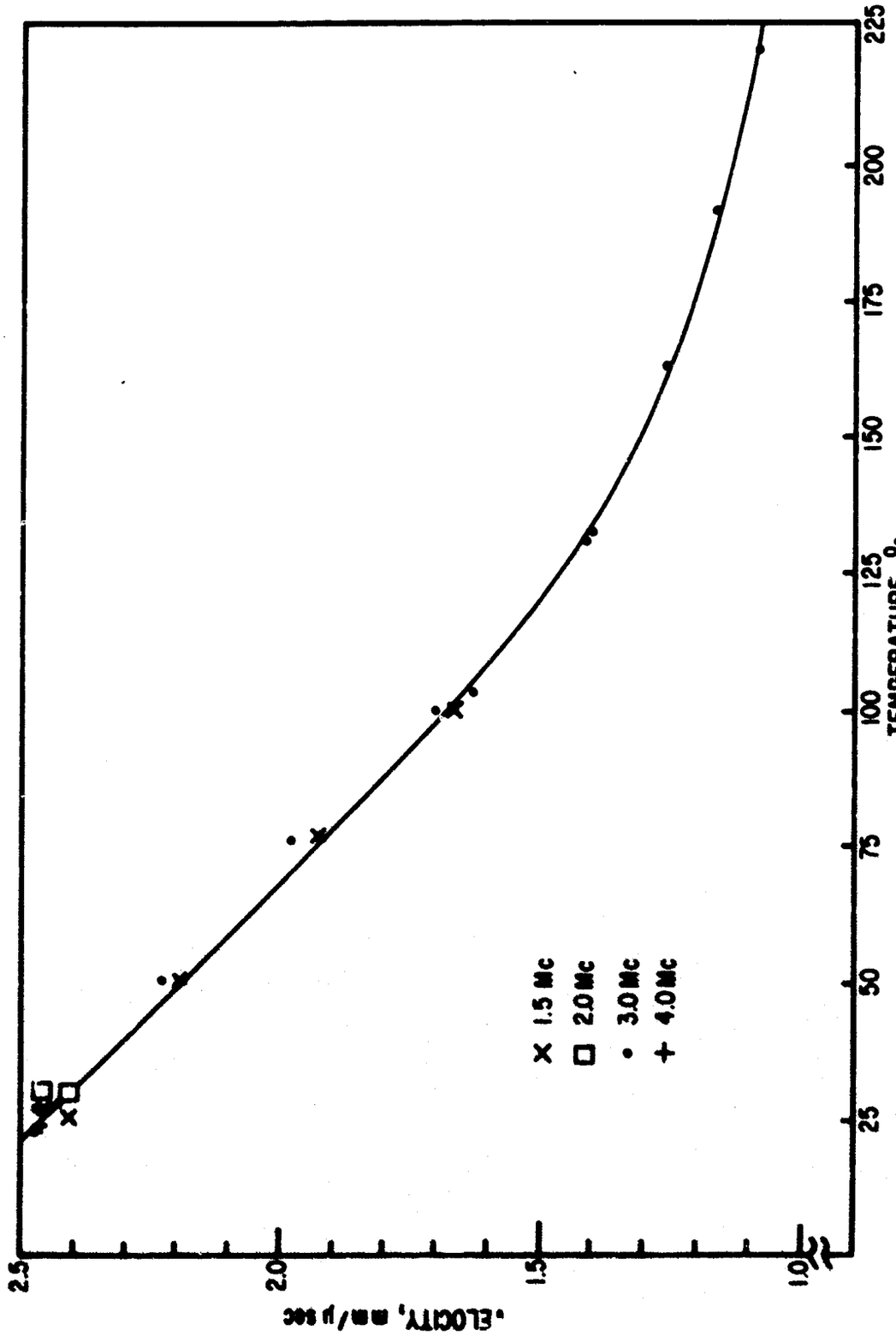

Figure 11. Longitudinal Wave Velocity vs Temperature in Castable 124 (density 1.23 g/cc)

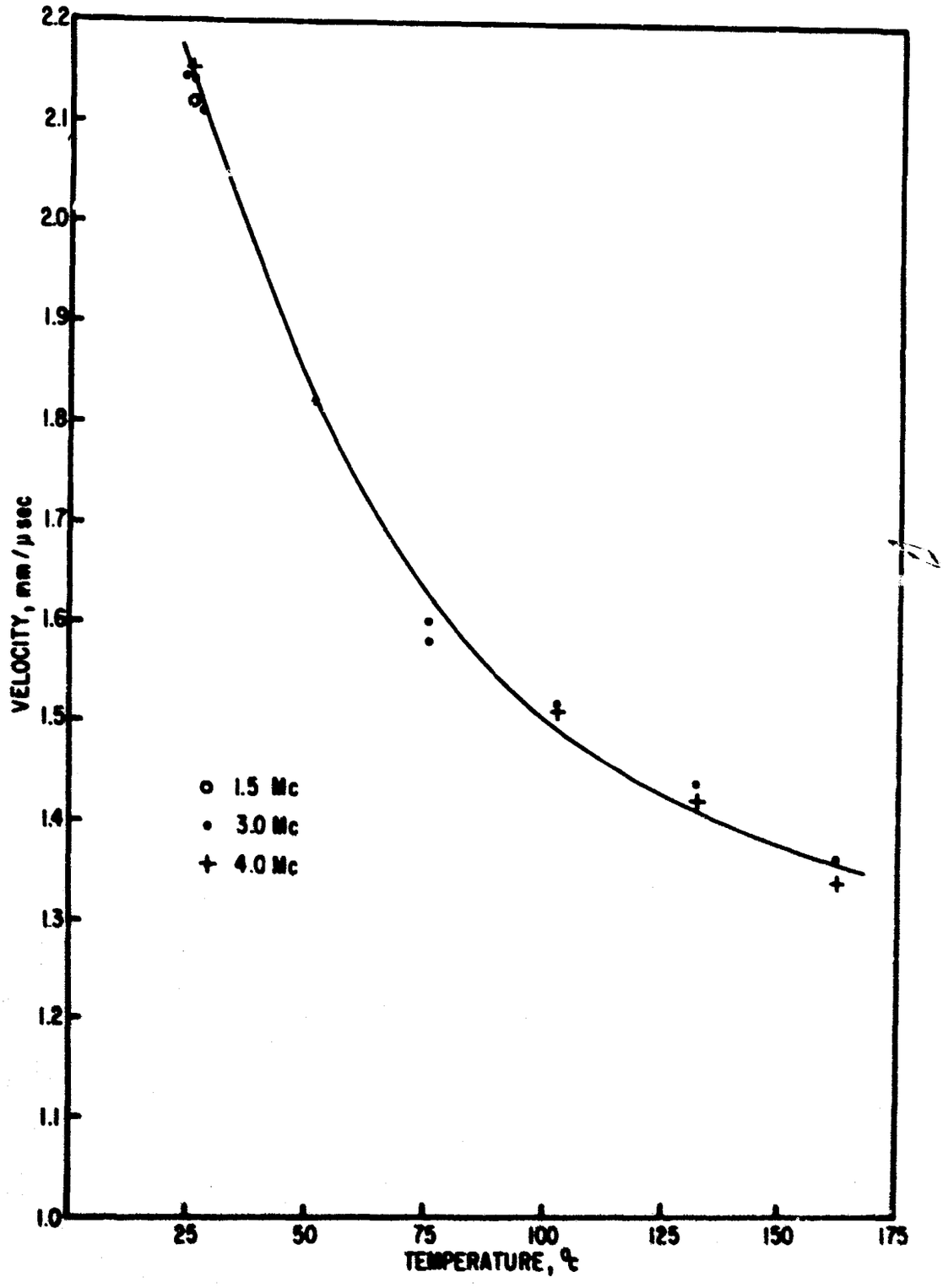

Figure 12. Longitudinal Wave Velocity vs Temperature in Avcoat 19 (density 1.07 g/cc)

with the values previously determined at room temperature for Avcoat 19 and was therefore used for the measurements at 50 and 75°C. To check the velocity values obtained by the echo technique, and to extend the temperature measurements, the single sample method was used to obtain room and high temperature values. At high temperatures the specimen became soft and somewhat distorted even under the approximately 1/3 psi pressure from the bonding clamp. However, dimension measurements on the sample at room temperature after exposure to 160°C showed a thickness decrease of only 0.4%, so that the high temperature values should be fairly insensitive to dimensional instabilities. The faces of the sample which were not protected by the buffer rods darkened significantly at 160°C, but the effect was only observed at the edges. A signal could not be reliably detected at higher temperatures in this material, so the velocity data are limited to this temperature.

Avcoat I (Fig. 13) exhibited behavior similar to that of Avcoat 19 at higher temperature in that the material became somewhat soft, and the signal was greatly attenuated. However, measurements were possible to ∿ 250°C using the single sample method, which checked reasonably well with the extrapolation of the values obtained by the comparison method at lower temperatures.

After exposure to 250°C, the sides of the Avcoat I specimen which were not protected by the oil film and buffer became excessively charred. However this effect was observed only for the exposed sides; the center of the specimen appeared to be unaffected except for some darkening. This material also showed greater dimensional change than did Avcoat 19. After exposure to 250°C, the thickness of the specimen was 2 percent lower than the original value.

Figure 14 shows the temperature dependence of velocity in chopped nylon phenolic (CNP), density 1.68 g/cc. The axis of propagation was approximately perpendicular to the reinforcing material (c-direction). As indicated in the graph, dispersion is not apparent in this frequency range, although the measurements are somewhat limited because the attenuation increased rapidly with frequency.

The velocity through pyrolytic graphite (density 2.19 g/cc) was measured in the a and c directions (parallel and perpendicular to the reinforcing layers, respectively), using the single sample method. As shown in figure 15, there appears to be no velocity dependence upon frequency; however, it is noted that there is about a 2 percent variation among the data points due to the small thickness of the sample available. The material contained alternate thin

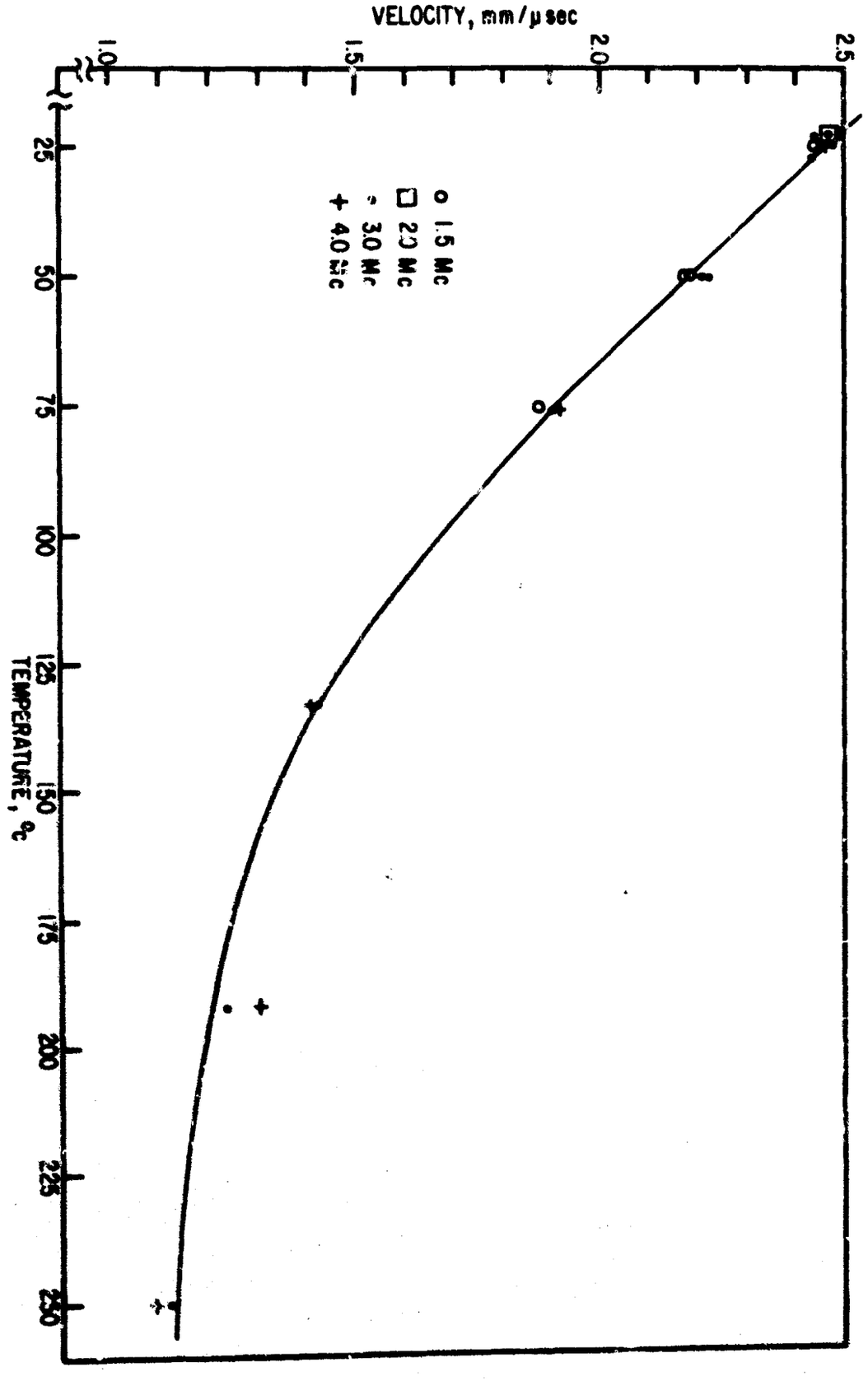

Figure 13. Longitudinal Wave Velocity vs Temperature in Avcoat I (density 1.10 g/cc)

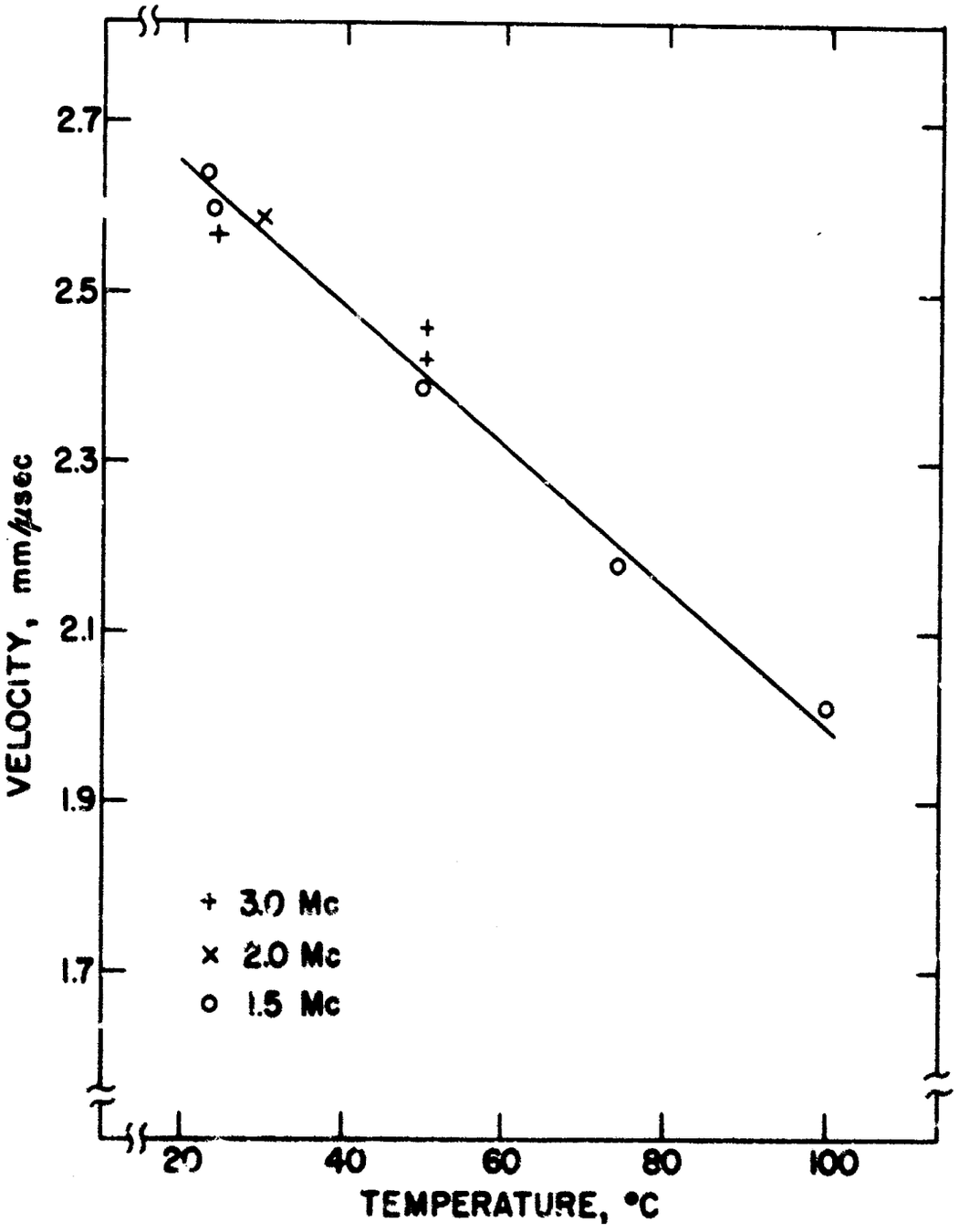

Figure 14. Longitudinal Wave Velocity vs Temperature in Chopped Nylon Phenolic (density 1.68 g/cc)

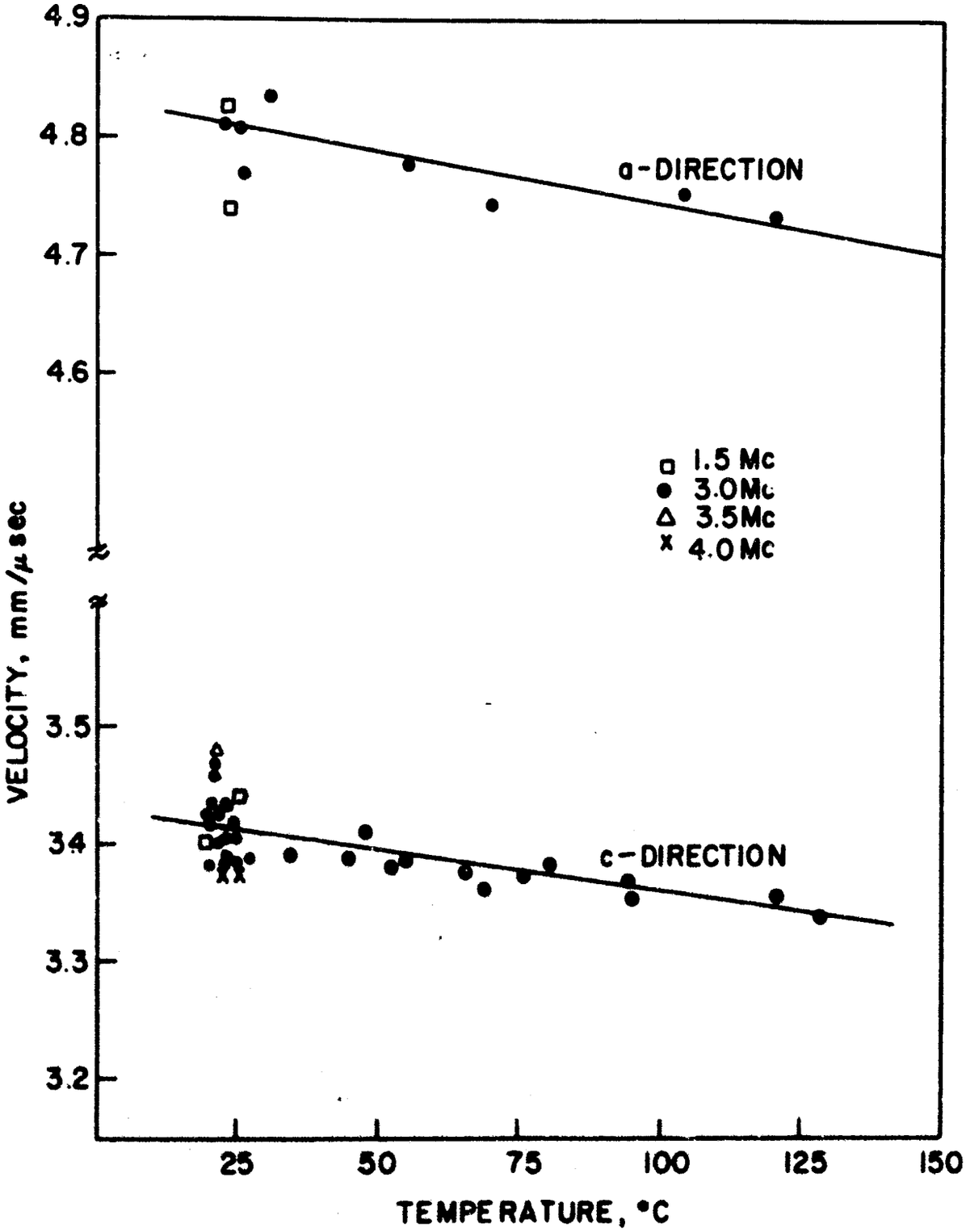

Figure 15. Longitudinal Wave Velocity vs Temperature in Pyrolytic Graphite (density 2.19 g/cc)

(0.05 - 0.10 mm) and thick (0.2-0.6 mm) layers so that the highest frequency used here corresponded to a minimum wavelength slightly greater than the maximum layer thickness. For values of wavelength much less than the layer spacing (corresponding to frequencies of 5.0 and 10.0 Mc) the output waveform was distorted to the point that reliable velocity information could not be obtained. The curves shown in figure 15 are corrected for thermal expansion of the sample using average values of the linear coefficients of thermal expansion for the two orientations.

Preliminary measurements on several laminated materials definitely established the conclusion that the velocity of propagation is a sensitive function of the angle of propagation through the layers. Three materials were consequently studied in detail with the specific aim of determining the angular dependence of velocity. For these measurements the single sample technique was used rather than the comparison method because of the difficulty in obtaining two samples with the same lamination angle. Wave velocities in these materials were studied as a function of lamination angle at several temperatures between 25° and 125°C.

The range of frequencies previously considered was chosen on the basis that the period of the waves corresponded approximately to pulse lengths of interest. The variation of frequency with layer thickness discussed above indicated negligible frequency dependence of velocity, within experimental variation, for the materials studied and the frequency range covered. For practically all the above materials the wavelength was much larger than the layer spacing at 3.0 Mc. This situation is true for the following three materials also, and all measurements are reported for a frequency of 3.0 Mc.

Figures 16 and 17 show the angular dependence of the longitudinal velocity in General Electric Phenolic Fiber Glass (PFG, density of 1.91 g/cc). The majority of PFG angular measurements were made at 30°C, although measurements at angles of 1°, 23°, 44°, and 89° were also made at temperatures of 50°C, 75°C, and 75°C. These measurements show the consistent shape of the velocity vs lamination angle curve as the temperature is varied.

The change in the velocity as a function of lamination angle in Phenolic Carbon (PC, density 1.48 g/cc) shown in figures 18 and 19 is less than the change observed in PFG. For this reason there is more uncertainty in drawing a unique curve to fit the data points. The chosen curve, however, appears to fit all data points better than any other simple curve.

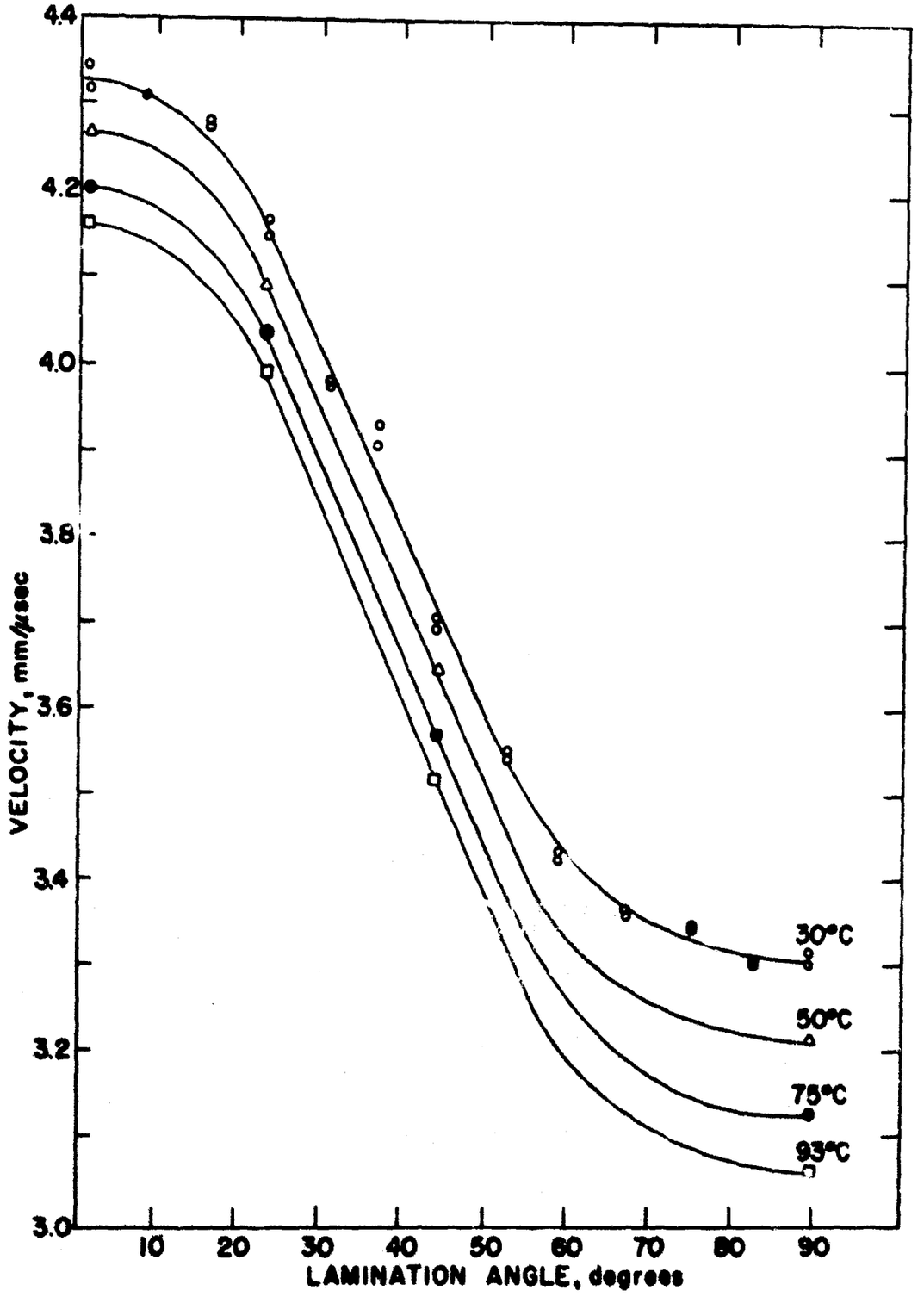

Figure 16. Longitudinal Wave Velocity vs Lamination Angle with Temperature as Parameter in GE Phenolic Fiber Glass (density 1.91 g/cc)

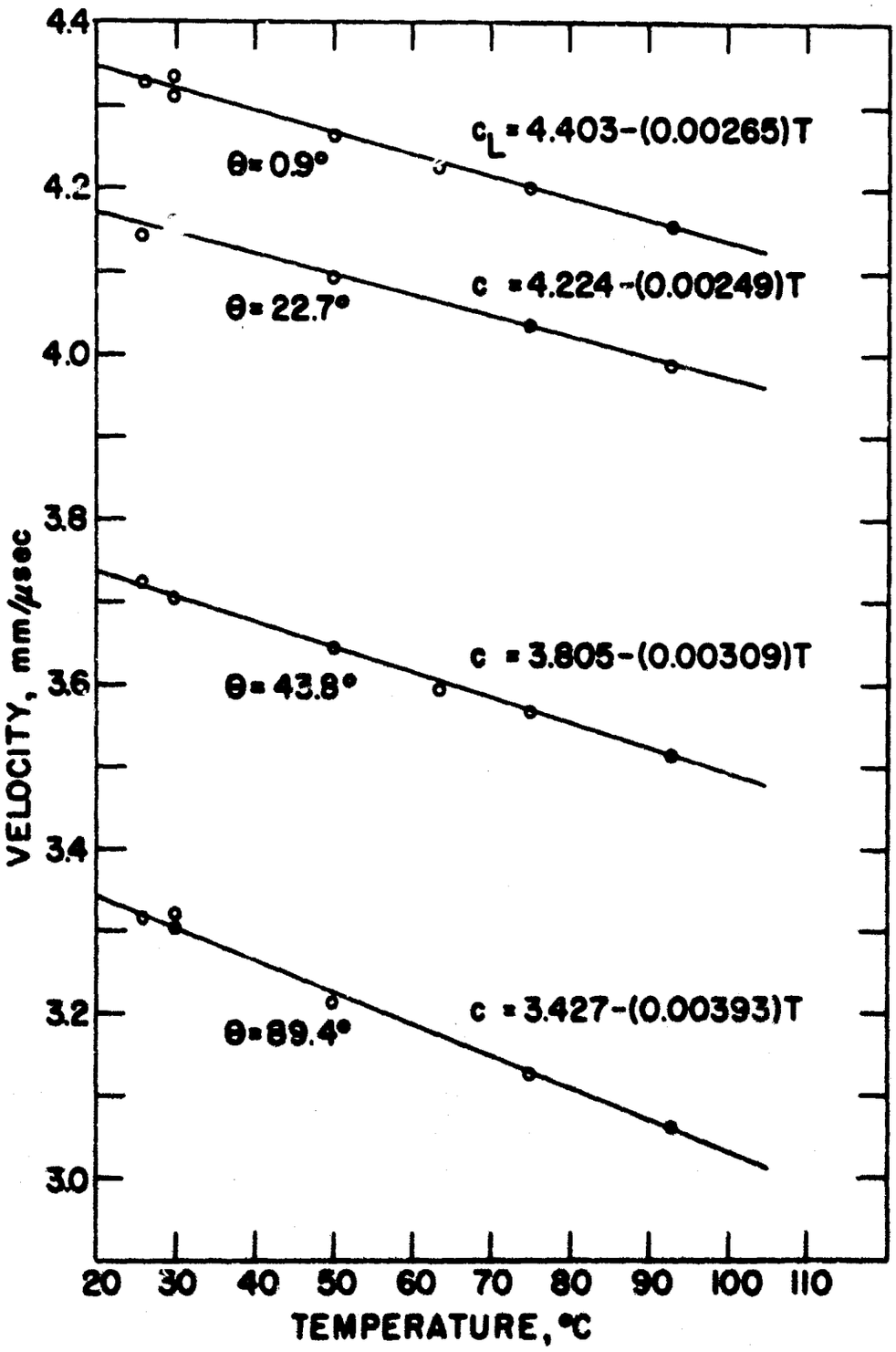

Figure 17. Longitudinal Wave Velocity vs Temperature with Lamination Angle as Parameter in GE Phenolic Fiber Glass

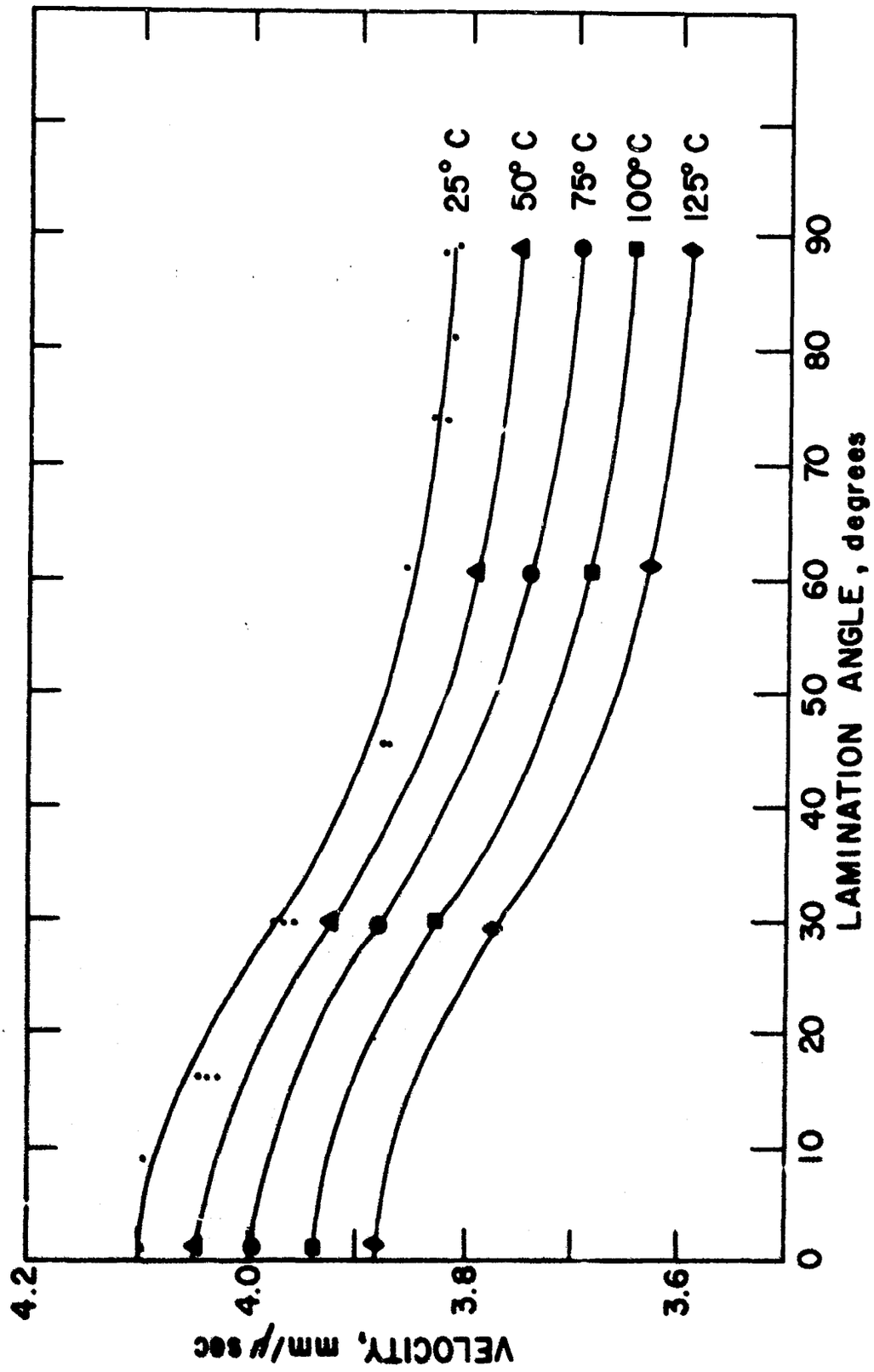

Figure 18. Longitudinal Wave Velocity vs Lamination Angles with Temperature as Parameter in Phenolic Carbon (density 1.48 g/cc)

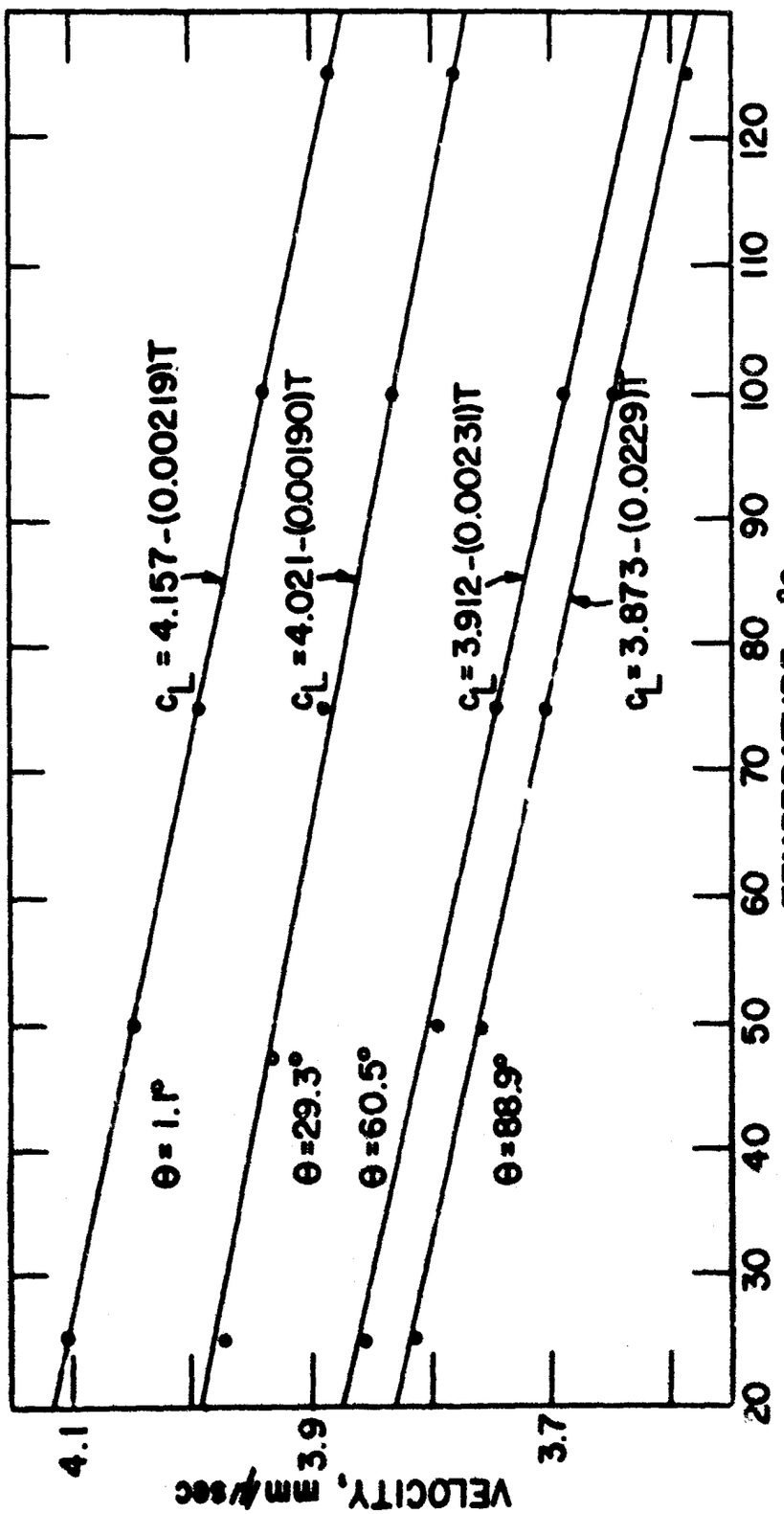

Figure 19. Longitudinal Wave Velocity vs Temperature with Lamination Angle as Parameter in Phenolic Carbon

In Tape Wound Nylon Phenolic (TWNP, density 1.21 g/cc) there is almost no dependence of wave velocity on the lamination angle (figures 20 and 21). In this case a straight line is used to fit the data points in figure 20. However, a curve with the same shape as the PFG and the PC curves, only with less vertical variation, fits the TWNP data equally well.

The similar shapes of the PFG, the PC, and the TWNP velocity vs lamination angle curves led to an attempt to predict these curves theroretically. Horio (Ref. 7) discusses the elastic moduli of layered paper from general considerations of elasticity. With his approach he derived an expression giving the stress to strain ratio (Young's modulus) for an arbitrary direction with respect to the plane layers. He found that the expression thus obtained fitted his experimental data quite well.

Since the wavelength of the ultrasonic waves in the present case is generally much larger than the layer spacing, his approach should be applicable to the present experimental data. At 3.0 Mc the number of complete layers/mm is about 4.5 for PFG, 3.0 for PC and 2.3 for TWPN. Here, a complete layer is considered to be a layer of the fiber glass cloth and a layer of phenolic. The wavelength (defined as $\lambda = \frac{c}{f}$, where c is the velocity and f is the frequency) at normal incidence and at 3.0 Mc for each case is 1.1, 1.25, and 0.9 mm, respectively. Following Horio's approach, the longitudinal wave velocity vs lamination angle curves are given by

$$\frac{1}{c_\theta^2} = \frac{\cos^2\theta}{c_0^2} + \frac{\sin^2\theta}{c_{90}^2} \qquad (2)$$

where θ is the angle between the normal and the plane of the layers, and c_0 and c_{90} are the velocities for parallel and normal angles of incidence, respectively. With equation (2) and a knowledge of the wave velocity at $\theta = 0°$ and 90°, the velocity for any angle of incidence can be estimated to within 2 percent. The curve thus obtained is shown for comparison with the actual curve of PFG in figure 22. The results of this work indicate that equation (2) can be applied to any material, such as pyrolytic graphite, if the wavelength is very much larger than the layer spacing, and if the velocities at angles of 0° and 90° with respect to the lamination layers are known.

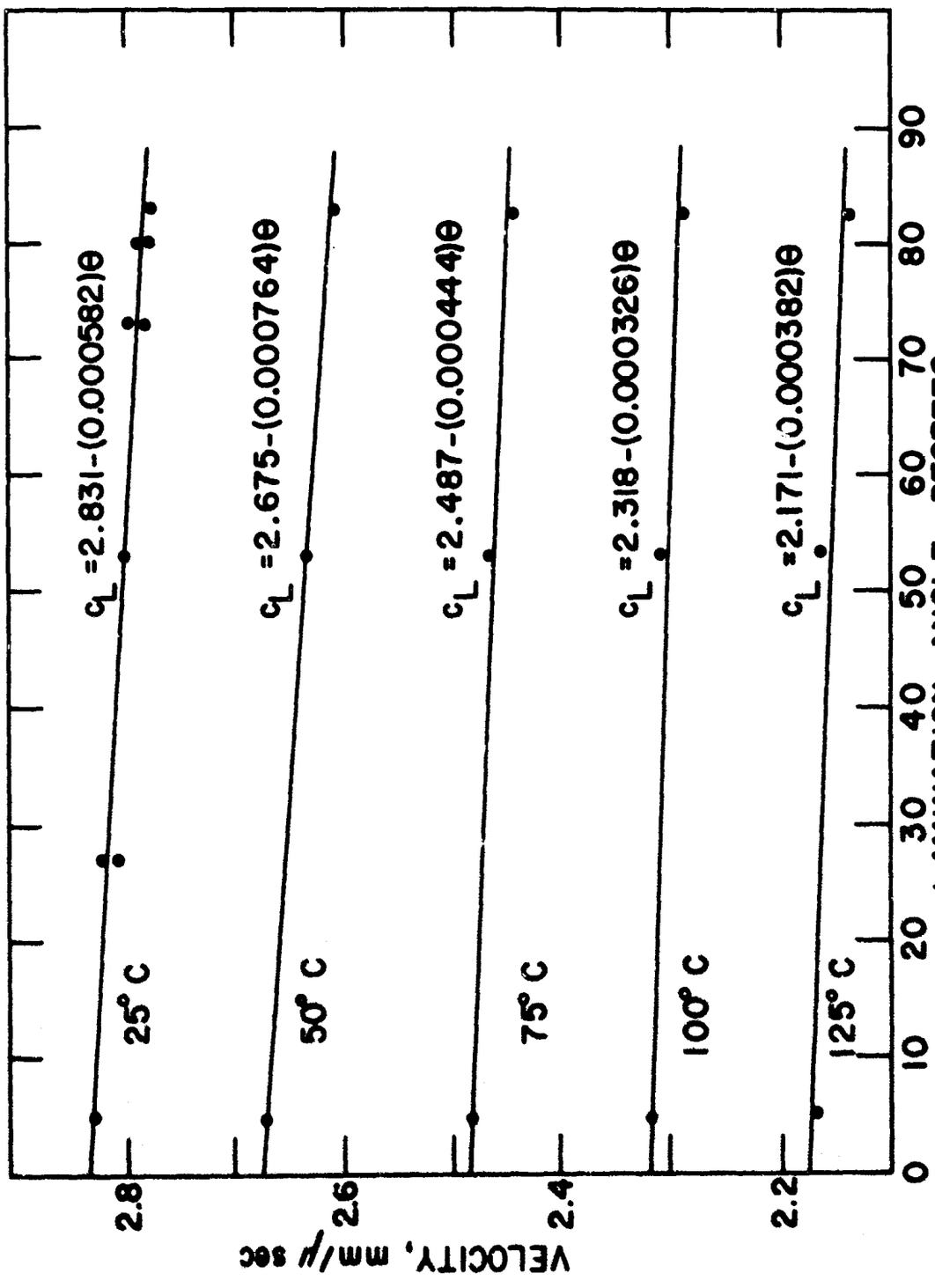

Figure 20. Longitudinal Wave Velocity vs Lamination Angle with Temperature as Parameter in Tape Wound Phenolic Nylon (density 1.21 g/cc)

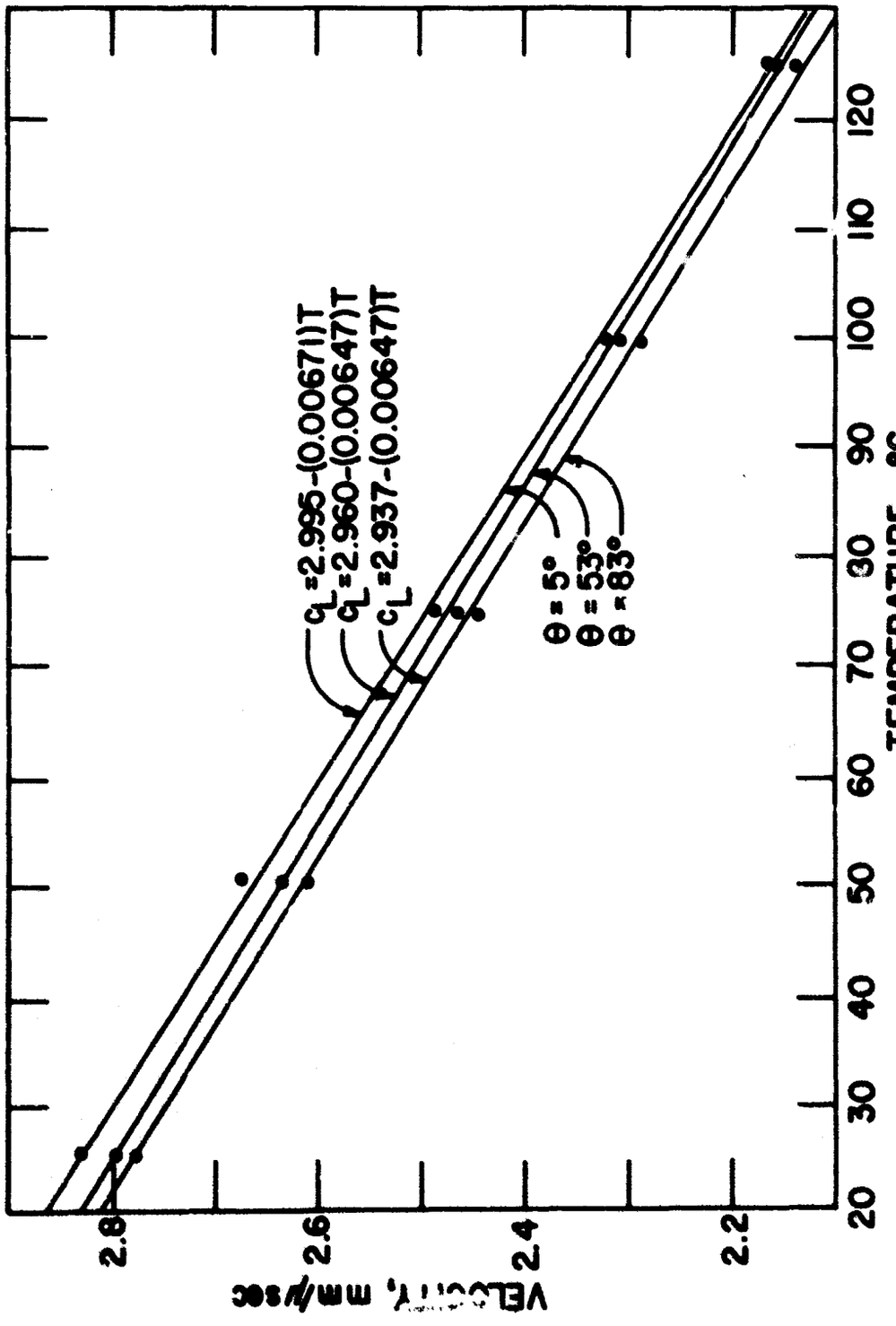

Figure 21. Longitudinal Wave Velocity vs Temperature with Lamination Angle as Parameter in Tape Wound Phenolic Nylon

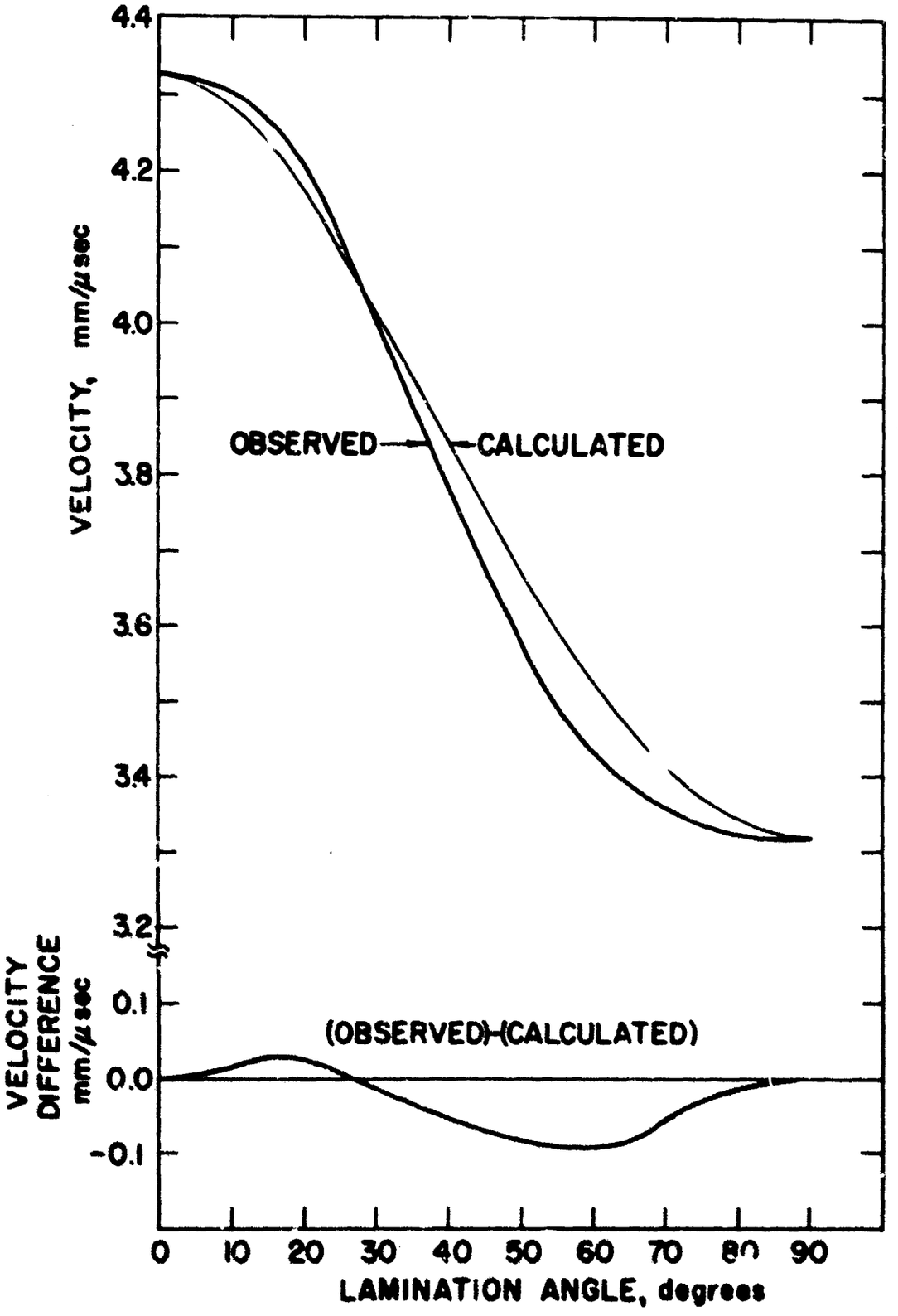

Figure 22. Longitudinal Wave Velocity in Phenolic Fiber Glass and the Difference Between the Observed and Predicted Values

Less complete velocity data were also obtained for a few other layered nose-cose materials. Rather limited information was obtained for two different configurations of AVCO Phenolic Fiber Glass (AVCO PFG).* When the angle of incidence of the waves is perpendicular to the reinforcing layers of glass (Fig. 23, lower curve) it was found that, for frequencies higher than about 1 Mc, the material apparently acts as a low-pass filter. When frequencies higher than this are transmitted into the sample, the received signal is observed to have a lower frequency than that of the input. At a frequency of 1 Mc or below, the transmitted and received signals are identical in frequency. However, the cutoff frequency of 1.0 Mc is not sharp, since the output frequency for 3.0 Mc input varies from 1.2 to 2.2 Mc, depending on the particular sample. The room temperature points shown for the lower curve (c-direction) in figure 23 were obtained for several different samples. It was found that even though the output frequencies at 3.0 and 4.0 Mc are significantly lower than the input, the velocity computed by the single sample technique agreed to within 1 percent of that computed by the comparison method when the first peaks were used as references. For this reason the temperature measurements were extended by the single sample method, because of excessive attenuation of the acoustic signals at high temperature.

The top curve shown in figure 23 represents the velocity in the a-direction through AVCO PFG. As for the lower curve, room temperature points were obtained by using several different samples, and the temperature measurements were extended by using one thin sample. For this orientation, the output frequency was slightly lower than the input, ranging from 2.0 to 2.5 Mc for 3.0 Mc input frequencies. For both orientations the reduced frequency effect appeared to be geometric, since the thinner samples always gave higher output frequencies for a given input than did the thicker samples. For this material the number of complete layers/mm is ~4, so that a frequency of 4.0 Mc corresponds to a wavelength of approximately three times a complete layer spacing.

Numerous efforts to take meaningful velocity measurements in Oblique Tape Wound Refrasil (OTWR)** were somewhat unsuccessful in that very erratic results were obtained. As in the case of the other anisotropic and inhomogeneous

---

*Density 1.71 g/cc

**Density 1.54 g/cc

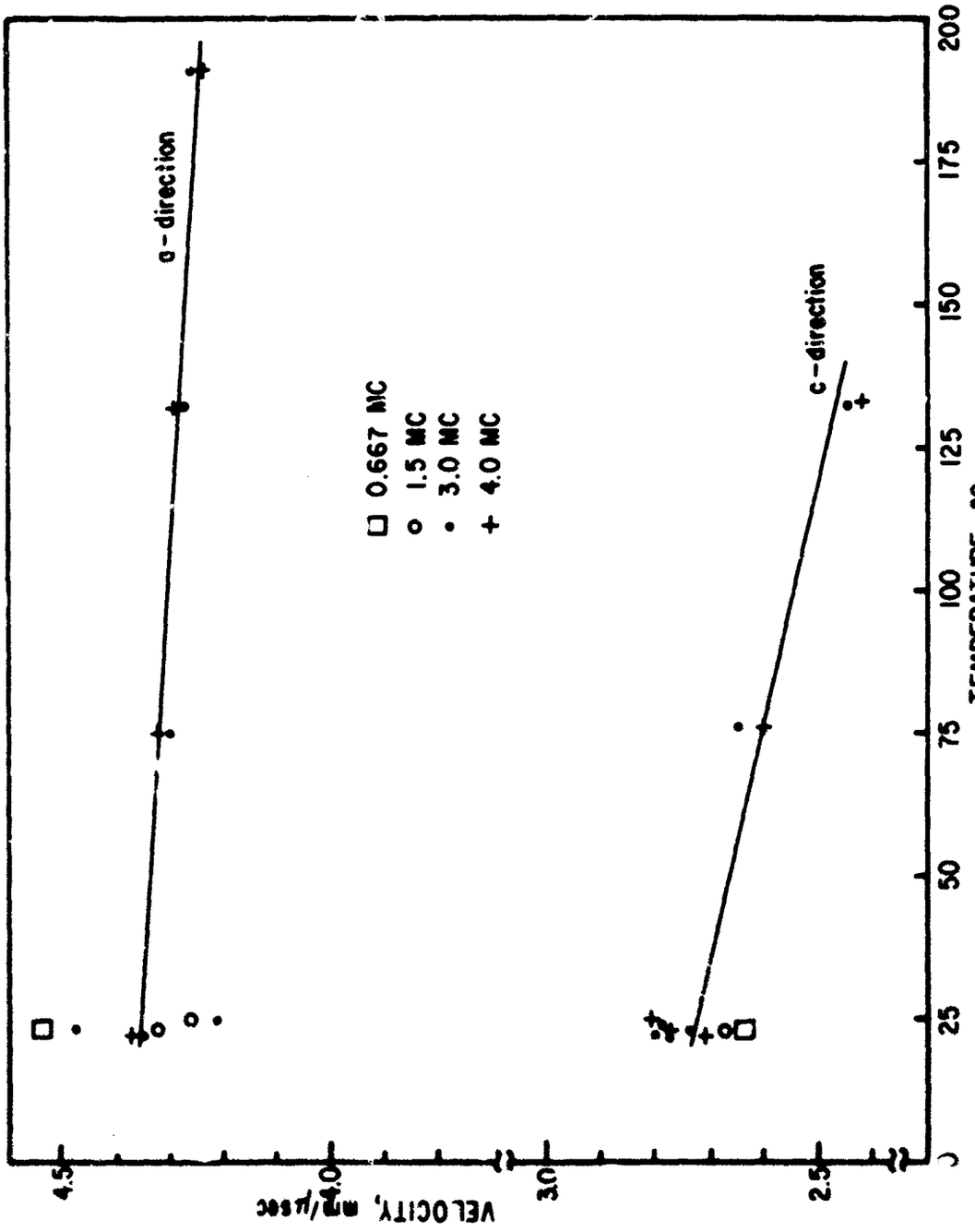

Figure 23. Longitudinal Wave Velocity vs Temperature in AVCO Fiber Glass (density 1.71 g/cc)

materials, different samples were cut so as to study the effect of the angle of incidence on the velocity of propagation. Since the layers in OTWR are very irregular (not planar), no single direction could properly be described as either perpendicular to, or parallel with, the layers. Figure 24 shows the curves representing the velocities in the perpendicular and parallel directions. It is interesting to note the fairly large difference in the velocity between 0.667 and 4.0 Mc for the upper curve. The situation is similar for the bottom curve, with velocities for 0.667 and 1.5 Mc waves being 2.003 and 2.036 mm/μsec, respectively. To check the consistency of this effect, the velocity was measured at another orientation (~45°) of OTWR, and the same effect was observed (the velocity at 1.5 Mc is 2.732 mm/μsec and at 3.0 Mc it is 2.890 mm/μsec). These effects suggest that this range of wavelengths must be comparable to the layer spacings. It was found that the spacing is 1 mm in OTWR, and in the frequency range of 0.667 to 4.0 Mc the wavelength ranges from 5 to 0.9 mm for the a-direction, and from 3 to 0.7 mm for the c-direction. As the wavelength is varied through this region, it would be expected that, because of geometric effects, the velocity should change significantly.

OTWR also behaved as a low pass filter with a cutoff frequency of approximately 1 Mc for the a-direction (all the reported frequencies were passed in the c-direction). The geometric effect of the cutoff frequency is predominant for this material. It was found that a 3-mm piece of OTWR (propagation in the a-direction) passed all frequencies to 4.0 Mc. For a thicker piece (6 mm) the output frequency consisted of a small amplitude 3.0-Mc wave superimposed on a higher amplitude wave whose frequency was approximately 0.67 Mc. For a still thicker piece (12mm) the 3.0-Mc carrier was completely absent, and the predominant frequency was 0.67 Mc. The same effect occurred for 6-Mc and 9-Mc inputs and is thought to be due to geometric effects. This effect has not been observed in most materials, except to a lesser extent in AVCO Phenolic Fiber Glass.

One thin piece of RAD-60 (density, 1.41 g/cc) was available for use as a sample. A measurement of velocity through this material was made as a function of temperature using the single sample technique. Figure 25 shows the relationship between velocity and temperature to ~200°C. It is interesting to note the curvature of the velocity curve in this region. For the materials previously studied it was found that the velocity curve normally showed either zero or positive curvature near 200°C whereas the curvature for this specimen was

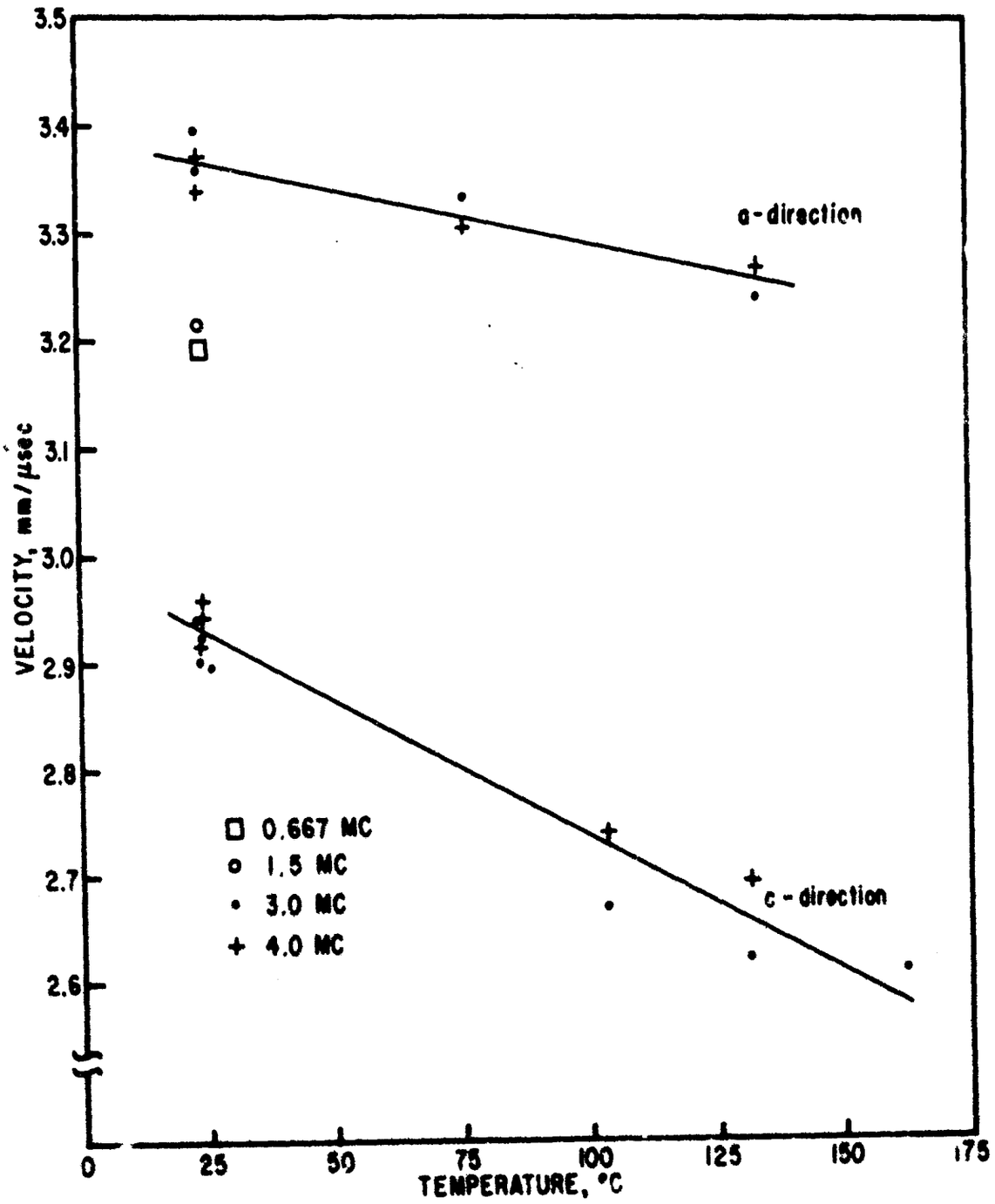

Figure 24. Longitudinal Wave Velocity vs Temperature in Oblique Tape Wound Refrasil (density 1.54 g

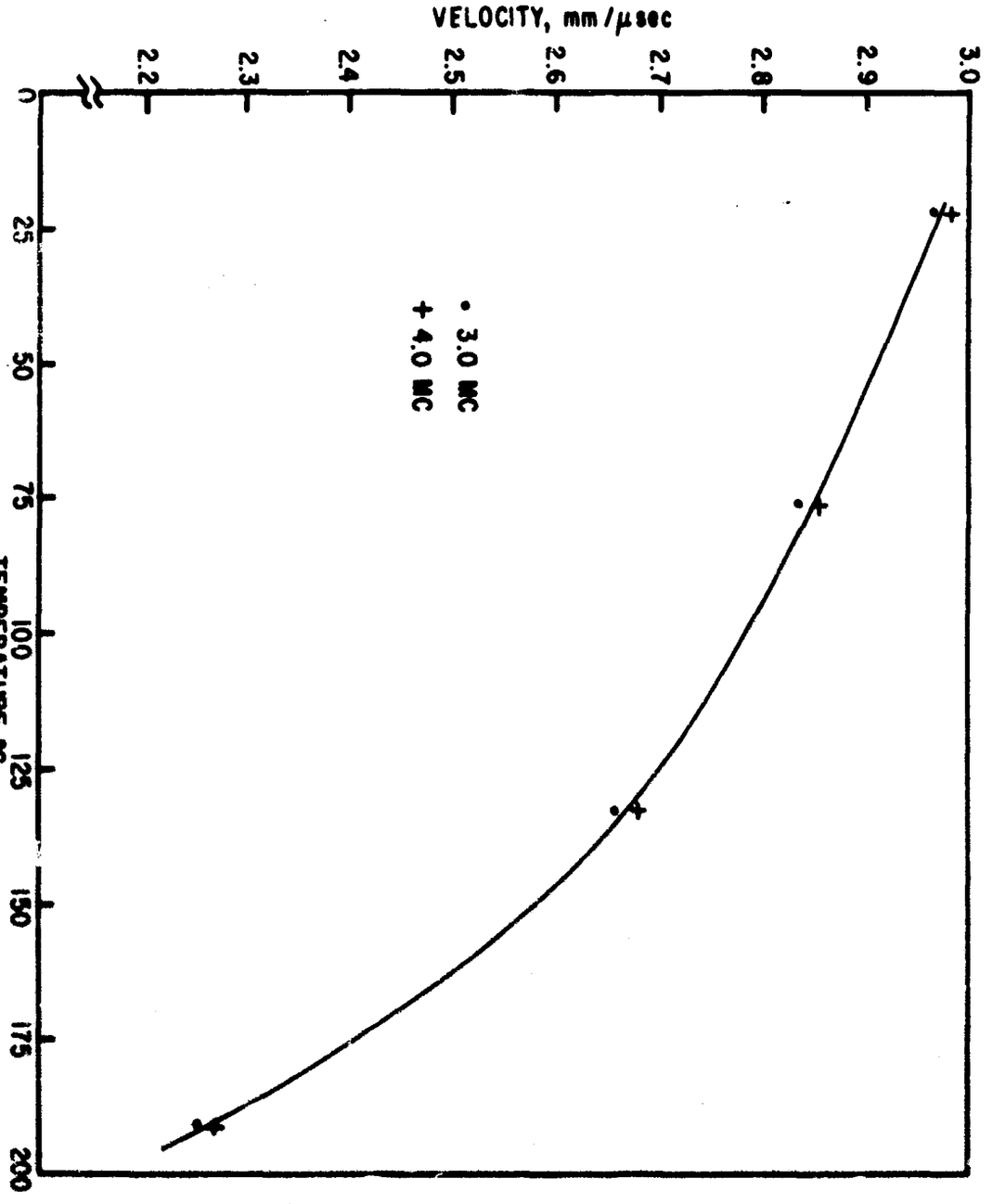

Figure 25. Longitudinal Wave Velocity vs Temperature in Rad 60 (density 1.41 g/cc)

negative in the same region. This material also exhibited some thermal degradation or physical change when exposed to 200°C, since a redetermination of the velocity at room temperature showed a decrease of ∿2 percent.

Figure 26 shows the velocity as a function of temperature in Rad 58E (density 1.26 g/cc), which is a composite of 85 percent silica fibers and 15 percent phenolic resin. The attenuation in this material is fairly high, and for that reason the curve is limited to approximately 135°C.

The ultrasonic velocities in the nose-cone materials discussed in this section are given in Table II. The values all correspond to 25°C, and the frequency range and direction of propagation with respect to the layers are indicated where applicable.

Fused Silica (density 1.93 g/cc) is also listed under this group of materials although it rightfully belongs in a class of its own. As in most of the materials previously discussed, the velocity-temperature variation in this material was obtained by using an oil bath for temperature regulation. It was observed, however, that the fused silica used in these measurements readily absorbed the oil from the temperature bath. Since the effect of this would be to increase the overall density of the specimen, one would expect a slight shift in the velocity. This shift would occur because the effect of the oil would be to slightly perturbate the stress-strain matrix and, consequently, to modify the equations of motion. However, measurements on the longitudinal velocity both before and after the sample had been immersed in oil showed no observed deviation due to oil absorption, and the temperature variation of the longitudinal velocity thus obtained is shown in figure 27. The data shown in figure 27 are corrected for thermal expansion and indicate that the velocity increases slightly with temperature to at least 125°C, contrary to the behavior in most materials.

Before concluding this section, some discussion concerning the accuracy of the measurements is in order. The sources of error inherent in this method of measuring ultrasonic velocities fall into four major categories. These are: (1) errors in sample thickness measurements, (2) transit time measurement errors, (3) errors in temperature measurements, and (4) systematic errors.

One problem of sample preparation was in machine shop technique. The early samples used in this study were cut on a lathe. This procedure was found satisfactory for the thicker samples and typically gave samples varying in thickness by no more than 0.05 percent. With the thinner and more flexible samples, however, the thickness variation was observed to be as high as $\pm$ 1.7 percent in some cases.

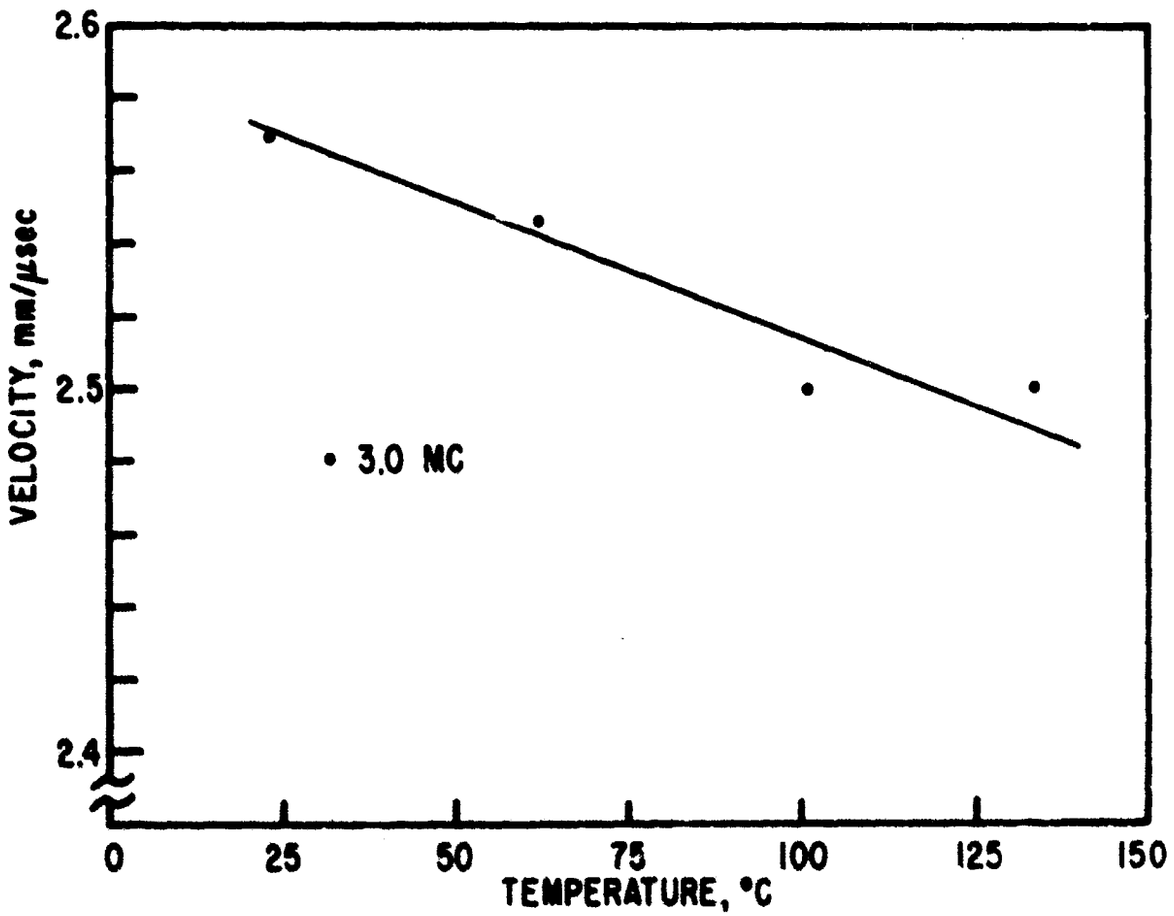

Figure 20. Longitudinal Wave Velocity vs Temperature in Rad 58B (density 1.26 g/cc)

Table II

LOGITUDINAL VELOCITY IN NOSE-CONE MATERIALS AT 25°C

Material	Density g/cc	Frequency Range Mc	Velocity mm/usec
Castable 124	1.23	1.5-4.0	2.45
Avcoat I	1.10	1.5-3.0	2.46
Avcoat 19	1.07	1.5-4.0	2.14
Chopped Nylon Phenolic	1.20		
c-direction		1.5-3.0	2.55
Pyrolytic Graphite	2.19		
a-direction		1.5-4.0	4.81
c-direction		1.5-4.0	3.42
G. E. Phenolic Fiber Glass	1.91		
a-direction		3.0	4.34
c-direction		3.0	3.33
Phenolic Carbon	1.48		
a-direction		3.0	4.10
c-direction		3.0	3.82
Tape Wound Nylon Phenolic	1.21		
a-direction		3.0	2.83
c-direction		3.0	2.77
AVCO Phenolic Fiber Glass	1.71		
a-direction		3.0-4.0	4.35
c-direction		3.0-4.0	2.72
Oblique Tape Wound Refrasil	1.54		
a-direction		3.0-4.0	3.36
c-direction		3.0-4.0	2.93
Rad 60	1.41	3.0-4.0	2.97
Rad 58B	1.26	3.0	2.70
Fused Silica	1.93	1.5-3.0	4.42

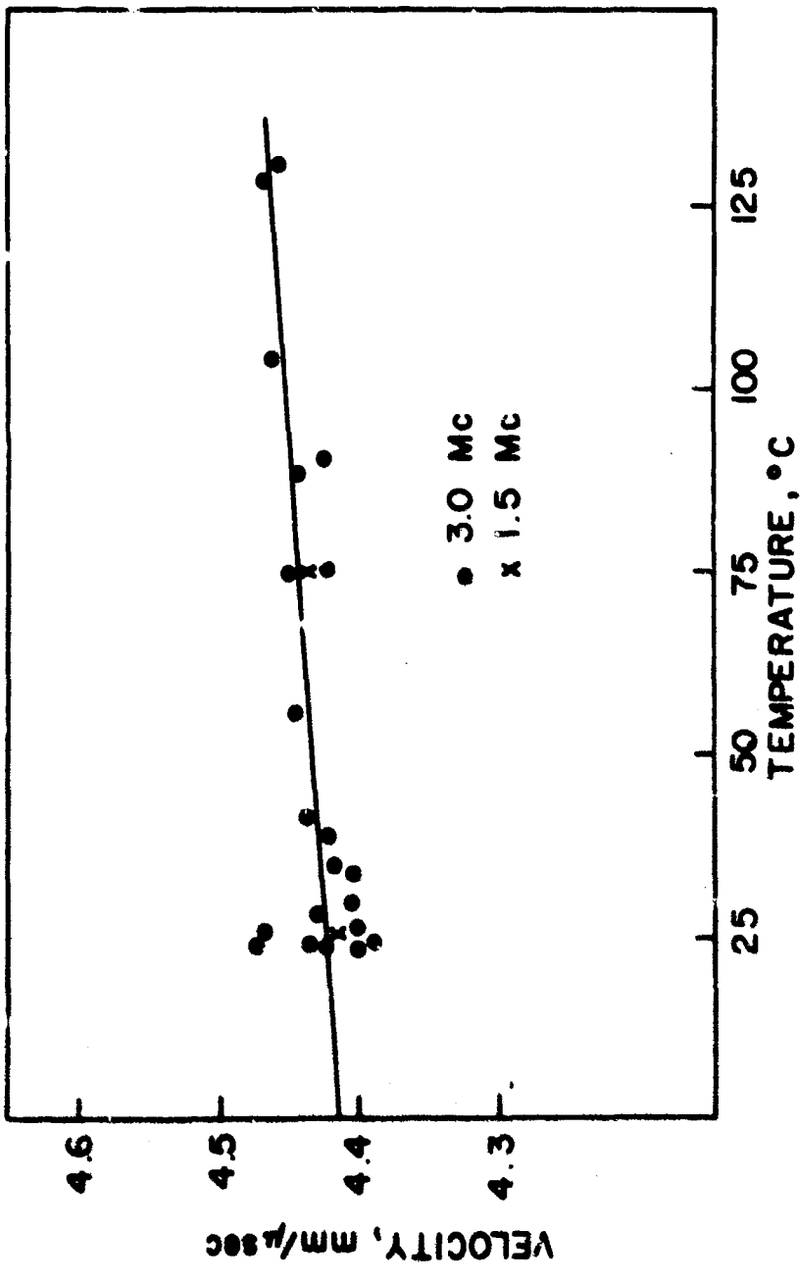

Figure 27. Longitudinal Wave Velocity vs Temperature in Fused Silica (density 1.93 g/cc)

Another problem associated with sample thickness was that some of the plastics studied in this work showed dimensional instability. Teflon, in particular, exhibited this characteristic. Teflon samples initially received from the machine shop were very uniform in thickness, but after repeated cycling to high temperatures it was noted that the velocity values were becoming increasingly erratic. When the samples were remeasured, it was discovered that they had become noticeably thicker and that opposite faces were no longer parallel. This phenomenum was at least partially due to the relaxation of strains imposed during the machining process. After this discovery uniform samples were obtained by using a milling process. Additionally, frequent checks were made of the sample dimensions between temperature measurements to reduce the error resulting from this cause.

The computed velocities for the common plastics discussed in the first section were corrected for thermal expansion using handbook values for the coefficients of linear expansion. In those cases in which the handbook gave a range of values the median value was used as indicated in Table III. Assuming that the correct values for the samples used were within the published range, the maximum possible velocity error due to the use of median values would be $\pm$ 0.5 percent for polyethylene at 100°C. This possible source of error would of course become less significant as the temperature was lowered, becoming nonexistent at room temperature.

When thermal expansion data were available for the nose-cone materials, they were used to correct the velocity temperature curves. In those cases where this information was not available, the thermal expansion was obtained by measuring the length change as a function of temperature. However, in comparing the values computed in this way with several available handbook values, it was found that the agreement in the velocity curves was within 0.5 percent at 100°C, considering the difference between the reported and the experimental values of thermal expansion. Table III lists the values of thermal expansion coefficients used for the previously mentioned materials. The letters a and c after the number indicate the a and c directions respectively.

Errors in time measurements might arise from three sources. Two of these, errors from the time mark generator and the oscilloscope, may well be considered negligible in comparison with other sources of error. The most important source of time error is due to the interpolation method of measuring time intervals and arises because of operator technique. The oscilloscope delay-potentiometer was read to three decimal places by visual interpolation between the finest

Table III

COEFFICIENTS OF LINEAR EXPANSION FOR SEVERAL COMMON PLASTICS AND NOSE-CONE MATERIALS

Material	Coefficients of Expansion (10^{-6} mm/mm °C)
Nylon (Poly Penco and Delrin Acetal)	92
Polyethlene (high and low density)	225
Plexiglas	90
Teflon	55
Avcoat I	90
Avcoat 19	150
Chopped Nylon Phenolic	63 (a)
Pyrolytic Graphite	18 (a) 26 (c)
Phenolic Fiber Glass	13 (a) 45 (c)
Tape Wound Nylon Phenolic	90 (a) 130 (c)
AVCO Fiber Glass	20 (a) 13 (c)
Oblique Tape Wound Refrasil	10 (a) 20 (c)
Rad 60	14
Rad 58B	40
Fused Silica	1.1

gradations on the scale. From reproducibility measurements between operators, it is doubted that the error in making any individual time measurements exceeded 0.01 μsec. Since the difference between elapsed times through two samples was typically in the range from 4 to 6 μsec, the relative uncertainty in time measurements was then not more than 0.5 percent.

The third type of error enumerated above concerns temperature measurements. Temperatures were measured with either a thermometer or a thermocouple and were recorded to the nearest degree. The instrument used was calibrated to the nearest degree over the range of interest. The typical effect of a temperature error can easily be determined from the linear graph of figure 8, where the functional relationship between velocity and temperature is seen to be approximately,

$$c = 2.58 - 0.0078(T-20) \qquad (3)$$

where c is the longitudinal velocity in mm/μsec, and T is in °C. An error of one half degree in temperature would cause an apparent error of 0.004 mm/μsec, which is a relative error of approximately 0.2 percent at the high temperature end of the curve.

The remaining sources of error other than those discussed above constitute the fourth category. The errors in this group are systematic, and, consequently, a numerical value cannot readily be assigned. The major premise of this experimental technique is that the acoustic units can be assembled accurately enough so that units assembled using different samples of the same material will differ ultrasonically only because of the differences in sample thickness. Because of the time required to statistically determine this factor, and because of the accuracy it would require, it was not feasible to determine this factor exactly. However, comparison with standards and the results obtained on the materials under study indicate that this error is insignificant in view of the limited accuracy required.

Another possible source of error was that involved in choosing the reference points on the transmitted and received pulses between which to measure the elapsed transit time. The received signals did not coincide exactly in shape with the transmitted signals, and some small amount of judgment was necessary to pick the proper reference points. Usually however, the oscillations were so clear and well defined that there was no serious doubt about the proper choice.

When the velocities were computed by using the transit times through three different samples of the same composition, three interrelated velocity values were obtained for each determination. This technique contributed greatly to the elimination of error and gave assurance that reasonably accurate values were obtained. However when reasonable care was exercised in assembling the acoustic unit, the accuracy of the single sample method was found to agree quite well with that obtained by the comparison method.

Because not enough measurements were made of the same quantity to permit a statistical error analysis, a series of maximum error calculations was made. These showed that the maximum relative uncertainty in velocity could be as high as 4 percent. Examination of the data points for which multiple velocity determinations were made on homogeneous materials reveals a maximum spread of less than 3 percent; it should be recalled, however, that these points include determinations made by different timing methods and at different frequencies. Another factor to be considered is that many of the early determinations were made with samples which were later found to be irregular in thickness. When homogeneous, isotropic samples of sufficient thicknesses were measured it was observed that the spread in velocity values rarely exceeded 1 percent, for a material measured at a particular temperature and frequency.

3. Longitudinal Velocity in Solid Epoxy Foams

This section presents data concerning the longitudinal bulk velocity in solid epoxy foams as functions of temperature and density. The different densities in this rigid material were obtained by varying the amount of blowing agent and epoxy resin, thereby obtaining the appropriate ratio of void to epoxy in the matrix of the resulting structure (Ref. 8). The resulting material exhibited a fine-cell, uniform, nondirectional structure completely free from grain and characterized by excellent machinability and dimensional stability.

Since the attenuation of longitudinal bulk waves in this material greatly exceeded that of the other materials studied, the acoustic experiment was slightly modified. The electronic apparatus necessary for the generation and detection of the ultrasonically pulsed signals was similar to that described before with the exception that an amplifier of about 70-db gain was inserted between the receiving attenuator and the oscilloscope. The transit time through the material was then obtained by the single sample technique using samples approximately 5mm thick. In place of the transformer oil, silicone grease was used for the coupling agent because it is more viscous and does not diffuse

away from the surface into the foam when the sample is exposed to high temperatures. The entire assembly as used for longitudinal measurements was held together by light spring tension (about 1/3 psi).

The longitudinal bulk velocity is plotted as a function of temperature with density as parameter in figures 28 and 29. Thermal expansion data was not available for this particular foam, so the curves are not corrected for thermal expansion. However, comparison with solid phenolic (Ref. 9) and silicone (Ref. 10) resins in the same density range indicates that the resulting error due to expansion is less than 1 percent at temperatures to 150°C. For the densities shown in figures 28 and 29, the samples had not been previously heat-treated, and the same general shape of the velocity curve is apparent for all densities.

Of particular interest is the existence of an inflection point in the velocity curve at a temperature of about 110°C, where there is a definite change in slope. Velocity inflection points are generally associated with some sort of phase transition relating to a change in one of the moduli. Similar behavior was previously noted for Teflon and has been observed in glass transition studies of polyethylene (Ref. 11). In this case, a permanent change in the color, density, and velocity was observed when the samples were exposed to temperatures higher than about 110°C. To this temperature, the velocity and density values were reproducible within experimental error. However, when the temperature increased beyond 110°C, a permanent dimensional change occured which caused a velocity decrease of 5 to 10 percent and a density increase of 5 to 15 percent at room temperature. The actual values were a function of the density and the temperature to which the samples had been exposed, the lower-density samples showing greater dimensional changes. The color also changed from the original neutral to various shades of brown, depending on the temperature to which the sample had been exposed.

Figure 30 shows the bulk velocity variation with temperature of two high density foams that had been previously heat treated and loaded with different amounts of aluminum. The aluminum filler used for loading was finely ground to an average particle size of less than 25 microns, thus insuring the nondirectional quality of the foam. The bottom curve corresponds to a light gray epoxy foam (density 0.371 g/cc) prepared in the same fashion as the lower density unloaded foams but filled with 8 percent aluminum by weight. The top curve represents a darker gray material (density 1.068 g/cc) prepared by mixing equal

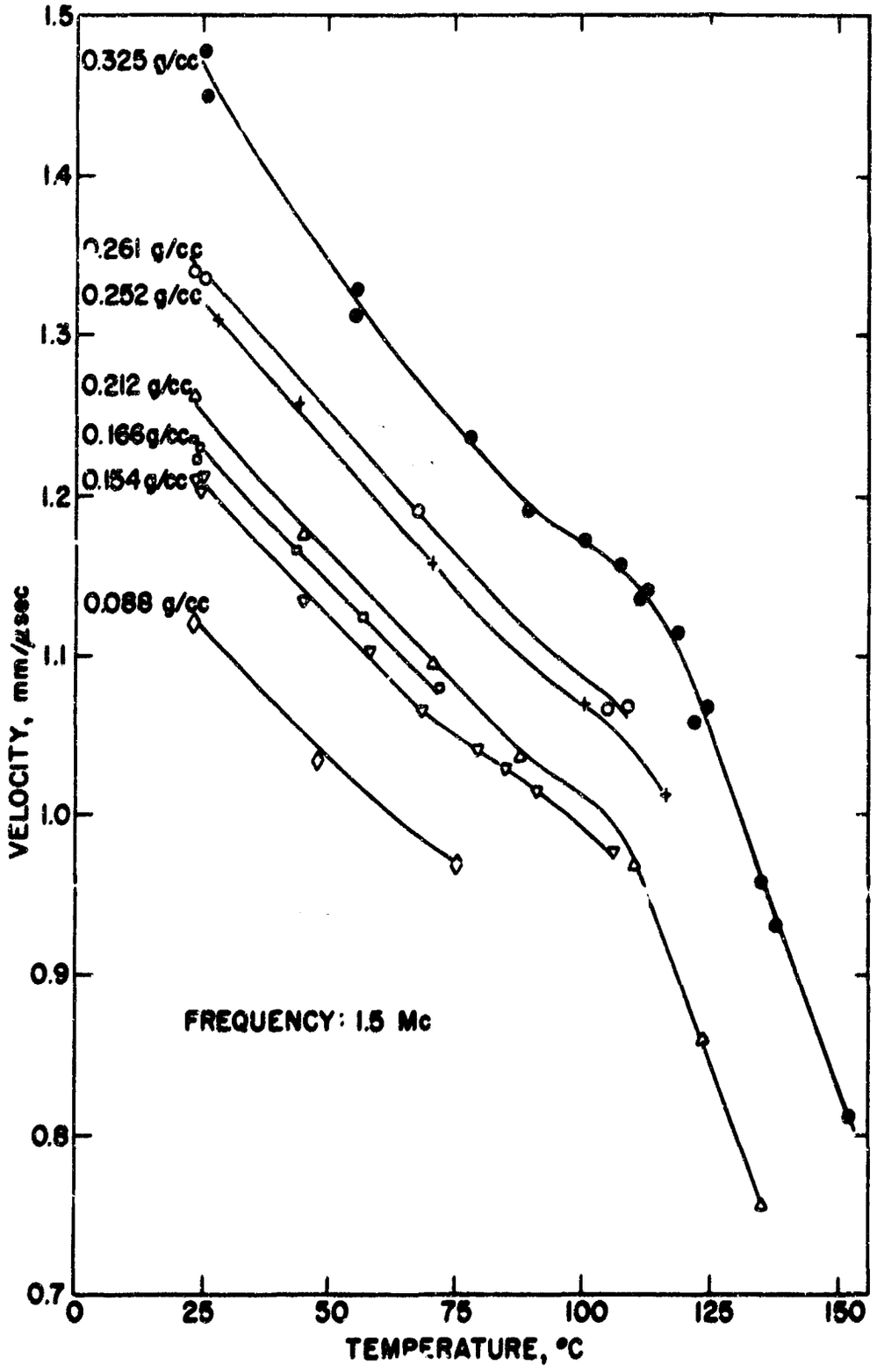

Figure 28. Longitudinal Wave Velocity at 1.5 Mc vs Temperature and Density in Solid Epoxy Foam

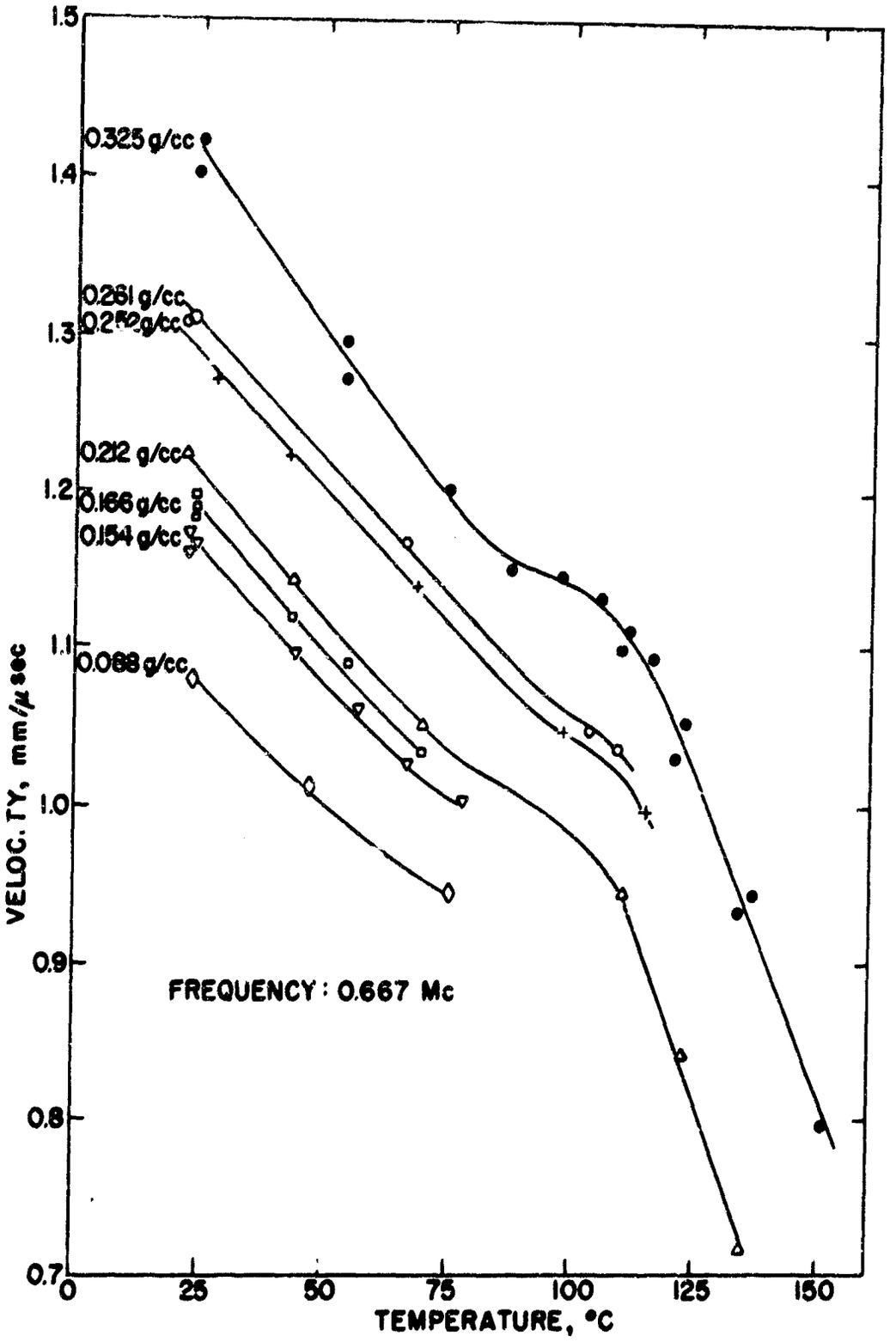

Figure 29. Longitudinal Wave Velocity at 0.667 Mc vs Temperature and Density in Solid Epoxy Foam

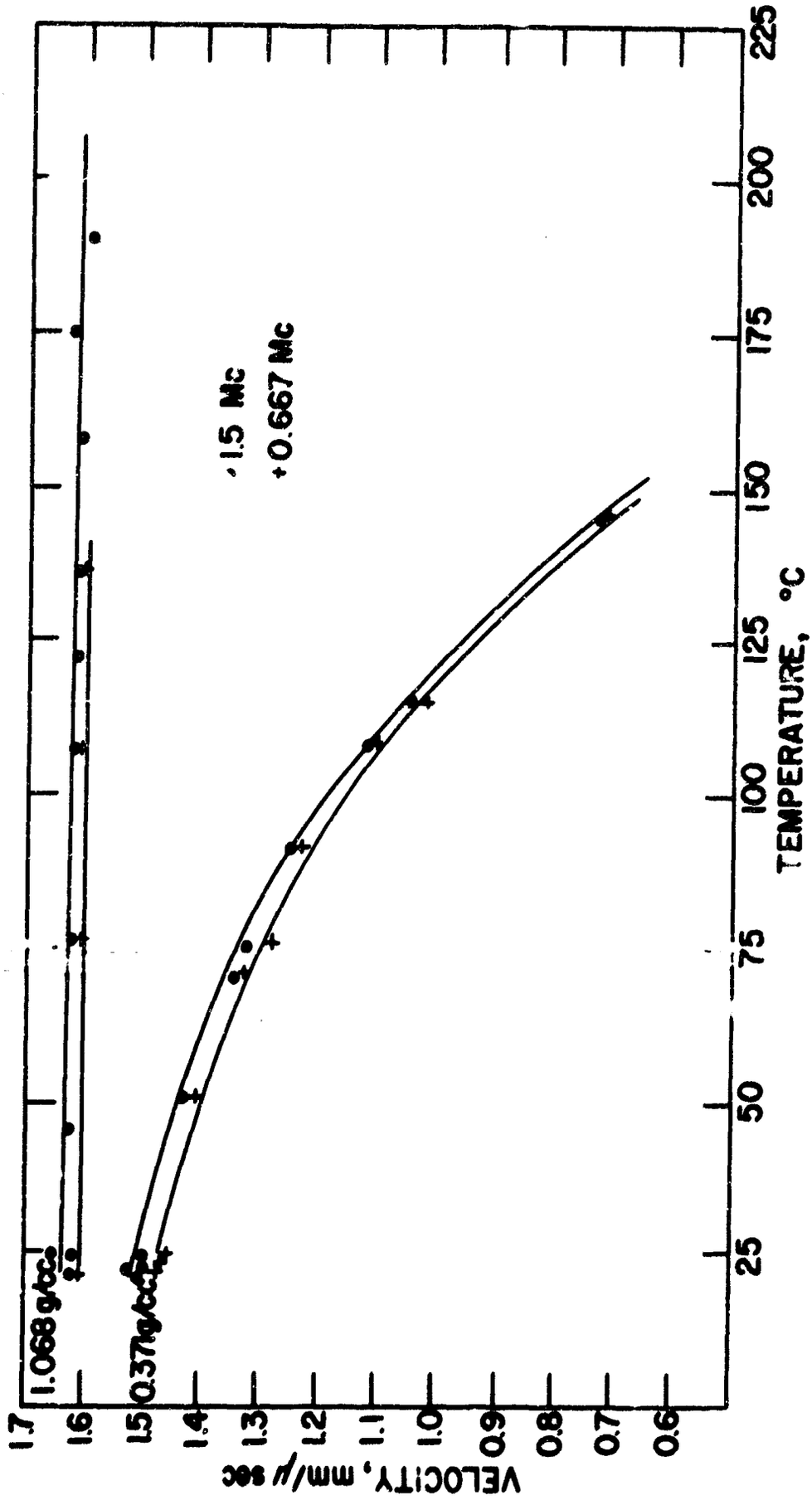

Figure 30. Longitudinal Wave Velocity vs Temperature for two Aluminum Loaded Foams

parts by weight of the finely powdered 8 percent loaded foam and solid epoxy resin (Ref. 8). Both materials had been previously heat treated at 250°C for several hours, and it is noted that an inflection point in the velocity does not exist for either material. The velocity and density for both materials were reproducible within experimental error at room temperature after the samples had been repeatedly cycled to high temperatures. High temperature information for the lower density material was limited to 150°C because of excessive attenuation of the signal at higher temperatures.

Figure 31 shows the attenuation in db/cm plotted as a function of temperature for the 0.325 g/cc sample. The attenuation is calculated from the relation,

$$\alpha = \frac{X_2 - X_1 - C}{d} \tag{4}$$

where X_1 and X_2 are the attenuator settings in db, for a standard amplitude signal with and without the sample inserted, and d is the thickness of the sample. C is a correction factor which accounts for the impedance mismatch at the two buffer-sample interfaces and, as shown in Appendix V, is given by

$$C = 20 \log \frac{\left(Z_1 + Z_2\right)^2}{4Z_1 Z_2} \tag{5}$$

Z_1 and Z_2 being the characteristic acoustic impedances of the sample and aluminum buffers.* Equation (4) does not account for interfacial effects such as the impedance of the silicone grease or the reproducibility of the bonding surface. The first effect was found to be negligible by comparison with attenuation measurements obtained by using two samples of different thicknesses. In the latter case the correction factor goes to zero since the same number and types of impedance mismatches are present in both assemblies. The value of d to be used in the resultant equation is the difference in thicknesses of the two samples.

*The longitudinal acoustic impedance of a medium is defined as $Z_1 = \rho_1 c_1$, where ρ_1 and c_1 correspond to the density and longitudinal velocity in the medium. A similar relation holds for transverse waves when c represents the transverse wave velocity

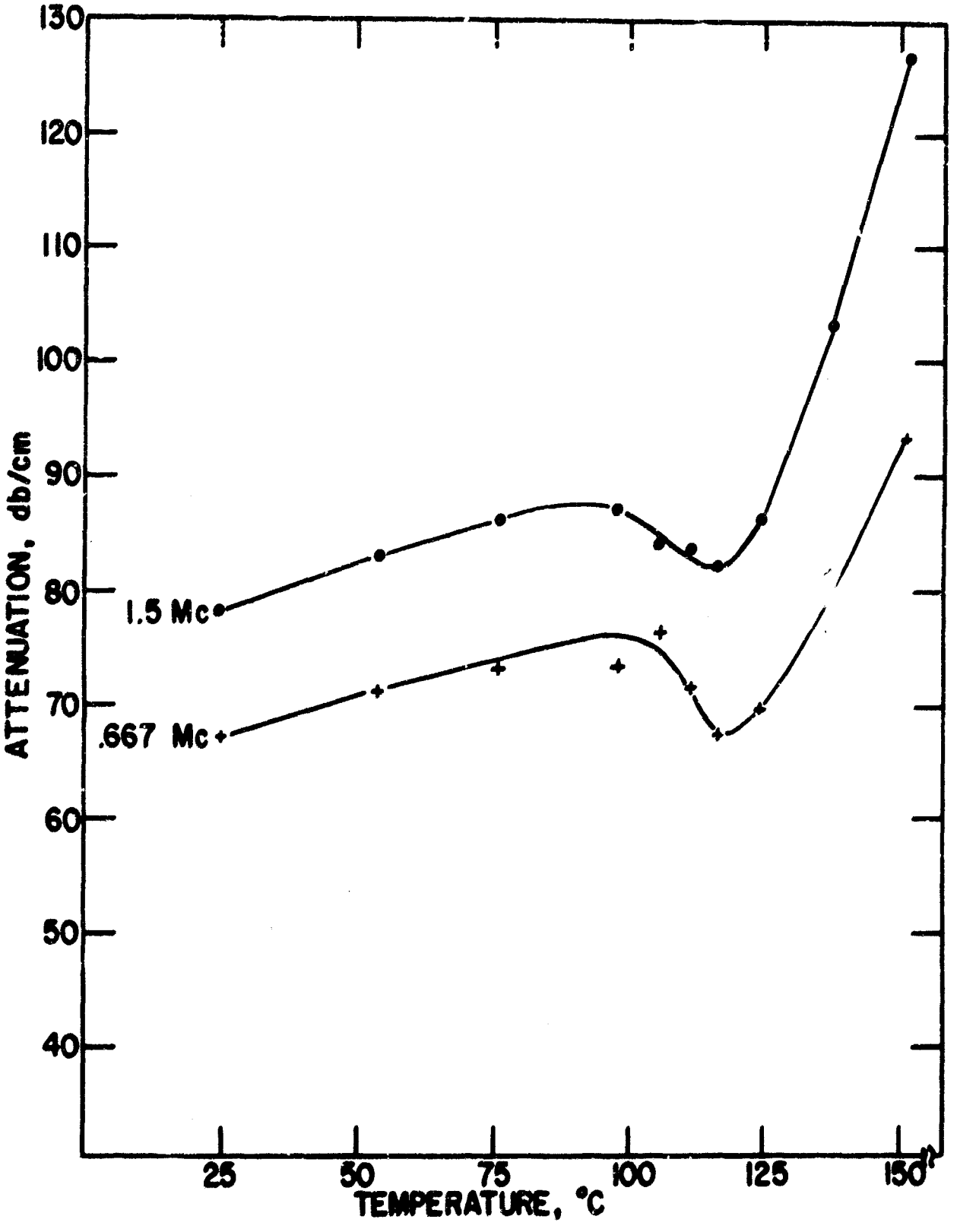

Figure 31. Longitudinal Wave Attenuation vs Temperature in Epoxy Foam (density 0.325 g/cc)

For both of the above methods the accuracy of the attenuation measurements was found to rely on the reproducibility of component assembly. For samples whose surfaces are not smooth, the amount of acoustic energy transferred is a sensitive function of the contact area wetted by the coupling agent. As more bond is added, better transfer of energy occurs since the area of contact, especially for the foam samples, is not limited to the area of a circle (if right circular samples are used). This occurs because the sample surfaces are fairly rough due to the porous structure of the foam. Therefore, the amount of bond and the applied pressure must be reproducible if accurate values of attenuation are desired. For these particular measurements, the precision of the attenuation measurements was found experimentally to be less than 20 percent. For the reasons discussed above the attenuation values should be considered relative rather than absolute.

Of particular interest in figure 31 is the existence of an inversion in the attenuation at about 110°C. It will be recalled that the velocity inflection occurred at this temperature and that a permanent change in the slope of velocity existed for higher temperatures. The situation is similar for the attenuation measurements; however, the effect seems to be much more pronounced and consequently a better indication of the presence of the transition.

Figure 32 shows the variation of velocity and attenuation as a function of frequency for the 0.325 g/cc sample at a constant temperature of 22°C. First, it is noted that extending the frequency to 4.0 Mc increases the velocity about 20 percent. This is a common characteristic of viscoelastic materials in that increasing the frequency is equivalent to lowering the temperature (Refs. 12, 13). The attenuation is also observed to increase with increasing frequency, and in this case an approximately linear relationship exists with frequency for both the attenuation and the velocity. Attenuation and velocity measurements were not possible beyond 4.0 Mc with the present technique because the attenuation increased very rapidly with higher frequencies.

Figure 33 shows the variation of attenuation and velocity with density for the unloaded samples at frequencies of 0.667 and 1.5 Mc. The velocity is seen to be essentially linear with density, monotonically increasing in the observed range. This result is to be expected since the effective stiffness should increase with increasing density, and, in fact, similar effects have been observed in density studies on polyethylene (Ref. 5). Over the same density range the attenuation is also found to be linear, decreasing with increasing density.

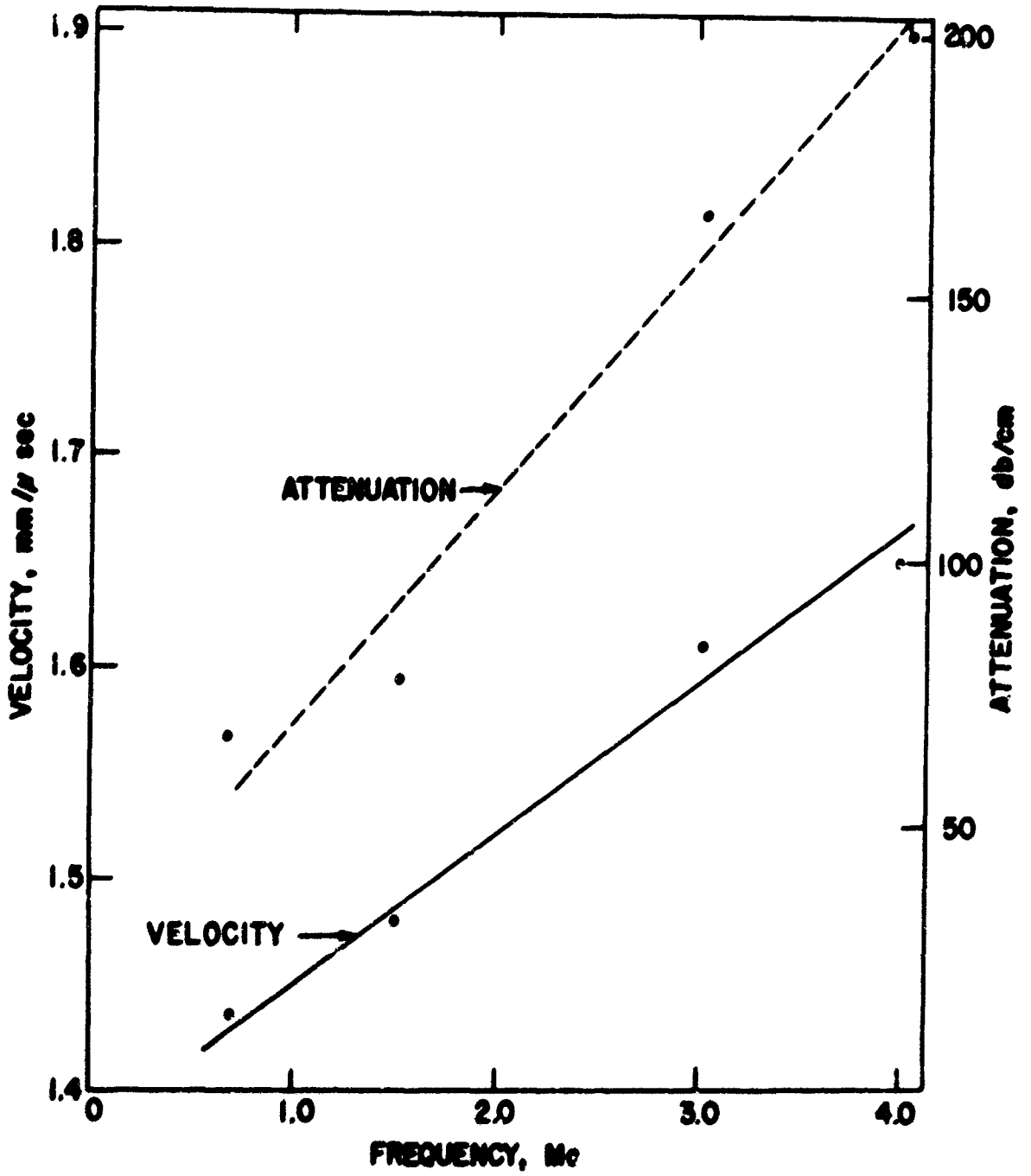

Figure 32. Longtitudinal Wave Velocity and Attenuation vs Frequency in Epoxy Foam of Density 0.325 g/cc

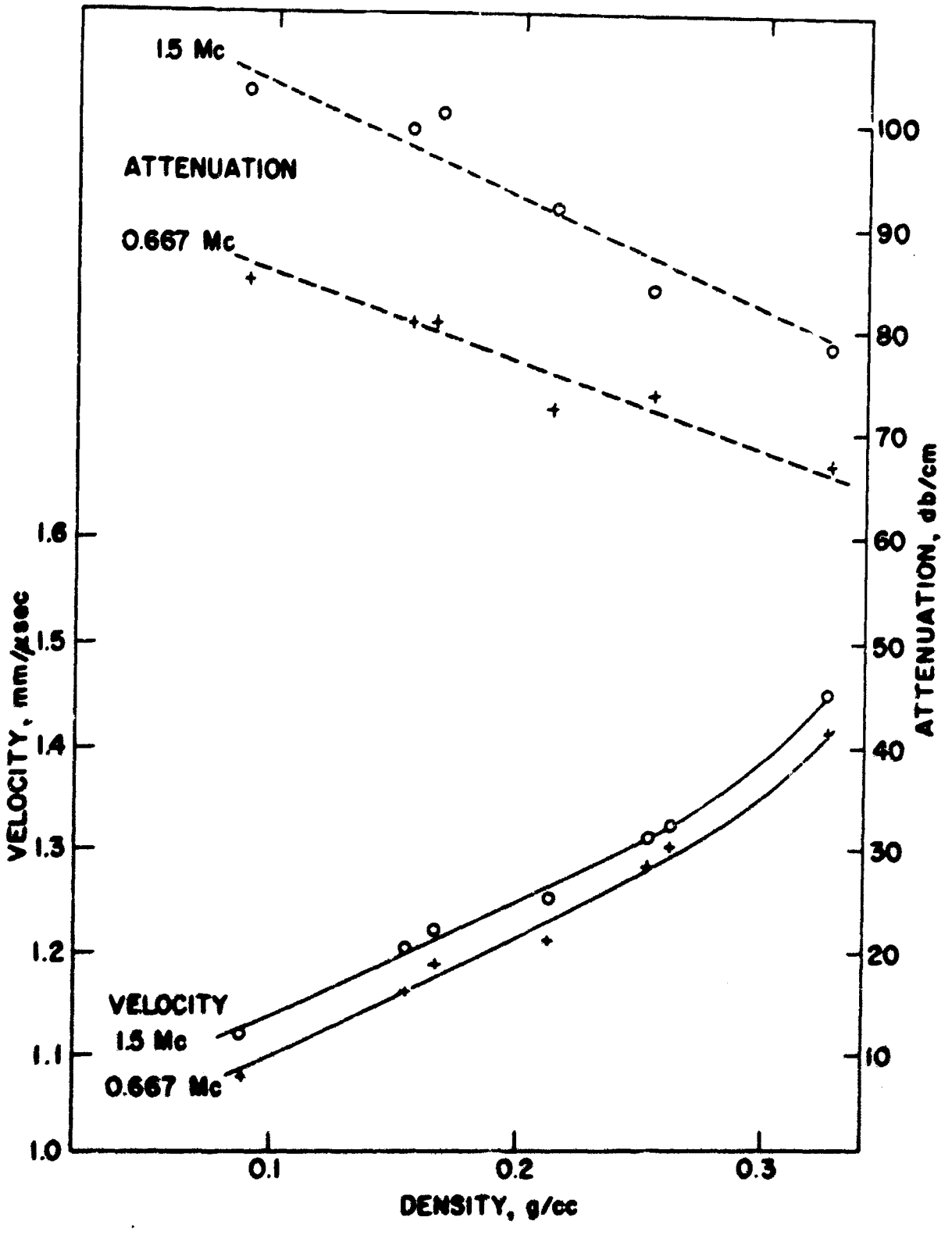

Figure 33. Longitudinal Wave Velocity vs Density in Solid Epoxy Foam

One further word on the accuracy of the velocity measurements is required at this point. As noted in figures 28 through 30, the difference in velocity among some of the curves is on the order of 1 to 2 percent. This magnitude of precision would be necessary to draw the individual curves of figures 28 and 29. As previously mentioned, the present technique has been found to give absolute accuracies on this order under favorable conditions, such as sufficient sample thickness, homogeneous, linear, nondispersive samples, and the use of thin coupling agents such as transformer oil. However, for these particular samples the above conditions are not entirely fulfilled and the accuracy is consequently limited by four major causes. First, as indicated previously, the thickness of the interfacial layer of silicone grease is a critical factor in the transit time reproducibility from one assembly to the next. However, this error was partially minimized by standardized techniques of assembling. By analyzing standards and using different sample thicknesses, it was found that the precision was well within 1 percent when careful attention was paid to the techniques of assembly.

The second error arises because of the very small thickness of the samples. This can result in a rather large percentage error in the transit time or can magnify any error due to sample nonuniformity. However, the former effect was small and fell into the category of the first source of error because of the excellent machinability of these solid foams. It was observed quite routinely that the magnitude of the thickness variation was on the order of 0.25 to 0.50 percent for samples up to 5mm thick. This tolerance was also found to hold even after the samples had been exposed to higher temperatures where dimensional changes might be expected to occur. Consequently, errors arising from the second source of error were not deemed significant.

The third source of error results from the fact that relatively large voids could sometimes be observed along the machined faces of the prepared sample. This is a quite obvious source of error since the velocity of propagation would be a function of the relative amount of epoxy encountered by the ultrasonic waves. The resultant sampling error is somewhat indicated by the top curve in figures 28 and 29. The curve, corresponding to the 0.325 g/cc sample, consists of points obtained from two different samples cut from the same block. The measured density of each sample was found to be the same, and in neither case do the points obtained from the two samples differ by more than 2 percent.

other samples checked for sampling error yielded specimens differing slightly in density and were consequently plotted as separate entities in figures 28 and 29.

The last source of error is by far the largest and depends upon the particular definition used in the calculation of velocity. These materials are obviously dispersive, as can be observed by noting the velocity variation with frequency in figure 32. Dispersion in elastic materials is generally due to purely geometrical consideration such as those arising in thin rods or plates, whereas in viscoelastic materials dispersion is produced by the properties of the solid (Refs. 14, 15, 16). In the latter case, high frequency waves travel faster than low frequency ones, which is consistent with the present experimental observations. But when the elastic properties vary with frequency, as in a dispersive medium, the interpretation of the results becomes uncertain, since there is not a unique velocity of propagation, and the velocity at which energy is transferred is the group velocity, c_g, which differs from the phase velocity, c_p, by an amount $\lambda \frac{dc_p}{d\lambda}$ (λ is used here as the wavelength).

As noted earlier, the transit time required for the pulse to traverse the sample was computed by measuring from one peak on the unrectified transmitted signal to the corresponding one on the received signal. When the input and output wave forms were not distorted (as was the case for most materials discussed previously), this method gave identical results within the capabilities of the technique, regardless of the peak used for reference. For the foam materials however, the calculation of the velocity was strongly dependent on which peak was used to measure the transit time. The possible reference peaks were limited to the first and second positive (or negative) peaks because of subsequent distortion of the remaining peaks of the output pulse. The velocity calculated using the second positive peak as reference instead of the first gave values which were about 8 percent lower at room temperature for 0.667- and 1.5-Mc input frequencies. The reasons for this apparent inconsistency is due to the above considerations and to the fact that the output frequency was in general lower than the input. For input frequencies of 0.667 to 4.0 Mc, the output ranged from 0.5 to 2.0 Mc. It was also noted that the output frequency slowly decreased with increasing temperature using these same frequencies. For an input of 0.333 Mc, the output was comparable, although velocity information could not be obtained because of extreme distortion of both input and output waveforms.

Since these foams are characteristic of visocoelastic solids, four independent measurements would be necessary to completely characterize the four constants

of propagation. These constants consist of the compressional and shear moduli associated with elastic behavior, plus the compressional and shear viscosities. To completely specify the propagation constants would then require shear wave velocity and attenuation measurements as well as the associated longitudinal measurements. Shear wave measurements were attempted in the present experiments by using appropriate coupling agents and extremely thin samples. But shear data was not possible with the present technique because of the extreme attenuation of the waves. This was to be expected at these temperatures and frequencies, since the longitudinal wave attenuation was high and since shear waves are, in general, attenuated much more than longitudinal waves.

A Differential Thermal Analysis (DTA) was performed on the 0.325 g/cc sample (Ref. 17) and thermograms were obtained to approximately 400°C. It was found that a glass transition occurs at 146°C with decomposition beginning at approximately 200°C and complete decomposition resulting at 408°C. Of particular interest was the existence of a small curing exotherm in the region of 50° to 145°C which disappeared on repeated heating. The material is a thermosetting resin and, as such, crosslinking of the polymer increases with increasing temperature. The resultant effect is probably such that the chemical structure changes with increasing cure, resulting in a permanent decrease in either the shear, the compressional modulus, or both, and consequently manifests itself in a decrease of the longitudinal velocity.

A word is in order about the behavior of the aluminum filled samples. Analyses of aluminum have shown that the longitudinal velocity, and consequently the effective modulus for propagation of longitudinal waves, is a slowly decreasing function of temperature to at least 125°C. One could assume that the properties of the foams should become more characteristic of the properties of aluminum as the percentage of aluminum increases. This assumption would in part be supported by the top curve of figure 30. However, as previously mentioned, the lower curve corresponds to a higher percentage of aluminum (8 percent versus 4 percent for the top curve) so that the assumption is apparently invalid or masked by more predominant characteristics. If the loading effect were compared with the combined effects due to density change, loading, and the epoxy itself, the behavior could be definitely attributed to a particular cause. But information on the variation of each effect with the other two held constant was not available, so that it was not possible to assign the differences in the two graphs of figure 30 to any one effect. It seems reasonable to assume that the

properties of epoxy and those inherent with the density are responsible for the difference in the two graphs, since the lower curve (higher percentage of aluminum) corresponds closely in shape to those obtained from the unloaded samples.

One further word is necessary to close the discussion on the solid foams. Static tests on the compressive, flexural, and tensile strengths, as well as moduli, indicate an increase of approximately an order of magnitude in these quantities when the density of the unloaded samples was increased fourfold (Ref. 8). The effective modulus for bulk wave propagation shows similar behavior, increasing by almost a factor of ten over the same density range. As shown in Appendix II, a relationship exists between the effective stiffness of a material and the velocity of propagation so that comparisons between the static and dynamic moduli can be made. The effective modulus is given approximately by (Ref. 15, 16),

$$\lambda + 2\mu = B_s + 4/3\mu = \rho c_\ell^2 \qquad (6)$$

where γ and μ are the Lame constants, which relate stress to strain in homogeneous, isotropic materials. B_s is the adiabatic bulk modulus, ρ is the density, and c_ℓ is the longitudinal wave velocity. Equation (6) is limited to situations involving low attenuation and no dispersion, where the phase and group velocities are equal. The equation as presented here neglects the high attenuation in the foam, the fact that the material is dispersive, and is presented only for comparison purposes.

Table IV summarizes the velocity through various densities of the epoxy foams at room temperature.

Table IV

LONGITUDINAL VELOCITY IN SOLID EPOXY FOAM AT 25°C

Density g/cc	Frequency Mc	Logitudinal Velocity mm/μsec
0.088	0.667	1.08
	1.5	1.12
0.154	0.667	1.16
	1.5	1.20
0.166	0.667	1.19
	1.5	1.22
0.212	0.667	1.21
	1.5	1.25
0.252	0.667	1.28
	1.5	1.31
0.261	0.667	1.30
	1.5	1.32
0.325	0.667	1.41
	1.5	1.45
	3.0*	1.61
	4.0*	1.65

*Temperature, 22°C

SECTION IV
APPLICATIONS

In recent y ars many laboratories have concentrated on measuring the high-temperature properties of materials. This is particularly true of space-age materials in that they must be capable of withstanding dynamic vibratory loadings at high temperatures. Thus, in many practical applications it is necessary to kn w the values of the elastic moduli of materials at high temperatures.

These values are necessary not only to the design engineer, but also to the physicist interested in the equation of state of materials that make up components of these systems. One method currently used for making these high temperature measurements is the standard tensile test employed in the static testing of materials (Ref. 18). The specimen is enclosed within a furnace and connected to the crossheads of a tensile machine, and stress-strain plots are made at elevated temperatures. This method of testing at high temperatures has many shortcomings. One is the difficulty in making strain measurements at high temperatures. In addition, the magnitude of the static elastic constant is always influenced, to some extent, by relaxation effects at elevated temperatures. Superimposed on the purely elastic deformation of the specimen are deformations associated with creep and elastic hysteresis. Thus, the values of the elastic modulus obtained by static methods can become very dependent upon the strain rate used in the test.

Since the propagation characteristics of small-amplitude elastic waves in a solid are governed by the elastic coefficients, a measurement of the different velocities of propagation, such as transverse and longitudinal velocities, allows a convenient calculation of the elastic constants. Ultrasonic wave velocity measurements are easily made as a function of temperature so that the variation of the elastic constants with temperature is readily obtained.

In anisotropic bodies, such as crystals, the number of constants necessary to specify the mechanical properties of the medium depends upon the particular symmetry system to which the crystal belongs. For example, for cubic symmetry three coefficients are necessary to specify the stress strain matrix and are commonly designated as c_{11}, c_{12}, c_{44}. In isotropic bodies the elastic behavior can be completely designated by two elastic constants, λ and μ, known as the

Lamé constants (Ref. 19). It is shown in Appendix II that the two velocities of propagation in an isotropic can be expressed as

$$c_\ell = \sqrt{\frac{\lambda + 2\mu}{\rho}}$$

$$c_t = \sqrt{\frac{\mu}{\rho}} \qquad (7)$$

where λ and μ have been defined, c_ℓ is the longitudinal wave velocity, c_t is the transverse velocity, and ρ is the density. The Lamé constant, μ, is identical with the shear modulus, G. Equation (7) applies to infinitesimal displacements in an infinite medium, i.e., where the wavelength is much smaller than the longitudinal or lateral dimensions of the specimen. The constants obtained from equation (7) are the adiabatic rather than the isothermal constants, since the velocity of propagation for ultrasonic waves in the low megacycle range is under the adiabatic response of the material (the thermal diffusivity is small at these frequencies). However, to compare with static measurements the conversion to the isothermal moduli involves the ratio of specific heats and is usually a small correction, on the order of a few percent (at low pressures).

Young's modulus, E, the shear modulus G, the bulk modulus B and Poisson's ratio σ can be expressed in terms of the Lamé constants for an isotropic medium as (Ref. 14)

$$E = \frac{\mu(3\lambda + 2\mu)}{\lambda + \mu}$$

$$G = \mu$$

$$B = \lambda + \frac{2}{3}\mu \qquad (8)$$

$$\sigma = \frac{\lambda}{2(\lambda + \mu)}$$

where it is understood that all of the moduli are the adiabatic moduli. Substituing for the Lamé constants in equation (7) yields the following formulas in terms of the longitudinal and shear wave velocities

$$E = \frac{\rho c_t^2 \left(3c_\ell^2 - 4c_t^2\right)}{c_\ell^2 - c_t^2}$$

$$G = \rho c_t^2$$

$$B = \frac{\rho \left(3c_\ell^2 - 4c_t^2\right)}{3} \qquad (9)$$

$$\sigma = \frac{c_\ell^2 - 2c_t^2}{2c_\ell^2 - 2c_t^2}$$

in cgs or mks units.

Nolle and Sieck (Ref. 4) discuss the mechanical behavior of a high-loss specimen in compression and shear. Their assumption is that for high-loss (high attenuation of acoustic signals) the moduli must be complex, with a real part associated with elastic behavior, and an imaginary part which is a function of frequency and viscosity. Following their notation, the complex modulus quantities connected with the observed velocity and attenuatio are given as

$$M^* = M_1 - iM_2$$

$$c^* = c_1 - ic_2 = \sqrt{\frac{M^*}{\rho}} \qquad (10)$$

where ρ is the density and M^* is the effective stiffness for a certain wave motion whose velocity is given by c^*. Direct solution of equations (10) gives

$$M_1 = \rho \left(c_1^2 - c_2^2\right)$$

$$M_2 = 2\rho c_1 c_2 \qquad (11)$$

Also, examination of the usual complex exponential expression for propagation shows that c_1 and c_2 are related to the observed phase velocity c, to the amplitude constant α (db/cm), and to M_1 and M_2 by the following relations

$$c_1 = \frac{c}{1 + \gamma^2}$$

$$c_2 = \frac{\gamma}{1 + \gamma^2} c \qquad (12)$$

$$M_1 = \frac{\rho c^2 (1 - \gamma^2)}{(1 + \gamma^2)^2}$$

$$M_2 = \frac{2\gamma}{1 - \gamma^2}$$

where $\gamma = \frac{\alpha c}{8.68\omega}$, α is the attenuation in db/cm, c is the observed phase velocity, and ω is the angular frequency. These equations were found to fit Nolle and Sieck's experimental data in Buna-N vulcanizate in the frequency range of 2 to 10 Mc and in the temperature range of -80°C to +80°C.

Since the effective complex stiffness for longitudinal waves is $B^* + 4/3\mu^*$, M_1 and M_2 represent, respectively, $(B_1 + 4/3\mu_1)$ and $(B_2 + 4/3\mu_2)$ when the longi-longitudinal velocities and attenuations are used in equation (12). From these equations it is found that when the attenuation is low ($\gamma \to 0$) the wave velocity equation reduces to that given by equations (8) and (9), viz., $B_1 + 4/3\mu_1 = \rho c_1^2$. Therefore, in this situation the bulk modulus could be evaluated from measurements on only the longitudinal and shear wave velocities. However, for high-loss specimens, such as some of the nose-cone materials encountered here, measurements on both the longitudinal and shear wave velocities as well as attenuations would be required to characterize the real and imaginary contributions to the bulk modulus.

In addition, measurements on both the longitudinal and shear wave velocity and attenuation indicate whether longitudinal wave attenuation is due principally to shear or compressional viscoelastic losses. If the imaginary components for the propagation of longitudinal and shear waves are calculated $B_2 + 4/3\mu_2$, and μ_2, respectively , then the fraction

$$\frac{4/3\mu_2}{B_2 + 4/3\mu_2} \qquad (13)$$

indicates how much of the longitudinal wave attenuation is due to pure shear losses. A value of unity would indicate that longitudinal wave attenuation is due entirely to shear losses.

Many other material characteristics, such as internal friction, strain rate effects, uniformity of density, existence of flaws, and specific heats, can be obtained by use of ultrasonic velocities and attenuations, and the interested reader is referred to the abundant literature on the subject (references 14, 15, 19).

Sound velocities have many applications in theoretical and experimental hydrodynamic studies of impulsively loaded materials. Many of these applications, such as calculations of rarefaction velocities, momentum transmission coefficients at impedance mismatches, and pulse lengths of strong shocks, are approximations since in many cases the corresponding quantities for the propagation of high pressure waves are not known. References 20 to 23 discuss, from experimental and theoretical points of view, some of the limitations and approximations involved in using ultrasonic velocities to describe the behavior of shock waves in the material under study. This report does not discuss the conditions and limitations of most of these approximations, and is concerned with some of the more quantitative applications.

One method of studying the properties of matter at high pressures is based on the use of strong shock waves. A determination of two of the wave parameters, for example its velocity of propagation and the velocity of the mass of material behind the shock transition, permits the pressure and density in the shock compression to be found by conserving momentum and mass across the shock front (Ref. 24). The assumptions usually made are that a steady state is eventually reached behind the shock front, and that the material under study acts as a fluid for the extremely high pressures encountered in a strong shock wave. The conservation laws then readily give a relationship between the shock and particle velocities. Also, by these conservation laws (Rankine - Hugoniot equations), relations between other material characteristics, such as pressure and density, can be deduced. The resultant experimental curve in the pressure-density plane is known as the Hugoniot curve, which is defined as the series of pressure, volume, and energy points generated by a series of single shocks applied to a material initially in a specific initial state. The Hugoniot equation of state for the material under study is then obtained from several hugoniots, starting from several initial states.

An interesting fact that has emerged from most Hugoniot measurements is that a plot of the shock velocity, U_s, versus particle velocity, u_p, yields a straight line (Ref. 24), which seems to hold if the material does not undergo a phase change. The relation thus experimentally obtained

$$U_s = a + \hat{b}u_p \tag{14}$$

represents the average behavior of the large number of substances investigated.

If the linear relation is presumed to hold all the way down to low pressures, where the particle velocity approaches zero, the shock velocity, and hence the constant a, should become identical to the "hydrodynamic" sound velocity. The hydrodynamic sound velocity, c_o, is defined as (Ref. 22)

$$c_o^2 = \left(\frac{\partial P_o}{\partial \rho}\right)_s \tag{15}$$

where P_o is the pressure corresponding to an infinitesimal deplacement, and S is the entropy. If the entropy is considered constant across the shock transition (which is usually assumed), Fowles (Ref. 22) indicates that this is equivalent to

$$c_o^2 = \left(\frac{\partial P_o}{\partial \rho}\right)_H \tag{16}$$

where H means that the derivative is evaluated along the Hugoniot. Since the adiabatic bulk modulus is defined as $-V\left(\frac{\partial P}{\partial V}\right)_s$, equation (16) reduces to

$$c_o^2 = \frac{B_s}{\rho_o} \tag{17}$$

if the assumption is made that the pressure is essentially hydrostatic in the limit of low pressure and that the Hugoniot can be approximated by an adiabat (see Appendix III). From the relations between the longitudinal and shear velocities and the elastic moduli given earlier, equation (17) can be expressed as (see Appendix III)

$$c_o^2 = c_l^2 - 4/3\ c_t^2 \tag{18}$$

Therefore, the extrapolation point a = c_o can be estimated from hydrostatic P-V data corrected to constant entropy (Ref. 24), or from the longitudinal and transverse velocities in the materials. The comparison between calculated values using equation (18) and extrapolated values is good for most metals, and some values are given in Appendix III. As shown in equation (18), the calculated value, c_o, is lower than the longitudinal velocity in the material, and this is generally true of the extrapolated values, if the Hugoniot experiments are performed at significantly high pressures. Figure 34 illustrates the typical variation between the longitudinal velocity and the extrapolated value of shock velocity.

If the linear relation (equation 14) is considered as an expansion of the shock velocity, Paul and Warschauer (24) show that the slope, b, should be given as

$$b = -1/4 \left[\frac{V^2 \left(\frac{\partial^2 P}{\partial V^2} \right)_s}{V \left(\frac{\partial P}{\partial V} \right)_s} \right] \qquad (19)$$

which can be further reduced to

$$b = 1/4 \left[1 + \left(\frac{\partial B_s}{\partial P} \right) \right] \qquad (20)$$

The quantity $\left(\frac{\partial B_s}{\partial P} \right)$, which is the change of the adiabatic bulk modulus with pressure, can be obtained from the pressure dependence of the longitudinal and transverse velocities. Table V shows the agreement between the values of the slope calculated from ultrasonic data compared to data obtained from shock experiments as listed by Paul (Ref. 24).

The data obtained from shock measurements is generally expressed in equation f state form as an expansion in the compression (Refs. 25,26)

$$P - P_o = \left(\frac{\partial P}{\partial \mu'} \right)_o \mu' + 1/2! \left(\frac{\partial^2 P}{\partial \mu'^2} \right)_o (\mu')^2 + 1/3! \left(\frac{\partial^3 P}{\partial \mu'^3} \right)_o (\mu')^3 + \ldots \qquad (21)$$

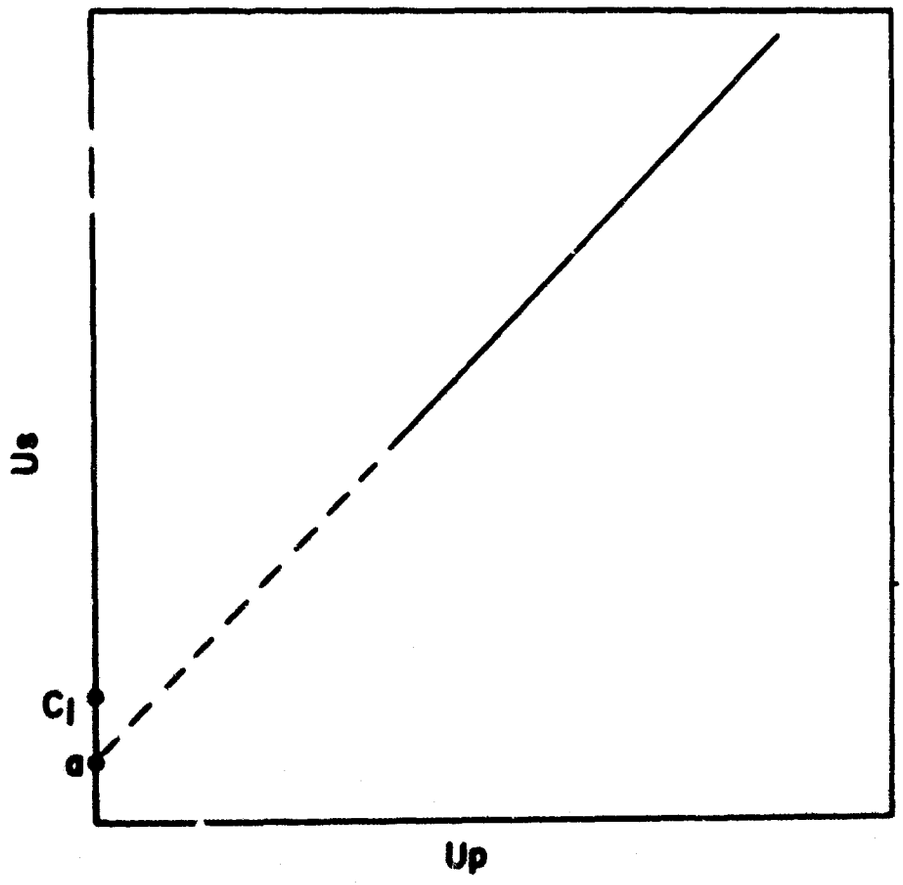

Figure 34. Relationship Between Shock Velocity and Particle Velocity for High Pressure Shocks

Table V

COMPARISON OF THE SLOPES OF THE
SHOCK VELOCITY VERSUS PARTICLE VELOCITY CURVE

Material	Ultrasonic, b	Shock, b
NaCl	1.35 $\pm$ .05	1.43 $\pm$ .02
Aluminum	1.54 $\pm$ .05	1.2 to 1.6
Copper	1.64	1.50
Silver	1.79	1.59
Gold	1.85	1.56
Sodium	1.15	1.2

where $\mu' = \frac{\rho}{\rho_o} - 1$ is the compression, and the zero subscript indicates that the derivatives are to be evaluated at the initial conditions. Since many experiments are made with pressures on the order of tens of kilobars or greater, P_o is usually neglected. Again, the first derivative can be related to the bulk modulus, which gives

$$\left(\frac{\partial P}{\partial \mu'}\right)_o = \frac{\rho_o}{\rho} \left[-V\left(\frac{\partial P}{\partial \rho}\right)_o \right] \tag{22}$$

which can be further related to the adiabatic velocities

$$\begin{aligned} \left(\frac{\partial P}{\partial \mu'}\right)_o &= \rho_o \left[c_\ell^2 - 4/3\ c_t^2\right] \\ &= \rho_c c_o^2 \end{aligned} \tag{23}$$

(For the assumptions involved in this derivation, see Appendix III). The longitudinal and transverse velocities can then be used to obtain a theoretical constant useful in describing experimental hydrodynamic data. The temperature dependence of the longitudinal and transverse velocities allows a convenient calculation of a constant to be used in experiments under varying temperature environments.

Normally, the equation of state used to describe impulsively loaded materials contains an additional term to equation (21) which involves the pressure dependence of the thermal energy, E, of the solid

$$P = a\mu' + b\mu'^2 + c\mu'^3 + \gamma \frac{\rho}{\rho_o} E \tag{24}$$

where γ is obtained from the Mie-Grueneisen equation of state (Ref. 22). This parameter enters into all calculations concerning the description of shock waves propagating through materials. As shown by Paul (Ref. 24), the Grueneisen ratio is defined as

$$\gamma = V\left(\frac{\partial P}{\partial E}\right)_V \tag{25}$$

Using thermodynamic relations and the relations among the velocities, this ratio can be expressed for isotropic materials as (see Appendix IV)

$$\gamma = \frac{\beta\left(c_\ell^2 - 4/3\ c_t^2\right)}{c_p} = \frac{\beta\ c_o^2}{c_p} \tag{26}$$

where β is the volume coefficient of expansion, and c_p is the specific heat. The coefficient calculated in this way for metals compares closely with that calculated from experimental shock wave data (Table VII, Appendix IV).

In another application, composite materials are used to reduce the magnitude of a high pressure impulse at a solid interface. This necessitates a knowledge of the reflection and transmission coefficients of a stress wave at the boundary. Allen (Ref. 27) discusses the applicability of a nonlinear approach to the calculation of the transmission coefficient, which in general exceeds that calculated from the linearized equations of motion. However, the derivation by the linearized approximation gives the transmission (t) and reflection (r) coefficients in terms of the acoustic impedances of the two solids as (Ref. 24)

$$r = \frac{\rho_{o2}c_2 - \rho_{o1}c_1}{\rho_{o1}c_1 + \rho_{o2}c_2} = \frac{Z_2 - Z_1}{Z_1 + Z_2}$$

$$t = \frac{2\rho_{o1}c_I}{\rho_{o1}c_1 + \rho_{o2}c_2} = \frac{2Z_1}{Z_1 + Z_2} \tag{27}$$

where the wave is propagating from medium 1 into medium 2, and the c_1 and c_2 are the shock velocities in the two media. Longitudinal velocities offer convenient approximations in the calculations of transmission coefficients when the equations of state are not known and can be used as approximations in equations (27).

The data presented earlier on the longitudinal velocity through laminated materials as a function of the angle of incidence also offers an attractive approach to the problem of shock reduction, since, as previously shown, the velocity is a sensitive function of the incident angle for some layered materials. A shock wave could then be attenuated by a material with a continuously varying

lamination angle, thus eliminating excess bonds between materials and possibly preserving desirable ablation characteristics. However, the approach is still tentative, and some theoretical work is needed to correlate the present acoustic measurements to the actual condition of high-intensity shock propagation.

SECTION V

CONCLUSIONS AND RECOMMENDATIONS

The temperature dependence of longitudinal and transverse velocities offers a convenient means of calculating many material properties as a function of temperature. The knowledge of mechanical properties at high temperatures is becoming an increasingly important requirement in hydrodynamic studies, and such knowledge is enhanced as experimental techniques and theoretical approaches become more sophisticated.

Many of the results obtained from sound velocities can be duplicated by other means, such as static tests in the case of the elastic moduli. However, ultrasonic measurements offer a check on the static results and perhaps apply more directly to hydrodynamic experiments because of the dynamic character of both.

Another consideration is that, in plastics relaxation effects can be important so that no simple relationship exists between the various mechanical properties of the material as determined by static and dynamic measurements. That is, mechanical properties such as the bulk modulus are a function of the strain rate. For example, the adiabatic bulk modulus calculated from velocity measurements can be considered to consist of two parts; one associated with an infinite relaxation time, which is a function of the lattice spacing, and one given by a finite relaxation time, relating to structural rearrangements. Such effects may be important in understanding the relationship between sound velocity measurements as obtained from the Hugoniot equation of state and those from ultrasonic measurements. Sound velocities at different frequencies should be useful in studying these relaxation phenomena.

Other parameters, such as the Grueneisen ratios calculated from sound measurements and shock measurements can be compared to give further theoretical insight of the hydrodynamic model of the material.

As mentioned earlier (equation 20), the slope of the shock velocity - particle velocity curve for metals can be estimated quite closely by means of ultrasonic pressure measurements. Similar ultrasonic experiments should be performed for the increasingly important plastics and nose-cone materials studied in high impulse experiments. Also, with the proper experiment and correct interpretation of data, the pressure dependence of ultrasonic velocities might be

used to explain the discrepancy in the lower pressure region of the shock velocity/particle velocity curve as shown in figure 34.

Theoretical investigations should be organized in two particular directions. First, the relations between the adiabatic longitudinal velocities and the mechanical properties of the laminated materials should be investigated in detail to correlate experimental data to hydrodynamic parameters such as the Grueneisen ratio, reflection coefficients, etc. Secondly, the temperature dependence of longitudinal velocities should be thoroughly investigated as to application in theoretical predictions of high-pressure experiments. For example, the results of the present experiments show that, in general, the longitudinal velocities in most nose-cone materials decrease with increasing temperature. This indicates that rarefaction velocities would likewise decrease with increasing temperature (the internal energy and temperature are higher behind the shock front) and consequently affect such parameters as shock width, since the rarefaction wave effectively terminates the impulse loading. (The impulse is determined by the relative wave front and rarefaction velocities. For a temperature gradient this relation changes if a velocity gradient exists for the rarefaction wave.)

Future ultrasonic/materials investigations at AFWL will involve a measurement of shear velocities as a function of both temperature and pressure for the materials reported here. Longitudinal measurements will likewise be made as a function of uniaxial stress and will be extended in temperature in an attempt to shed light on some of the above problem areas.

APPENDIX I

INTERNAL TEMPERATURES OF THE SAMPLES

During the course of the investigation, sample temperatures were controlled by either a thermostatically controlled oven or an oil bath. The temperature was determined by reading the temperature of the oil or the air temperature near the sample and not the internal temperature of the sample itself. Therefore, to eliminate any temperature gradients in the sample it was necessary to determine the time required for the sample to obtain a uniform temperature. An experimental study was conducted to determine the internal temperatures of the samples as a function of time.

Samples were prepared by drilling small holes in various places of the sample geometry and by inserting iron-constantan thermocuple wires as shown in figure 35. Internal temperature gradients were then determined by measuring the output of each thermocouple. The measurements were made by first bringing the environment to the desired temperature, inserting the sample, and measuring the temperature at each position in the sample as a function of time.

A variety of temperatures were used as the ambient temperature, as indicated in the following graphs, although it was observed that for the range studied the time required for equilibration was fairly independent of initial temperature.

Figures 36 and 37 show the temperature curves obtained by heating samples of Plexiglass and low-density polyethylene in a 70°C oil bath. It is observed that temperature equilibrium is reached in about one hour in both materials.

Figures 38 and 39 show the internal temperature variation in AVCO fiberglass and OTWR at temperatures of 217°C and 212°C, respectively. For these measurements the oven, rather than the oil bath, was used to control the temperature environment. It is noted that the same form of temperature curve exists for both methods, which implies that the waiting period is independent of the original temperature over this range of temperatures.

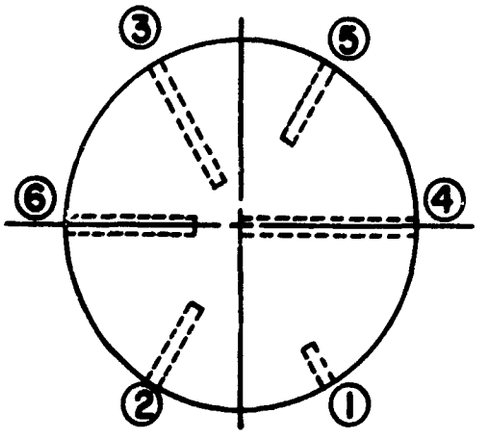

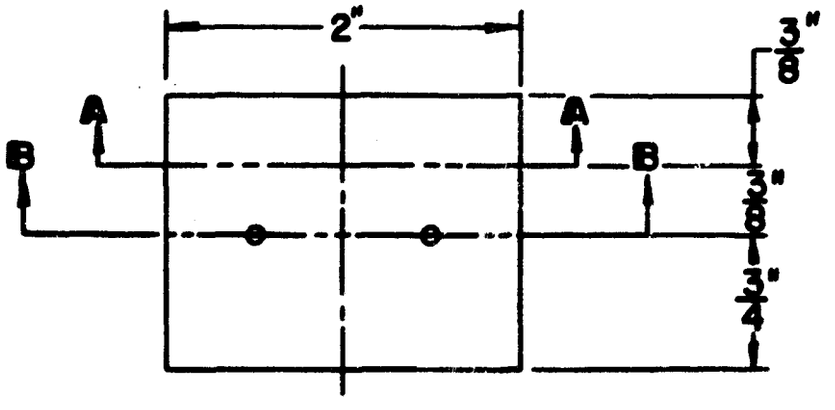

SECTION A-A

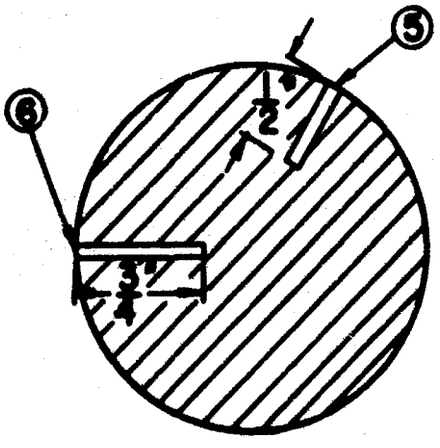

SECTION B-B

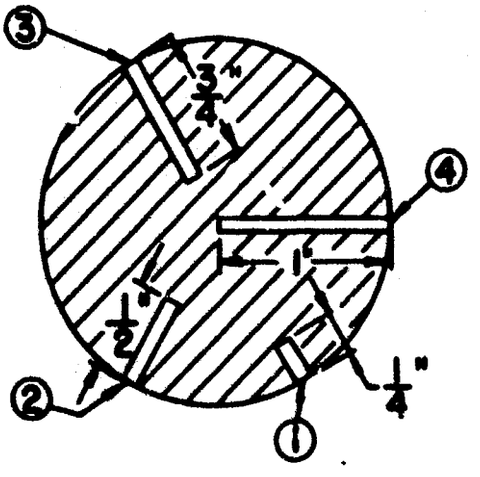

Figure 35. Sketches of Samples Used in Study of Sample Heating

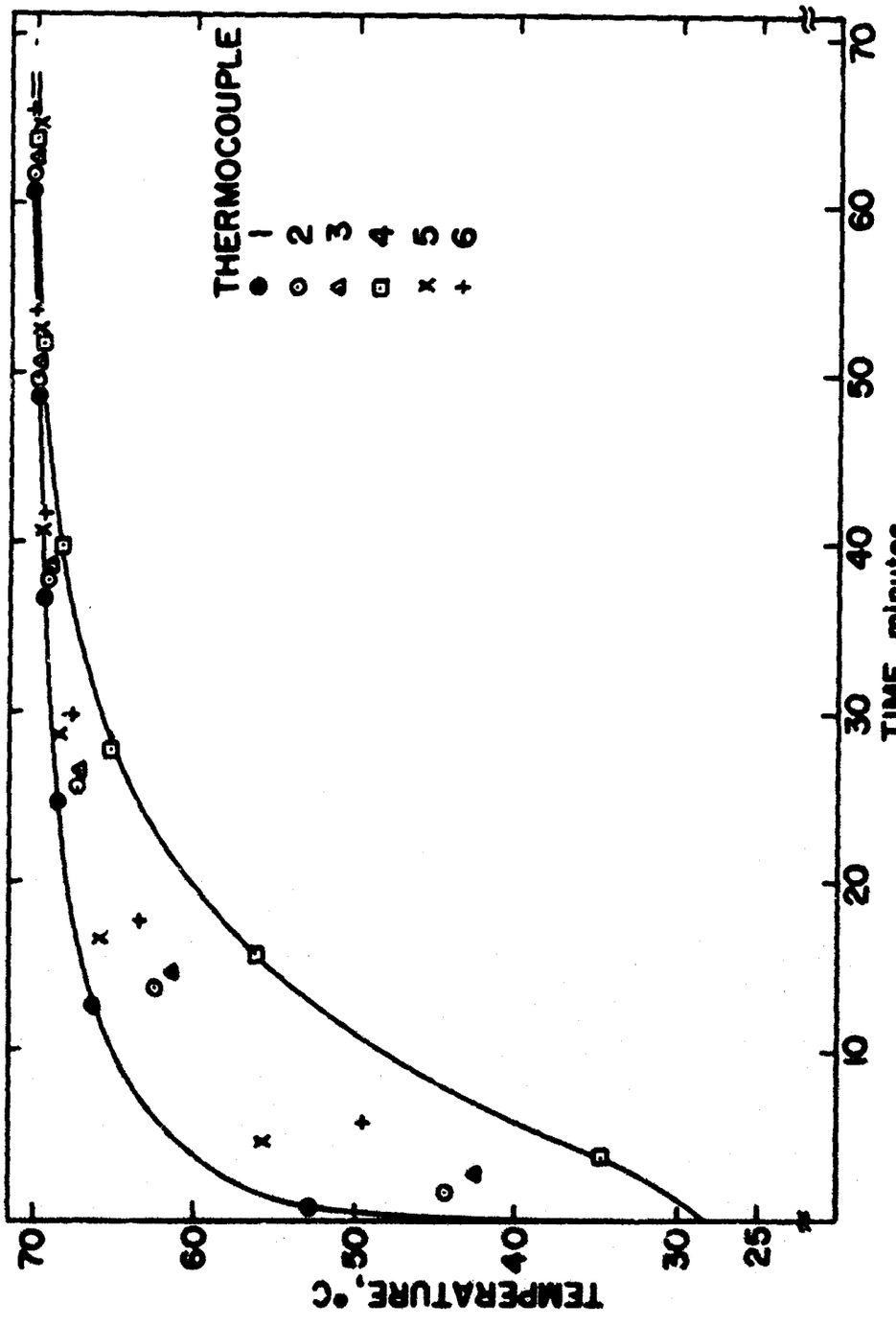

Figure 36. Internal Temperatures of Plexiglass Sample; Initial Temperature of Bath, 70° ± 1/2 °C

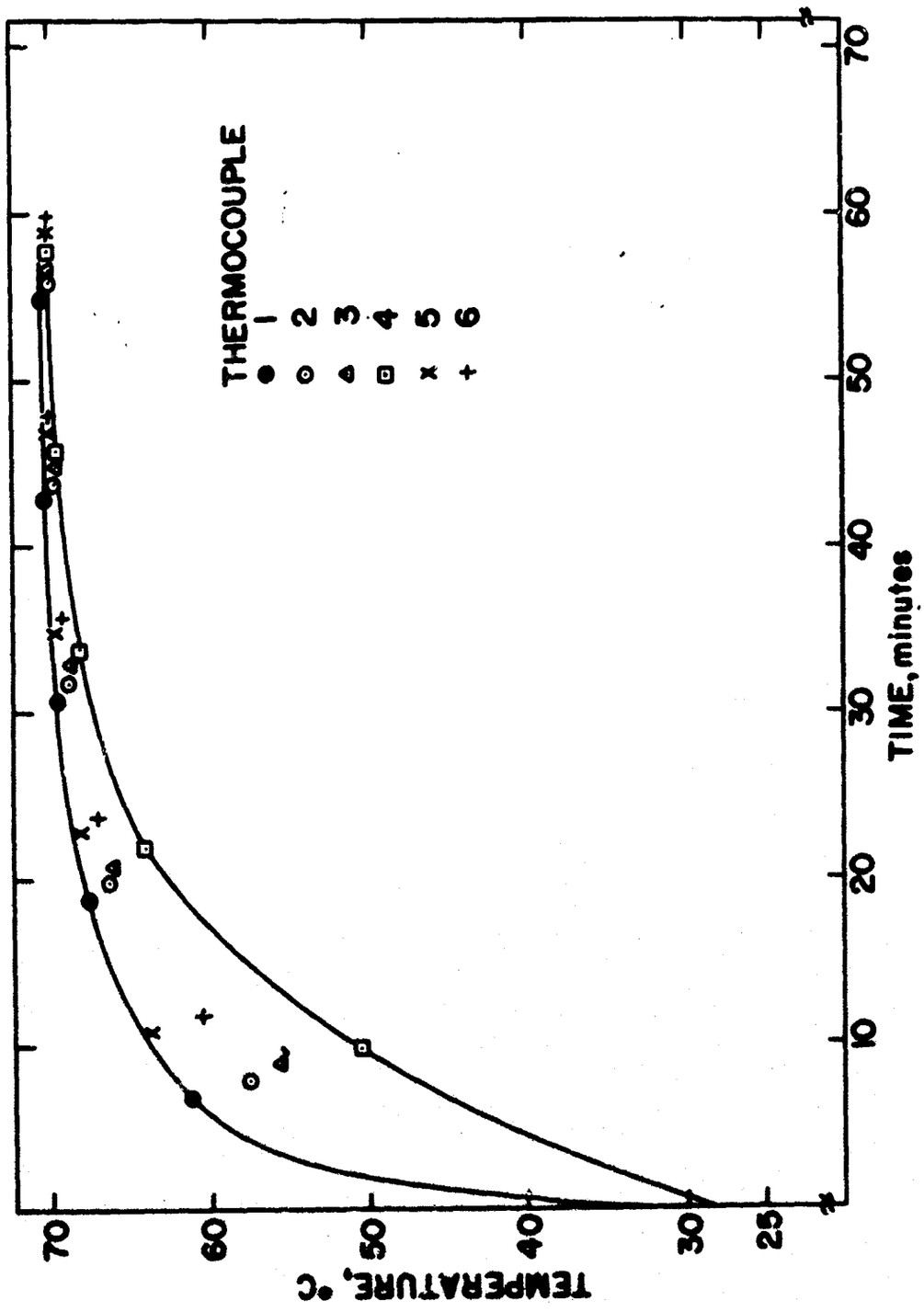

Figure 37. Internal Temperatures of Polyethylene Samples; Initial Temperature of Bath, 70° ± 1/2 °C

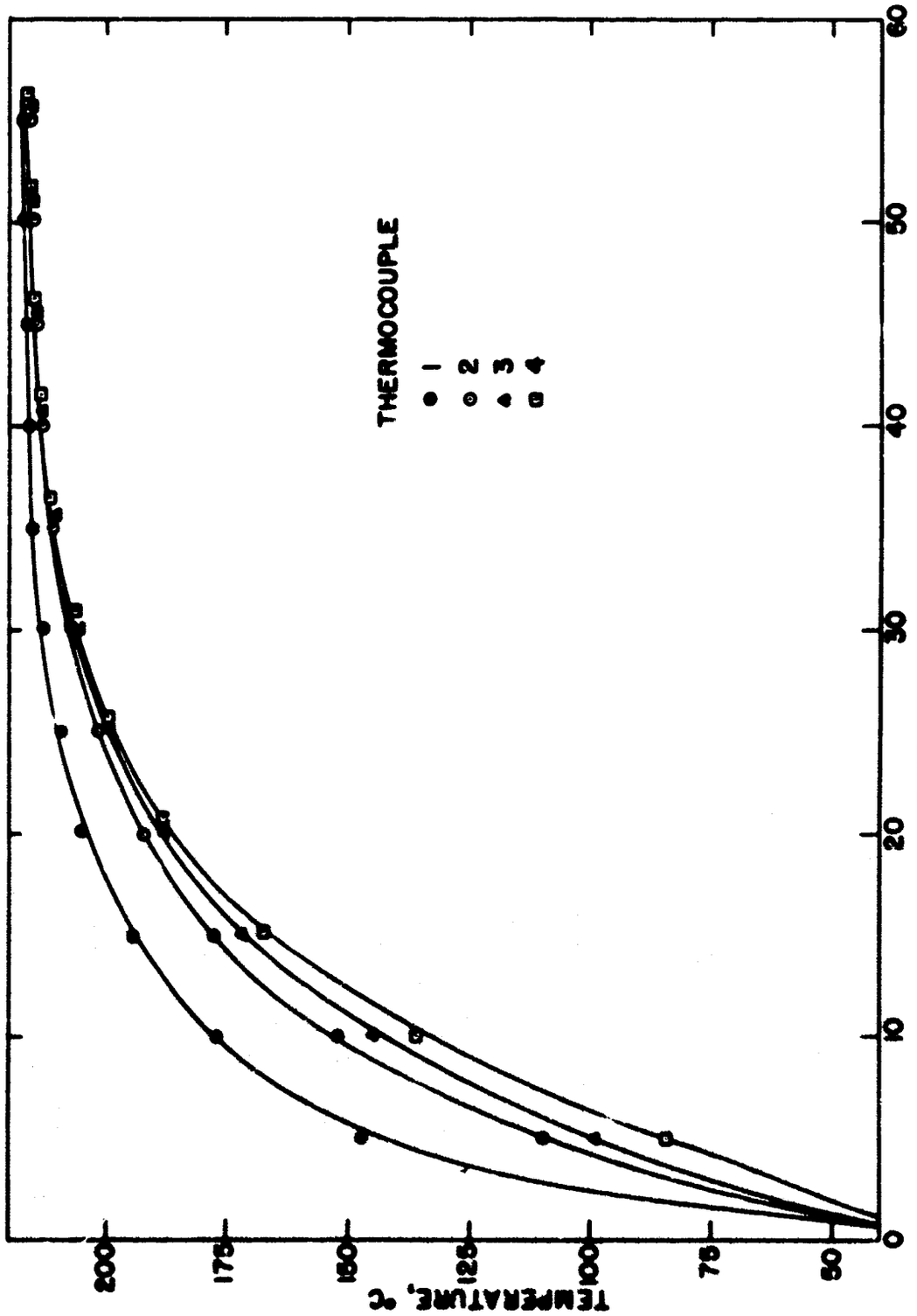

Figure 38. Internal Temperatures of AVCO Fiber Glass; Initial Temperature of Oven, 217° ± °C

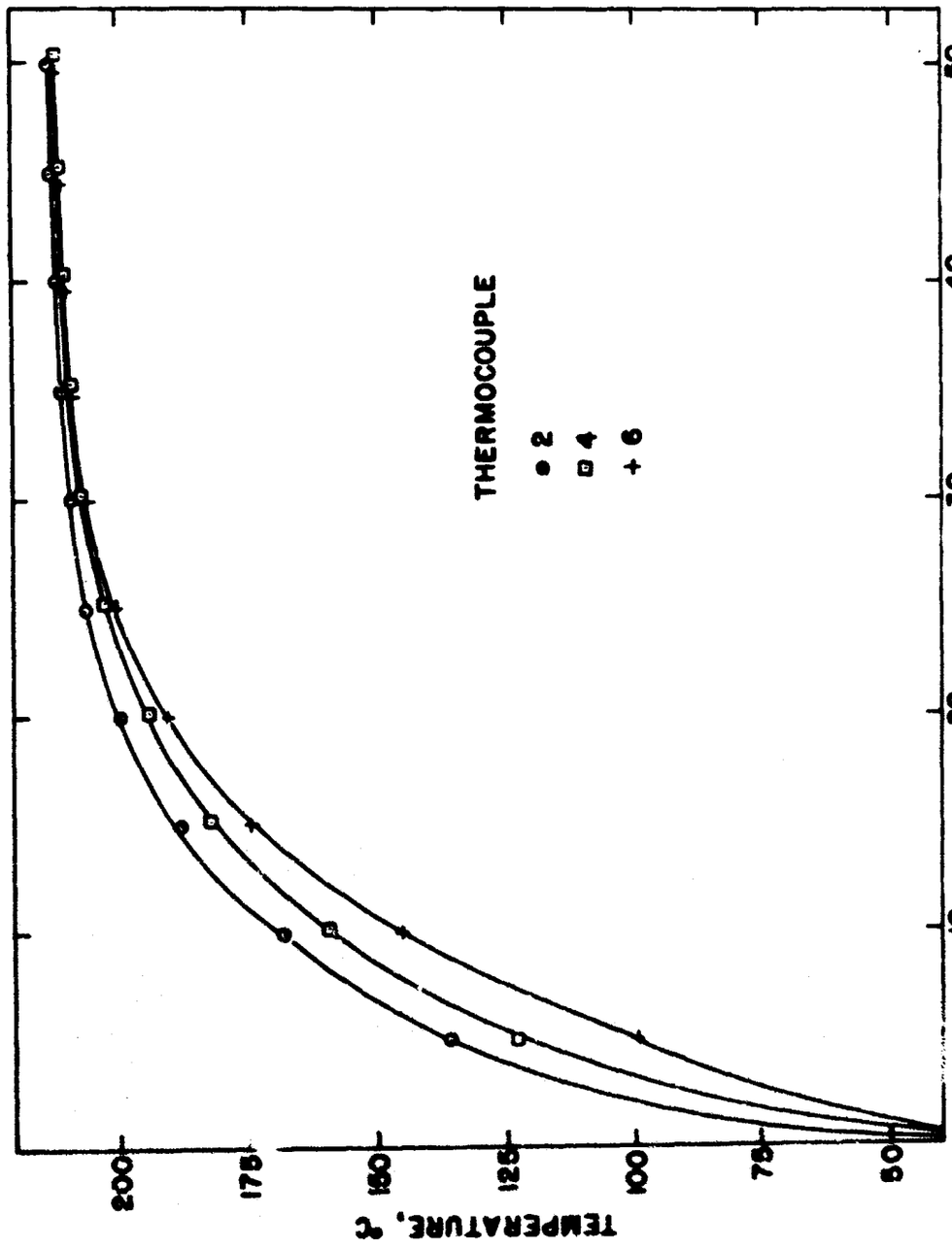

Figure 39. Internal Temperatures of OTWR; Initial Temperature of Oven, 212° ± 1 °C

APPENDIX II

DERIVATION OF EQUATIONS OF MOTION FOR ULTRASONIC WAVES

The generalized form of Hook's law up to the elastic limit is given by (Ref. 14).

$$\sigma_{xx} = c_{11}\varepsilon_{xx} + c_{12}\varepsilon_{yy} + c_{13}\varepsilon_{zz} + c_{14}\varepsilon_{yz} + c_{15}\varepsilon_{zx} + c_{16}\varepsilon_{xy}$$

$$\sigma_{yy} = c_{21}\varepsilon_{xx} + c_{22}\varepsilon_{yy} + c_{23}\varepsilon_{zz} + c_{24}\varepsilon_{yz} + c_{25}\varepsilon_{zx} + c_{26}\varepsilon_{xy}$$

$$\sigma_{zz} = c_{31}\varepsilon_{xx} + c_{32}\varepsilon_{yy} + c_{33}\varepsilon_{zz} + c_{34}\varepsilon_{yz} + c_{35}\varepsilon_{zx} + c_{36}\varepsilon_{xy} \qquad (28)$$

$$\sigma_{yz} = c_{41}\varepsilon_{xx} + c_{42}\varepsilon_{yy} + c_{43}\varepsilon_{zz} + c_{44}\varepsilon_{yz} + c_{45}\varepsilon_{zx} + c_{46}\varepsilon_{xy}$$

$$\sigma_{zx} = c_{51}\varepsilon_{xx} + c_{52}\varepsilon_{yy} + c_{53}\varepsilon_{zz} + c_{54}\varepsilon_{yz} + c_{55}\varepsilon_{zx} + c_{56}\varepsilon_{xy}$$

$$\sigma_{xy} = c_{61}\varepsilon_{xx} + c_{62}\varepsilon_{yy} + c_{63}\varepsilon_{zz} + c_{64}\varepsilon_{yz} + c_{65}\varepsilon_{zx} + c_{66}\varepsilon_{xy}$$

where the coefficients are the elastic constants of the material. The first letter in the subscript of the stress (σ_{ij}) denotes the direction of the stress and the second letter defines the plane in which it is acting. The identical subscripts on the strain (ε_{ij}) refer to extensional and shearing strains. For the elastic energy to be an univalued function of the strain, any coefficient c_{ij} must equal the coefficient c_{ji} (Ref. 14). The number of independent coefficients is thus reduced from 36 to 21. If the material has axes or planes of symmetry, the required number of independent coefficients is correspondingly reduced. For example, cubic symmetry requires only three independent constants, c_{11}, c_{12}, and c_{14}.

In an isotropic material the values of the coefficients must be independent of the chosen coordinate system. This constrains the matrix to two coefficients which are commonly known as the Lame constants, λ and μ. Kolsky (Ref 14) then shows that

$$c_{12} = c_{13} = c_{21} = c_{23} = c_{31} = \lambda$$

$$c_{44} = c_{55} = c_{66} = \mu \tag{29}$$

$$c_{11} = c_{22} = c_{33} = \lambda + 2\mu$$

Equations (28) may then be written as

$$\sigma_{xx} = \lambda\Delta + 2\mu\varepsilon_{xx}; \quad \sigma_{yy} = \lambda\Delta + 2\mu\varepsilon_{yy}; \quad \sigma_{zz} = \lambda\Delta + 2\mu\varepsilon_{zz}$$

$$\sigma_{yz} = \mu\varepsilon_{yz}; \quad \sigma_{zx} = \mu\varepsilon_{zx}; \quad \sigma_{xy} = \mu\varepsilon_{xy} \tag{30}$$

where $\Delta = \varepsilon_{xx} + \varepsilon_{yy} + \varepsilon_{zz}$ represents the change in volume and is called the dilatation.

To obtain the equation of motion for an elastic medium the net forces acting on a small parallelepiped of volume $\delta x\delta y\delta z$ are equated to the rate of change of the momentum in any direction. Consider the net force in the x direction. This is given from the definition of the subscripts on the stresses as

$$\left(\sigma_{xx} + \frac{\partial\sigma_{xx}}{\partial x}\delta x\right)\delta y\delta z - \sigma_{xx}\delta y\delta z + \left(\sigma_{xy} + \frac{\partial\sigma_{xy}}{\partial y}\delta y\right)\delta x\delta z$$

$$- \sigma_{xy}\,\delta x\delta z + \left(\sigma_{xz} + \frac{\partial\sigma_{xz}}{\partial z}\delta z\right)\delta x\delta y - \sigma_{xz}\delta x\delta y \tag{31}$$

where the origin is placed at one corner of the parallelpiped. By Newton's second law of motion the net force is equated to the rate of change of mass times velocity in the x-direction

$$\left(\frac{\partial\sigma_{xx}}{\partial x} + \frac{\partial\sigma_{xy}}{\partial z} + \frac{\partial\sigma_{xz}}{\partial z}\right)\delta x\delta y\delta z = \rho\left(\frac{\partial^2 u}{\partial t^2}\right)\delta x\delta y\delta z \tag{32}$$

where ρ is the density and u is the displacement in the x - direction. Similar equations apply when the displacements in the y and z - directions (v and w, respectively) are considered. The resulting equations for the three directions then become

$$\rho \frac{\partial^2 u}{\partial t^2} = \frac{\partial \sigma_{xx}}{\partial x} + \frac{\partial \sigma_{xy}}{\partial y} + \frac{\partial \sigma_{xz}}{\partial z}$$

$$\rho \frac{\partial^2 v}{\partial t^2} = \frac{\partial \sigma_{yx}}{\partial x} + \frac{\partial \sigma_{yy}}{\partial y} + \frac{\partial \sigma_{yz}}{\partial z} \qquad (33)$$

$$\rho \frac{\partial^2 w}{\partial t^2} = \frac{\partial \sigma_{zx}}{\partial x} + \frac{\partial \sigma_{zy}}{\partial x} + \frac{\partial \sigma_{zz}}{\partial z}$$

Substituting from equation (30) gives for the equation of motion in the x - direction.

$$\rho \frac{\partial^2 u}{\partial t^2} = \frac{\partial}{\partial x}\left(\lambda\Delta + 2\mu\epsilon_{xx}\right) + \frac{\partial}{\partial y}\left(\mu\epsilon_{xy}\right) + \frac{\partial}{\partial z}\left(\mu\epsilon_{xz}\right) \qquad (34)$$

Now consider a point in the undisplaced position which has coordinates $(x + \delta x, y + \delta y, z + \delta z)$, and let the displacement which it has undergone have components $(u + \delta u, v + \delta y, w + \delta w)$. If δx, δy, and δz are sufficiently small,

$$\delta u = \frac{\partial u}{\partial x}\delta x + \frac{\partial u}{\partial y}\delta y + \frac{\partial u}{\partial z}\delta z$$

$$\delta v = \frac{\partial v}{\partial x}\delta x + \frac{\partial v}{\partial y}\delta y + \frac{\partial v}{\partial z}\delta z$$

$$\delta w = \frac{\partial w}{\partial x}\delta x + \frac{\partial w}{\partial y}\delta y + \frac{\partial w}{\partial z}\delta z$$

where $\frac{\partial u}{\partial x}$, $\frac{\partial v}{\partial y}$, $\frac{\partial w}{\partial z}$ represent the fractional expansions and contractions of infinitesimal line elements parallel to the x, y, z direction, respectively, and are respectively denoted by ϵ_{xx}, ϵ_{yy}, ϵ_{zz}. The pairs $\frac{\partial w}{\partial y} + \frac{\partial v}{\partial z}$, $\frac{\partial u}{\partial z} + \frac{\partial w}{\partial x}$, $\frac{\partial v}{\partial x} + \frac{\partial u}{\partial y}$ correspond to the components of shear strain in the planes denoted by their suffixes. These quantities are defined as

$$\varepsilon_{yz} = \frac{\partial w}{\partial y} + \frac{\partial v}{\partial z}$$

$$\varepsilon_{zx} = \frac{\partial u}{\partial z} + \frac{\partial w}{\partial y} \qquad (36)$$

$$\varepsilon_{xy} = \frac{\partial v}{\partial x} + \frac{\partial u}{\partial y}$$

Rotations of the element about a point are given as the difference of the partial derivatives, which Kolsky (Ref. 14) defines as

$$2\bar{w}_x = \frac{\partial w}{\partial y} - \frac{\partial v}{\partial z}$$

$$2\bar{w}_y = \frac{\partial v}{\partial z} - \frac{\partial w}{\partial x} \qquad (37)$$

$$2\bar{w}_z = \frac{\partial v}{\partial x} - \frac{\partial u}{\partial y}$$

Using these definitions the equations of motion become

$$\rho\frac{\partial^2 u}{\partial t^2} = (\lambda + \mu)\frac{\partial \Delta}{\partial x} + \mu\nabla^2 u$$

$$\rho\frac{\partial^2 v}{\partial t^2} = (\lambda + \mu)\frac{\partial \Delta}{\partial y} + \mu\nabla^2 v \qquad (38)$$

$$\rho\frac{\partial^2 w}{\partial t^2} = (\lambda + \mu)\frac{\partial \Delta}{\partial z} + \mu\nabla^2 w$$

Manipulation of these equations gives

$$\rho\frac{\partial^2\Delta}{\partial t^2} = (\lambda + 2\mu)\nabla^2\Delta$$

$$\rho\frac{\partial^2\bar{w}_x}{\partial t^2} = \mu\nabla^2\bar{w}_x \qquad (39)$$

The first equation shows that the dilation Δ is propagated through the medium with velocity $\left[\frac{\lambda + 2\mu}{\rho}\right]^{1/2}$, while the second corresponds to a rotation propagated with a velocity $\left[\frac{\mu}{\rho}\right]^{1/2}$. Thus, waves in the interior of an isotropic elastic solid may be propagated with two different velocities. Waves involving no rotation travel with velocity $c_\ell = \left[\frac{\lambda + 2\mu}{\rho}\right]^{1/2}$ and waves involving no dilation travel with velocity $c_t = \left[\frac{\mu}{\rho}\right]^{1/2}$.

APPENDIX III

COMPARISON OF ADIABATIC LONGITUDINAL VELOCITY AND THE EXTRAPOLATED SHOCK VELOCITY

As shown in Appendix II the longitudinal wave velocity for small stresses in a homogeneous, unbounded, isotropic medium is given by

$$c_\ell = \sqrt{\frac{\lambda + 2\mu}{\rho}} \tag{40}$$

where λ and μ are the adiabatic Lamé constants. As previously shown, for infinitesimal displacements the equations governing a longitudinal wave propagating in the x - direction ($\varepsilon_{yy} = \varepsilon_{zz} = 0$) are given as

$$\sigma_{xx} = (\lambda + 2\mu)\varepsilon_{xx} \tag{41}$$

Since $\varepsilon_{xx} = \frac{\partial u}{\partial x}$, where u is the displacement of a point in the body by the stress σ_{xx}, Morgan (Ref. 26) shows that equation (40) can be written as

$$c_\ell = \sqrt{\frac{\sigma_{xx}}{\rho}\,\frac{\partial x}{\partial u}} = \sqrt{\frac{\partial \sigma_{xx}}{\partial \rho}} \tag{42}$$

This equation applies only when the induced stresses imposed on the sample by the wave are small.

If a large stress is induced in the material by some means such as that produced by a high velocity impact, the wave velocity, $U_s = \sqrt{\left(\frac{\partial P}{\partial \rho}\right)_s}$, will be constant and independent of the stress level if the induced stress is less than the elastic limit. In this region the elastic constants alone determine the slope of the one-dimensional strain curve which has a slope of $\lambda + 2\mu$. When plastic yielding occurs the curve tends to parallel the hydrostat which has a slope of $\left(\lambda + \frac{2}{3}\mu\right)$ (Ref. 28). This transition regio. where the strain slope changes from $\left(\lambda + \frac{2}{3}\mu\right)$ is usually called the Hugoniot elastic limit.

In this discussion it is assumed that shear effects have an important effect on the equation of state. Consider the stress-strain plot in figure 40. Below the elastic limit (point A) any stress disturbance will propagate with a constant velocity as normally measured in the laboratory. For pressures between A and B, where B refers to the inflection point at which $\left(\frac{\partial P}{\partial \rho}\right)$ starts increasing with increasing ρ, the stress wave propagation velocity decreases with increasing stress. The wave will thus break up into a two wave structure - the elastic portion traveling at the dilatational velocity and the plastic portion traveling with a velocity given by the value of $\left(\frac{\partial P_x}{\partial \rho}\right)$ at that pressure, where P_x refers to the one dimensional stress.

From the point B to C, $\left(\frac{\partial P_x}{\partial \rho}\right)$ increases with increasing stress level, with the net effect of an unstable shock wave preceeded by an elastic and plastic precursor. For pressures greater than that corresponding to point C the velocity of propagation of the disturbance is greater than the elastic wave velocity and a single shock front occurs.

For a fluid or material in which μ is zero the stress strain curve of figure 40 does not show the inflection behavior and $\left(\frac{\partial P}{\partial \rho}\right)$ is a monotonically increasing function of the strain after the elastic limit is exceeded (if no phase transitions are present). Morgan (Ref. 26) states that in this region the bulk modulus is then given by λ rather than $\lambda + \left(\frac{2}{3}\mu\right)$.

Morgan (Ref. 26) discusses the extrapolated shock velocity from a theoretical point of view for two situations. His predictions indicate that for measurements taken in the region where the inflection due to shear rigidity occurs (see figure 40), the use of $\sqrt{\left(\frac{\partial P}{\partial \rho}\right)_s}$ as the wave velocity and the extrapolation of the data to zero pressure yields the sound velocity as normally measured for very small stresses. The extrapolated velocity should then be given as

$$U_s(P = 0) = c_l = \sqrt{\left(\frac{\lambda + 2\mu}{\rho}\right)_{P = 0}} \qquad (43)$$

The AVCO report (Ref. 26) states that for pressures well above the inflection point the shear rigidity, μ, can be neglected relative to the magnitude the volume compressibility, λ, as previously noted. In this region it has been found experimentally that the shock velocity is usually a linear function of

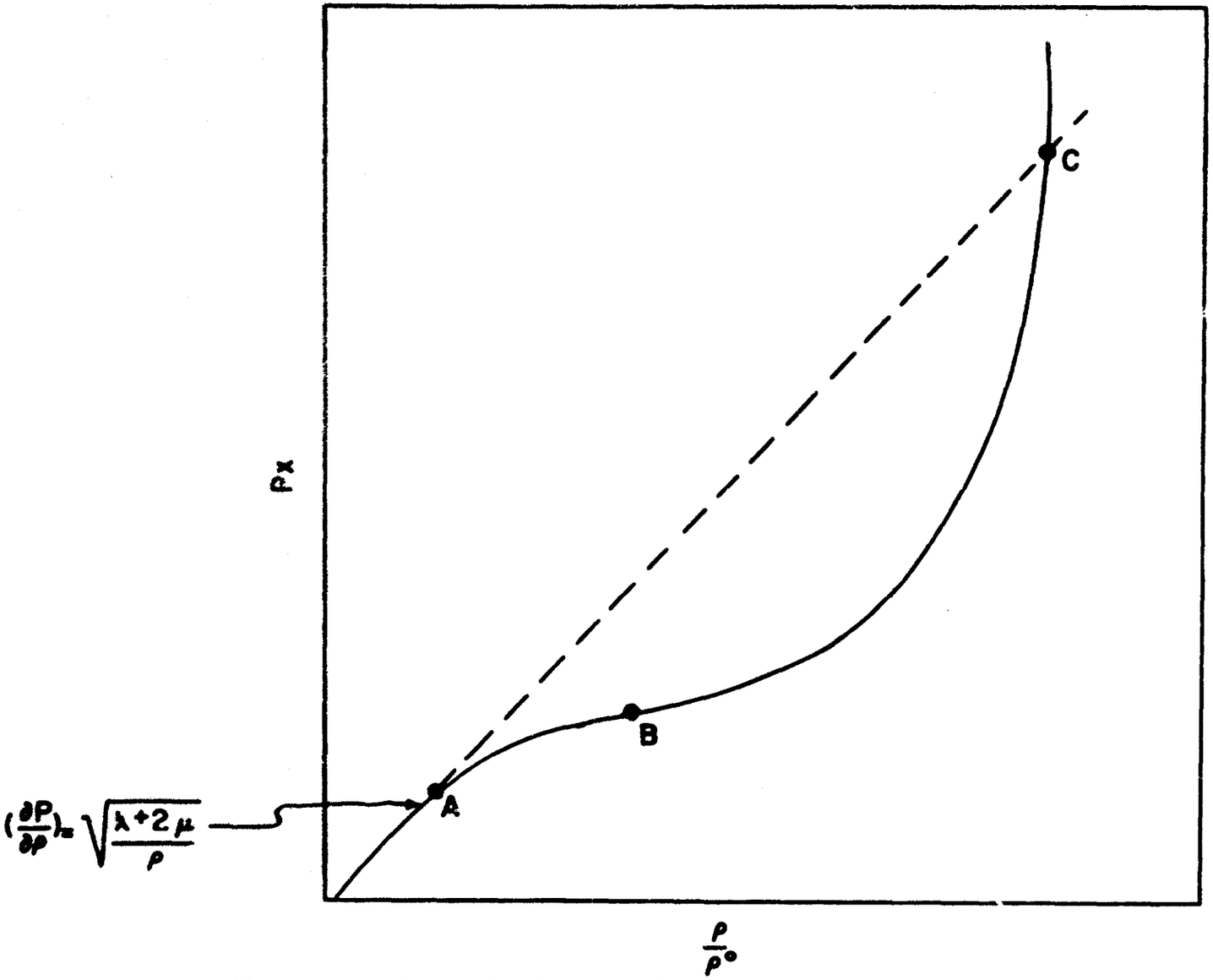

Figure 40. Dynamic Stress-Strain Curve for a Material with Shear Rigidity

the particle velocity. Thus, using this hypothesis, the report shows that the extrapolated value of shock velocity should be

$$U_s(P = 0) = \sqrt{\left(\frac{\lambda}{\rho}\right)_{P=0}} = c^* \qquad (44)$$

From the relations given in equation (39), equation (44) can be expressed as a function of longitudinal and transverse velocities at atmospheric pressure. Table VI lists some experimentally extrapolated velocities $U_s(P = 0)$ and the corresponding predicted values, c*, of equation (44) as listed in the AVCO report. It is noted that AVCO's predicted values are generally lower than the actual extrapolated values, particularly in the case of Beryllium.

The table also lists the adiabatic longitudinal velocities at atmospheric pressure, c_ℓ, and some values under the heading c_o which will presently be explained.

Table VI

COMPARISON OF EXTRAPOLATED SHOCK VELOCITIES AND CALCULATED VALUES

Metal	c_ℓ mm/μsec	$U_s(P = 0)$ mm/μsec	c* mm/μsec	c_o mm/μsec
Gold	3.24	3.059	2.77	2.94
Beryllium	12.89	7.975	2.96	7.80
Magnesium	5.77	4.493	3.82	4.57
Nickel	6.04	4.667	4.32	4.95
Tin	3.32	2.668	2.39	2.64
Zinc	4.21	3.042	2.43	3.15
Aluminum	6.42	5.32	4.75	5.37
Silver	3.65	3.215	2.85	3.13

The predicted value of the extrapolated shock velocity as given by equation (18) can be derived using the assumption of the Hugoniot equation of state that the pressure can be expressed

$$P(\mu') = \left(\frac{\partial P}{\partial \mu'}\right)_o \mu' + 1/2!\left(\frac{\partial^2 P}{\partial \mu'^2}\right)_o \mu'^2 + 1/3!\left(\frac{\partial^3 P}{\partial \mu'^3}\right)\mu'^3 + \ldots \qquad (45)$$

neglecting the term involving the internal energy. Assuming that $P(\mu')$ is continuous, that is, that inflective or transitive behavior does not exist the definition of the shock velocity can be used to calculate the value in the limit of $P \to P_o$, $\mu' \to o$

$$U_s^2(P = 0) = \lim_{\mu' \to o} \left(\frac{\partial P}{\partial \rho}\right)_s = \left(\frac{\partial P}{\partial \mu}\right)_{o\,s} \qquad (46)$$

Using the relation

$$\mu' = \frac{\rho}{\rho o} - 1 = \frac{V_o}{V} - 1 \qquad (47)$$

equation (46) becomes

$$U_s^2(P = 0) = \left[\frac{-V\left(\frac{\partial P}{\partial V}\right)_s}{\rho}\right]_o \qquad (48)$$

where the derivative is to be evaluated at the initial conditions. From the definition of the adiabatic bulk modulus, equation (48) can be expressed as

$$U_s^2(P = 0) = \frac{B_s}{\rho o} \qquad (49)$$

This last step results in the same extrapolated value of shock velocity that is predicted in the AVCO report (equation 44) if it is assumed that the bulk modulus at high pressure is given by λ and should consequently extrapolate to $\lambda_{P=0}$ under normal conditions. It is assumed here that the extrapolated value corresponds to a hydrostatic compression and thus is related to the bulk modulus $\left[\lambda + \frac{2}{3}\mu\right]$ as measured under atmospheric pressure. This assumption is partially supported by Bridgman's measurements on the isothermal compressibilities. His data in the upper pressure range generally agree to within a few percent of the data in the lower pressure range ($\sim$100 kb) of dynamic experiments (for example, see Walsh's comparison (Ref. 29) and some of Bridgman's original data (Ref. 30)). Bridgman's data for the compression $\frac{\Delta V}{V_o}$ are fitted by a quadratic expression in pressure: $\frac{\Delta V}{V_o} = -aP-bP^2$, where a is the isothermal compressibility (reciprocal of isothermal bulk modulus $\left[\lambda + \frac{2}{3}\mu\right]$ and b is a constant. If Bridgman's data, corrected to the adiabat (to correspond to the approximately adiabatic dynamic measurements), are assumed to be a continuous extension of the dynamic measurements, than the slope of static curve near zero pressure should correspond to the extrapolated slope of the dynamic curve. Under these assumptions the extrapolated shock velocity should be given as the square root of $(\lambda + 2/3\mu)_{P=o}$, which by equation (9) can be further related to longitudinal and shear velocities.

$$U_s^2(P = o) = c_l^2 - 4/3\ c_t^2 \qquad (50)$$

which was previously defined as c_o. The assumptions used in evaluating this derivative near zero pressure also apply to the justification of equation (23) since the derivative in both cases is the same.

The actual situation is much more complicated than this simple treatment, and some of the assumptions used here are certainly not valid in all cases. However, it is interesting to note in Table VI the fair agreement between the predicted values of extrapolated shock velocity, c_o, from equation (50) and those obtained by experimental extrapolation $U_s(P = o)$.

Equation (50) rests upon the assumptions that (1) the data can be expressed by a smooth curve of the form of equation (45), (2) that the Hugoniot is sufficiently near the adiabat, so that $U_s^2 = \left(\frac{\partial P}{\partial \rho}\right)_s$ is valid, (3) that no transitions or inflections occur in the observed pressure range, (4) that the shock

velocity is given by a linear relation with the particle velocity, and (5) that the internal energy term in the pressure can be neglected.

Assumptions (1) and (3) are in general justified for pressure experiments above 100 kb (Ref. 29). The Hugoniot is usually within a few percent of the adiabat so that assumption (2) is a fair approximation. As mentioned earlier, the linear relationship between shock and particle velocity represents only the average behavior of a large number of substances. Therefore, assumption (4) must be evaluated for the individual experiment. The effect that the energy term has on the predictions of equation (50) is not now known, but might be responsible for some of the discrepancies in Table VI.

APPENDIX IV

EVALUATION OF GRUENEISEN RATIO FROM A KNOWLEDCE OF SOUND VELOCITIES

The Gruenelsen constant is defined as (Ref. 26),

$$\gamma(V,T) = V\left(\frac{\partial P}{\partial E}\right)_V = \frac{V}{c_v(V,T)}\left[-\frac{\left(\frac{\partial V}{\partial T}\right)_P}{\left(\frac{\partial V}{\partial P}\right)_T}\right] \tag{51}$$

where V is the specific volume $\frac{1}{\rho}$, E is the internal energy, and c_v is the specific heat at constant volume. Now,

$$\beta \equiv \frac{1}{V}\left(\frac{\partial V}{\partial T}\right)_P$$

$$B_T \equiv -V\left(\frac{\partial P}{\partial V}\right)_T \tag{52}$$

where β is the volume coefficient of expansion and B_T is the isothermal bulk modulus. It is desired to express equation (52) in terms of the acoustic velocities, which are obtained under adiabatic conditions. This implies that the associated elastic moduli must be the adiabatic rather than the isothermal moduli. With this in mind and applying the relation between the adiabatic and isothermal bulk modulus the last part of equation (52) becomes,

$$\frac{B_s}{B_T} = \frac{c_p}{c_v} \tag{53}$$

Using this relation and the first part of equation (52) yields for equation (51)

$$\gamma(V,T) = \frac{\beta B_s}{\rho c_p} \tag{54}$$

The adiabatic bulk modulus is defined in terms of the Lamé constants for an isotropic homogeneous medium (Ref. 1) as

$$B_s = \lambda + \frac{2}{3}\mu \tag{55}$$

The dilatational, c_ℓ, and transverse, c_t, velocities in an isotropic medium are shown in Appendix II to be

$$c_\ell = \sqrt{\frac{\lambda + 2\mu}{\rho}}$$

$$c_t = \sqrt{\frac{\mu}{\rho}} \tag{56}$$

so that with equations (55) and (56) equation (54) becomes,

$$\gamma(V,T) = \frac{\beta}{c_p}\left[c_\ell^2 - 4/3\ c_t^2\right] = \frac{\beta}{c_p}\ c_o^2 \tag{57}$$

Equation (57) gives the value of the Grueneisen constant for isotropic materials as determined from sound velocity measurements and compares closely with that computed by other means. The following table shows some values of the ratio γ_s computed from shock measurements and extracted from the AVCO report (Ref. 26) and the corresponding values γ_u calculated from sonic measurements. The necessary quantities used in equation (57) were handbook values.

TABLE VII

COMPARISON OF GRUENEISEN RATIOS CALCULATED FROM SHOCK MEASUREMENTS TO THOSE CALCULATED FROM ULTRASONIC VELOCITIES

Material	γ_s	γ_u
Beryllium	1.17	1.29
Copper	2.04	2.40
Magnesium	1.46	1.56
Tin	2.03	2.05
Zinc	2.38	2.30
24 ST Aluminum	2.13	2.25
Silver	2.47	2.45

APPENDIX V

CALCULATION OF TRANSMISSION COEFFICIENTS AT IMPEDANCE MISMATCHES

The purpose of this section will be to derive the correction factor C used in equation (4). Consider the following sketch:

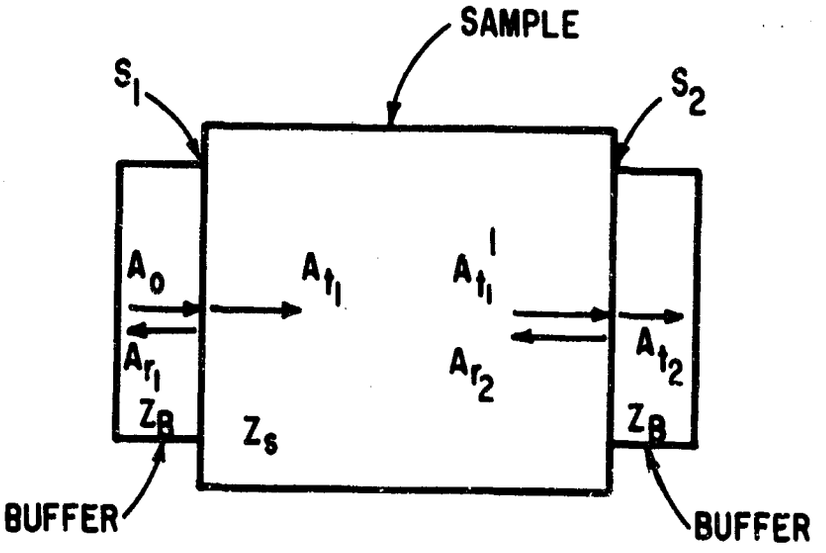

Here a sample of impedance $Z_s(=\rho_s c_s)$ is inserted between two buffers of impedance $Z_B(=\rho_B c_B)$. Neglecting the small loss through the buffers the input amplitude A_o and the output A_{t_2} is measured. From the ratio of these two signals it is desired to calculate the amplitudes A_{t_1} and A_{t_1}' which give a measure of attenuation of the signal through the specimen.

At surface S_1 the transmission ratio is given by $t = \frac{2Z_S}{Z_B + Z_S}$ so that the amplitude A_{t_1} is given by

$$A_{t_1} = \frac{2Z_S}{Z_B + Z_S} A_o \qquad (58)$$

and at surfaces S_2, A_{t_2} is given by

$$A_{t_2} = \frac{2Z_B}{Z_B + Z_S} A_{t_1}' \tag{59}$$

Now the natural logarithm of the two amplitudes A_{t_1}'/A_{t_1} is by definition, the attenuation through the sample in Nepers, $-\alpha$ where e^{α} is the ratio of the amplitude at a point x to that at the point x + dx. The corresponding attenuation in decibels per unit length L is $L = 20\log_{10}(e^{\alpha}) = 8.686\,\alpha$. By definition

$$\frac{A_{t_1}'}{A_{t_1}} = e^{-\alpha d} \tag{60}$$

where d is the sample thickness.
Taking logs

$$\alpha d \log_{10} e = \log_{10} \frac{A_{t_1}}{A_{t_1}'}$$

$$20\alpha \log_{10} e = \frac{1}{d}\, 20\log_{10} \frac{A_{t_1}}{A_{t_1}'} \tag{61}$$

or

$$L = \frac{1}{d}\, 20\log_{10} \frac{A_{t_1}}{A_{t_1}'}$$

Substituting in the values of A_{t_1} and A_{t_1}' in terms of known quantities A_o, A_{t_2}, gives for L

$$L = \frac{1}{d}\left[20\log \frac{2Z_A}{Z_B + Z_S} A_o - 20\log \frac{Z_B + Z_S}{2Z_B} A_{t_2} \right] \tag{62}$$

$$L = \frac{1}{d}\left[20 \log \frac{A_o}{A_{t_2}} - 20 \log \frac{\left(Z_B + Z_S\right)^2}{4Z_B Z_S}\right] \qquad (63)$$

$$= \frac{1}{d}\left[20 \log \frac{A_o}{A_{t_2}} - C\right]$$

This correction factor C is the one defined in equation (4) and accounts for the impedance mismatch at the boundaries. For materials in which the impedances are similar to that of aluminum the correction factor is negligible. However, for the foam materials the impedance mismatch between the buffer and specimen was very large so that the correction factor was on the order of 20 db.

This correction does not account for other influences such as surface defects, impedance of the bond, etc. which must be evaluated in other ways. However, for the high loss epoxy foam discussed in Section III, the term C in equation (63) was found to be the most significant factor in correcting for the total loss.

REFERENCES

1. Sullivan, P. F., "Bonding Methods and a Bonding Clamp for Ultrasonic Measurements," J. Acoust. Soc. Am., 34, p. 1879, December 1962.

2. Tu, L. Y., Brennan J. N. and Sauer, J. A. "Dispersion of Ultrasonic Pulse Velocity in Cylindrical Rods," J. Acoust. Soc. Am., 27, p. 550, May 1955.

3. Eros, S., and Reitz, J. R., "Elastic Constants by the Ultrasonic Pulse Echo Method," J. Appl. Phys. 29, p. 683, April 1958.

4. Nolle, A. W., and Sieck, P. W. "Longitudinal and Transverse Ultrasonic Waves in a Synthetic Rubber," J. Appl. Phys. 23, p. 888, August 1952.

5. Davidse, P. D., Waterman, H. I., and Westerdyk, J. B., J. Polymer Sci., 59, p. 389, 1962.

6. Anderson, R., Sandia Corporation, Albuquerque, New Mexico, private communication.

7. Horio, M., and Onogi, S., J. Appl. Phys. 22, p. 971, July 1951.

8. Mead, M., D & R Pilot Plants, Inc., Hazardville, Conn., private communication.

9. Pears, C. D., et al., The Thermophysical Properties of Plastic Materials from - 50°F to over 700°F. TDR No. ML-DTDR 64-87, II, AF Materials Laboratory, p. 56, 1964.

10. Howse, P. T. et al., The Thermal Properties of Some Plastic Panels, TR 60-657, Wright Air Development Division, Wright-Patterson AFB, Ohio, p. 57, 1960.

11. Dunegan, H., Lawrence Radiation Laboratory, Livermore, Calif., private communication.

12. Nolle, A. W., J. Polymer Sci, 5, pp 1-54, 1950.

13. Ivey, D. G., Mrowca, H. I., and Guth, E., J. Appl. Phys., 20, p. 486, 1949.

14. Lamb, H., Stress Waves in Solids, Dover Publications, Inc., New York, 1963.

15. Mason, W. P., Electromechanical Transducers and Wave Filters, D. Van Nostrand Co., Inc., New York, p. 304, 1964.

16. Mason, W. P., Baker, W. O., McSkimin, H. J., and Heiss, J. H., Phys. Rev. 75, p. 936, 1949.

17. Urzendowski, Sr. Rosalie, AFWL, Kirtland AFB, NM, private communication.

18. Dunegan, H. L., "High Temperature Dynamic Modulus Measurements by Use of Ultrasonics," Materials Evaluation, June 1964.

19. Mason, W. P., ed., Physical Acoustics, Vol I, Part A, Academic Press, New York, 1964.

20. Al'tshuler, L. V., et al., JETP 11, No. 4, October 1960.

21 Guenther, A. H., "Production of Strong Shocks in Plastics by Ultra-Short Impulsive Loading," ASTM, Special Technical Publication No. 336, 1962.

22. Fowles, G. R., Attenuation of the Shock Wave Produced in a Solid by a Flying Plate, Poulter Laboratories Technical Report, 009-59, August 1959.

23. Stuiver, W., Effects of Pulse-Spreding on Thick Base Laminates, Poulter Laboratories Technical Summary Report No. 4, SRI Project No. PGU-3772, July 1963.

24. Paul, W., Warschauer, D. M., Solids Under Pressure, McGraw-Hill Book Company, Inc., San Francisco, 1963.

25. Penning, J. R., et al., "Negative Equation - of - State and Spall Criteria", RTD-TDR-63, prepared under AF Contract AF 29(601)-5363, July 1963.

26. Morgan, D. T., et al., (U) "Optimizing Reentry Vehicle Materials to a High-Altitude Nuclear Effect," RTD-TDR-63-3018, August 1963. (Secret RD)

27. Allen, R. G., (U) "A Study of X-Ray Countermeasure Methods," AFSWC-TDR-62-86, October 1962. (Secret RD)

28. Lundergan, C. D., Barker, L. M., Herman, W., J. Appl. Phys. 35, April 1964.

29. Walsh, J. M., et al., Phys. Rev. 108, p. 196, October 1957.

30. Bridgman, P. W., Proc. Amer. Acad., 77, p. 189, 1949.

Unclassified

Security Classification

DOCUMENT CONTROL DATA - R&D

(Security classification of title, body of abstract and indexing annotation must be entered when the overall report is classified)

1. ORIGINATING ACTIVITY (Corporate author)	2a. REPORT SECURITY CLASSIFICATION
Air Force Weapons Laboratory Kirtland Air Force Base, New Mexico	Unclassified
	2b GROUP

3. REPORT TITLE

ULTRASONIC WAVE VELOCITY - TEMPERATURE STUDIES IN SEVERAL PLASTICS, PLASTIC FOAMS, AND NOSE-CONE MATERIALS

4. DESCRIPTIVE NOTES (Type of report and inclusive dates)

April 1964 to June 1965

5. AUTHOR(S) (Last name, first name, initial)

Asay, James R., Lt, USAF; Dorr, Anton J., Lt, USAF; Arnold, Ned D., Capt, USAF; Guenther, Arthur H., Dr.

6. REPORT DATE	7a. TOTAL NO. OF PAGES	7b. NO. OF REFS
March 1966	118	30

8a. CONTRACT OR GRANT NO.	9a. ORIGINATOR'S REPORT NUMBER(S)
b. PROJECT NO. 5710	AFWL-TR-65-188
c. SUBTASK 15.018	9b. OTHER REPORT NO(S) (Any other numbers that may be assigned this report)
d.	

10. AVAILABILITY/LIMITATION NOTICES This document is subject to special export controls and each transmittal to foreign governments or foreign nationals may be made only with prior approval of AFWL (WLRE), Kirtland AFB, NM 87117. Distribution is limited because of the technology discussed in the report.

11. SUPPLEMENTARY NOTES	12. SPONSORING MILITARY ACTIVITY
	AFWL (WLRE) Kirtland AFB, NM

13. ABSTRACT An experimental study with two specific aims was conducted at the Air Force Weapons Laboratory: (1) to show the relationship between temperature and velocity of longitudinal ultrasonic waves through several plastics and nose-cone materials and (2) to establish a convenient apparatus for the determination of elastic properties of materials. The velocity-temperature data were needed for use in another research project where certain inputs were necessary to more completely describe materials under shock-loaded conditions. The experimental procedure was based on measuring the transit times required for ultrasonic waves in the low-megacycle range to pass through samples of different thicknesses. The resulting accuracy for most of the measurements is within about 1 to 2 percent. The temperature range of the measurements extended between room temperature and about 125°C, with a few measurements to 250°C. Velocity-temperature curves were determined for nylon, low- and high-density polyethylene, plexiglass (polymethylmethacrylate), Delrin Acetal, teflon. Curves were also drawn for several re-entry vehicle nose-cone materials, including chopped nylon phenolic, Castable 124, Avcoat I and 19, pyrolytic graphite, General Electric Phenolic Fibre Glass, Phenolic Carbon, Tape Wound Nylon Phenolic, Rad 58B, Rad 60, and some solid epoxy foams. Less complete data were obtained for Avco phenolic fiber glass and Oblique Tape Wound Refrasil. The angular dependence of velocity was measured for several layered materials, and it was found that the velocity was very dependent on the direction propagation. For most of the materials studied the velocity was found to decrease more or less linearly with increasing temperature and normally was about 9 - 20 percent lower at 100°C than at room temperature.

DD FORM 1 JAN 64 1473

Unclassified

Security Classification

Unclassified

Security Classification

14. KEY WORDS	LINK A		LINK B		LINK C	
	ROLE	WT	ROLE	WT	ROLE	WT
Ultrasonics						
Longitudinal velocity in nose-cones						
Temperature dependence of velocity						
Velocity in laminates and composites						
Dependence of velocity and lamination angle						
Velocity in solid epoxy foam						
Dependence of velocity and density						
Adiabatic velocity in nose-cones						

INSTRUCTIONS

1. ORIGINATING ACTIVITY: Enter the name and address of the contractor, subcontractor, grantee, Department of Defense activity or other organization *(corporate author)* issuing the report.

2a. REPORT SECURITY CLASSIFICATION: Enter the overall security classification of the report. Indicate whether "Restricted Data" is included. Marking is to be in accordance with appropriate security regulations.

2b. GROUP: Automatic downgrading is specified in DoD Directive 5200.10 and Armed Forces Industrial Manual. Enter the group number. Also, when applicable, show that optional markings have been used for Group 3 and Group 4 as authorized.

3. REPORT TITLE: Enter the complete report title in all capital letters. Titles in all cases should be unclassified. If a meaningful title cannot be selected without classification, show title classification in all capitals in parenthesis immediately following the title.

4. DESCRIPTIVE NOTES: If appropriate, enter the type of report, e.g., interim, progress, summary, annual, or final. Give the inclusive dates when a specific reporting period is covered.

5. AUTHOR(S): Enter the name(s) of author(s) as shown on or in the report. Enter last name, first name, middle initial. If military, show rank and branch of service. The name of the principal author is an absolute minimum requirement.

6. REPORT DATE: Enter the date of the report as day, month, year, or month, year. If more than one date appears on the report, use date of publication.

7a. TOTAL NUMBER OF PAGES: The total page count should follow normal pagination procedures, i.e., enter the number of pages containing information.

7b. NUMBER OF REFERENCES: Enter the total number of references cited in the report.

8a. CONTRACT OR GRANT NUMBER: If appropriate, enter the applicable number of the contract or grant under which the report was written.

8b, 8c, & 8d. PROJECT NUMBER: Enter the appropriate military department identification, such as project number, subproject number, system numbers, task number, etc.

9a. ORIGINATOR'S REPORT NUMBER(S): Enter the official report number by which the document will be identified and controlled by the originating activity. This number must be unique to this report.

9b. OTHER REPORT NUMBER(S): If the report has been assigned any other report numbers *(either by the originator or by the sponsor)*, also enter this number(s).

10. AVAILABILITY/LIMITATION NOTICES: Enter any limitations on further dissemination of the report, other than those imposed by security classification, using standard statements such as:

(1) "Qualified requesters may obtain copies of this report from DDC."

(2) "Foreign announcement and dissemination of this report by DDC is not authorized."

(3) "U. S. Government agencies may obtain copies of this report directly from DDC. Other qualified DDC users shall request through _____."

(4) "U. S. military agencies may obtain copies of this report directly from DDC. Other qualified users shall request through _____."

(5) "All distribution of this report is controlled. Qualified DDC users shall request through _____."

If the report has been furnished to the Office of Technical Services, Department of Commerce, for sale to the public, indicate this fact and enter the price, if known.

11. SUPPLEMENTARY NOTES: Use for additional explanatory notes.

12. SPONSORING MILITARY ACTIVITY: Enter the name of the departmental project office or laboratory sponsoring *(paying for)* the research and development. Include address.

13. ABSTRACT: Enter an abstract giving a brief and factual summary of the document indicative of the report, even though it may also appear elsewhere in the body of the technical report. If additional space is required, a continuation sheet shall be attached.

It is highly desirable that the abstract of classified reports be unclassified. Each paragraph of the abstract shall end with an indication of the military security classification of the information in the paragraph, represented as *(TS), (S), (C), or (U)*

There is no limitation on the length of the abstract. However, the suggested length is from 150 to 225 words.

14. KEY WORDS: Key words are technically meaningful terms or short phrases that characterize a report and may be used as index entries for cataloging the report. Key words must be selected so that no security classification is required. Identifiers, such as equipment model designation, trade name, military project code name, geographic location, may be used as key words but will be followed by an indication of technical context. The assignment of links, rules, and weights is optional